Student thesis series INES nr 629

Evaluating a new hydraulic implementation in LPJ-GUESS for three sites in north Europe

Carl Holmquist

2023
Department of
Physical Geography and Ecosystem Science
Lund University
Sölvegatan 12
S-223 62 Lund
Sweden

Carl Holmquist (2023).

Evaluating a new hydraulic implementation in LPJ-GUESS for three sites in north Europe.

Utvärdering av en ny hydraulisk inkludering i LPJ-GUESS för tre områden i norra Europa.

Master degree thesis, 30 credits in *Subject of degree*

Department of Physical Geography and Ecosystem Science, Lund University

Level: Master of Science (MSc)

Course duration: *January* 2022 until *January* 2023

Disclaimer

Evaluating a new hydraulic implementation in LPJ-GUESS for three sites in north Europe

---

Carl Holmquist

Master thesis, 30 credits, in Physical Geography and Ecosystem Analysis

Supervisor: Thomas Pugh

Lund University

Supervisor: Annemarie Eckes-Shephard

Lund University

Exam committee:

Anders Ahlström, Lund University

Vaughan Phillips, Lund University

Acknowledgements

Thanks to Philip Papastefanou for the detailed explanation of LPJ-GUESS-HYD and for answering questions related to the model. I extend my gratitude to my supervisors, Annmarie Eckes-Shephard and Thomas Pugh, for the excellent guidance, support in setting up the model and improvement suggestions for my report writing. I also acknowledge ICOS Sweden for provisioning of data and I would like to thank Maj-Lena Finnander Linderson for answering questions related to the flux data. ICOS Sweden is funded by the Swedish Research Council as a national research infrastructure.

Table of contents

List of abbreviations

Abbreviation	Description
CUT	Constant Ustar Threshold
DGVM	Dynamic Global Vegetation Model
ET	Evapotranspiration
GPP	Gross primary production
HF	Hydraulic failure
HTM	Study site Hyltemossa
LAI	Leaf area index
LPJ-GUESS-HYD	Lund Potsdam Jena general ecosystem model hydraulic version
NOR	Study site Norunda
OAT	Once at a time
PFT	Plant function type
PWS	Plant water-regulation strategies
RRMSE	Relative root mean square error
SVB	Study site of Svartbeget
VPD	Vapor pressure deficit
VUT	Variable Ustar Threshold

Abstract

Drought is projected to increase in frequency and intensity and impacts trees with increased water stress and increased mortality rate. Water stresses can cause hydraulic failure-related mortality or carbon starvation due to tree species having different strategies to deal with water stresses. LPJ-GUESS-HYD (Hydraulic implementation of a new plant hydraulics scheme in LPJ-GUESS) was developed to include strategies plants are taking to deal with drought. The new model is an enhanced version of LPJ-GUESS, introducing parametrizations of hydraulic mechanisms in plants. LPJ-GUESS (Lund-Potsdam-Jena general ecosystem simulator) is a state-of-the-art ecosystem model, which combines a Dynamic Global Vegetation Model (DGVM) with a more detailed representation of vegetation dynamics, to simulate vegetation at a regional scale.

The aim of this study was therefore to evaluate a new version of the dynamic global vegetation model LPJ-GUESS-HYD with an upgraded hydraulic implementation by testing the model results' accuracy to observed data and the behaviour of mostly hydraulic parameters, never tested in Sweden. A parameter calibration was done to improve the hydraulic model representing GPP (gross primary production) and ET (evapotranspiration). After two calibrations the model was improved with a final mean RRMSE of around 40% aggregated using all sites and model outputs (ET and GPP). The hydraulic model underestimated ET while the standard version represented ET fluxes better, with a lower site mean RRMSE compared to observations. The hydraulic model predicted GPP better than ET, even if the model tends to overestimate the carbon fluxes for HTM and NOR. A One At a Time (OAT) sensitivity test of LPJ-GUESS-HYD was done to evaluate which parameters cause the highest variability in model outputs representing GPP and ET fluxes. The yearly mean changes during the simulation period (2010-2019) of carbon and water fluxes showed high sensitivity to isohydricity (λ), optimal forcing pressure to maintain canopy conductance ($\Delta\Psi_{max}$), maximum sapwood conductivity (Ks_{max}), water potential representing 50% loss of conductance (Ψ_{50}) and the ratio of intercellular to ambient CO2 (λ_{max}). Cavitation slope (d) (how fast air bubbles form in the tree xylem and preventing water from being pulled upward) and the proportion of resistance located below ground and above ground (b) showed negligible sensitivity for all sites. Recommendations for further studies are varied and range from testing parameter interactions to including additional parameters in an improved sensitivity test and calibration. It is crucial to further evaluate the hydraulic model to improve the water fluxes predictions and to go beyond the scope of the current observations to strengthen climate change prediction, including how ecosystems react to increase drought conditions in future scenarios.

1 Introduction

Forests cover around 30 percent of the terrestrial surface on earth, account for around 45% of global terrestrial carbon stocks, and sequester around 25% of human-emitted carbon dioxide annually (Allen et al. 2010, Choat et al. 2018, Hartmann et al. 2018). Forests provide a range of important ecosystem services like maintaining biodiversity, erosion prevention and hydrologic balance (Choat et al. 2018, Hammond et al. 2019). Forests are facing many negative consequences for climate change, for instance drought (Seidl et al. 2017). In the future drought events are projected to increase in frequency and intensity (IPCC 2021). The negative consequences for forests during a climate change driven drought include increased water stress, increased mortality rate, decreased carbon sequestration, and reduced growth (reduced GPP leads to reduced carbon fixed in biomass) (Allen et al. 2010). Soil moisture is the most important factor regulating stomatal conductance. With a root signal (hormone or hydraulic) stomata can respond to dry conditions in the soil (Christmann et al. 2017; Hammond et al. 2019).

In dry conditions, tree species can be categorizing into applying two strategies of stomatal regulation, an isohydric and an anisohydric strategy, see fig. 1 (Papastefanou et al. 2020, Schulze et al. 2019). Trees applying the isohydric strategy maintain the water potential of their cells by decreasing stomatal conductance (closure of stomata), but trees with anisohydric strategy keep the stomata open and decrease their leaf water potential. Anisohydric trees can therefore maintain photosynthesis and transpiration (Papastefanou et al. 2020, Schulze et al. 2019), under lower soil water content than isohydric trees, but with increased risk for hydraulic failure (water loss by transpiration from the leaves is much greater than the water uptake) (Schulze et al. 2019). Isohydric trees with rapid stomatal closure, experience carbon limitation/starvation (Kannenberg et al. 2022). Carbon limitation can further lead to detrimental depletion of stored sugars and starches (Kannenberg et al. 2019). The benefit of stomatal closure is that trees can avoid excessive xylem tensions, caused by higher demand of transpiration than a water uptake by the roots can serve (Garcia-Forner et al. 2017, Schulze et al. 2019). Simplified, for anisohydric species, the risk for damage (cavitation) related to water stress is more likely but for isohydric species, carbon limitation is more likely in dry conditions, but in prolonged climatic dryness conditions isohydric species are exposed to risk to cavitation due to water stress (Salazar-Torosa et al. 2018). Garcia-Forner et al. (2017) showed that an isohydric tree most likely died from hydraulic failure by greater reduction of hydraulic conductance in xylem than an anisohydric tree under long drought.

An increase of xylem water tension occurs when the transpiration is much greater than the uptake of water by the roots caused by a dry soil environment. Further, this leads to cavitation (breakage of the water column in xylem cells by small air bubbles) of xylem vessels, or embolism (the bubbles expand) and conductivity loss (Schulze et al. 2019). This loss of xylem conductivity increases tree mortality (Hammond et al. 2019).

To explain drought resistance and mortality mechanism for plants an iso/anisohydric classification is widely used (Garcia-Forner et al. 2017), but in recent years these strategies are increasingly seen as a continuum and not a dichotomy. Stomatal control and water potential regulation can be less interdependent (Martínez-Vilalta & Garcia-Forner, 2017). Understanding and predicting drought effects on forest ecosystems are important for linking climate change to forest health (Allen et al 2010) and understanding tree mortality (Hartmann et al. 2018). Understanding how ecosystems are responding to climate-driven change is a challenging task and that includes how vegetation responds to drought events (Hartmann et al. 2018, Papastefanou et al. 2020). Ecosystems have different

vegetation types with different hydraulic systems and strategies that respond to soil dryness (Papastefanou et al. 2020). Strategies of stomatal regulation play a crucial part in how species respond to drought. Dynamic vegetation models simulate ecosystem responses to climate change through interactions between carbon-, water-and nutrient cycles (Papastefanou et al. 2020). These models in most cases only include simple implementations of plant hydraulics, but a few of them include more developed implementation, e.g., in LPJ (Hickler et al. 2006), in the Ecosystem Demography model 2 (Xu et al. 2016) and in the stomatal optimization model based on xylem hydraulics (SOX model) that was coupled to a DGVM called TRIFFID (Eller et al. 2018). Still today, most of the models have problems accurately representing the critical processes that govern hydraulics-induced tree mortality by failing to explicitly represent the tree`s hydraulic system (Hartmann et al. 2018). To deal with this issue, a new version of LPJ-GUESS, LPJ-GUESS-HYD has been developed to deal with the tree`s hydraulic system. Precisely as Papastefanou et al. (2020), parameters in LPJ-GUESS-HYD can be changed to control regulation mechanisms of water potential, for instance isohydricity and hydraulic conductivity, and this is implemented as different plant water regulation strategies (PWS). LPJ-GUESS-HYD can be evaluated in different ecosystems and with different PWS in tree species. It is not obvious how different ecosystems fluxes like gross primary production (GPP) and evapotranspiration (ET) reacts to the changes of isohydricity and hydraulic conductivity, when coexisting species in an ecosystem may have a variety of isohydricity behaviour. Therefore, it is difficult to correctly model the impact of isohydricity at ecosystem level (Konings & Gentine 2017).

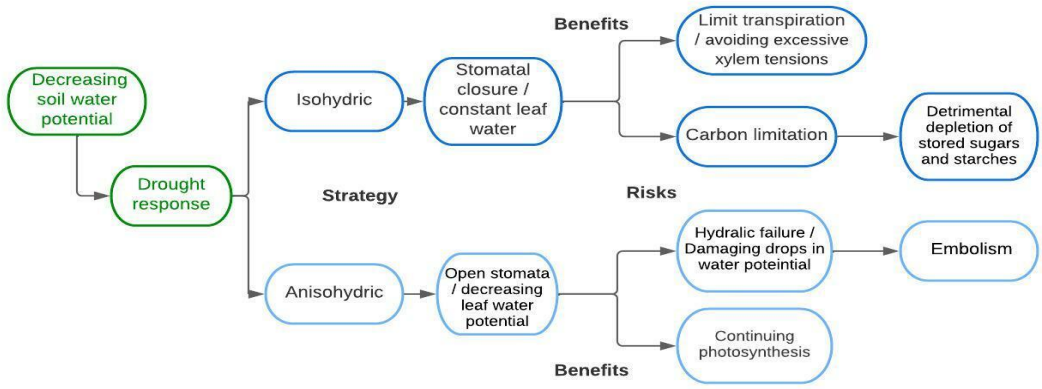

FIGURE 1: *The classical iso/anisohydric concept build on two strategies of responding to drought based on Kannenberg et al. (2022), Papastefanou et al. (2020) and Garcia-Forner et al. (2017).*

1.1 Aim

This study aims to evaluate a new version of the dynamic global vegetation model LPJ-GUESS with an upgraded hydraulic implementation (Papastefanou et al., in review). This includes testing the model results' accuracy to observed data (eddy flux measurements) for three Swedish sites, Norunda (NOR), Hyltemossa (HTM) and Svartberget (SVB). The new version of LPJ-GUESS has not been tested against observations of carbon and water fluxes at the site level in North Europe. Therefore, the aim is also to evaluate if the model can be improved by changing several model parameters and secondly if carbon and water fluxes are sensitive to these parameters, with and without the effects of competition.

This thesis addresses these issues for Swedish boreal sites by answering several research questions. First, improving model results is a necessary baseline for further studies to go beyond the scope of the

current observations to strengthen climate change prediction, including how ecosystems react to increase drought conditions in future scenarios.

1.2 Research questions:

- **(RQ1)** Does the more detailed representation of plant hydraulic strategy, and are there unique solutions for the choice of parameters that improve model performance in simulating land-atmosphere exchanges of carbon and water at three boreal forest sites?

- **(RQ2)** Are the variables of evapotranspiration and gross primary production sensitive to hydraulic parameters in these environments.

- **(RQ3)** How can altered hydraulic parameters for spruce affect the sensitivity test in a forest with competing species (spruce, pine, and birch)?

To be able to answer the first research question, LPJ-GUESS-HYD outputs should be compared to the LPJ-GUESS (standard version) with the old hydraulic implementation based on Sitch et al. (2003). Also in the first question, a parameter calibration should be done, with one change for one species tested in an iterative procedure to find a local minimum of Relative Root Mean Square Error (RRMSE). For the second question, a parameter sensitivity test should be done with all chosen species/PFTs included (spruce, birch and pine), but with parameter change for spruce only. The third question, a second sensitivity test without PFT/species competition, is compared to the first sensitivity test. In the second sensitivity test, only spruce is included to avoid that species competition affecting the sensitivity test, made by altered hydraulic traits for spruce. This is important to be sure that the change in the evapotranspiration (ET) and gross primary production (GPP) is caused by the change of the spruce parameter and not affected by the other species parameters settings.

It is hypothesized that (1) a higher sensitivity to soil water change for the new model improves the model performance ET and GPP (2) Both carbon and water fluxes like GPP and ET will prove sensitive to isohydricity and sapwood hydraulic conductivity changes for chosen sites, Hyltemossa (HTM), Norunda (NOR) and Svartberget (SVB). Because isohydricity regulates leaf water potential with altered soil water potentials, which in turn governs in- and outflows of carbon and water through the canopy conductance. If isohydricity changes to more anisohydric behaviour, the tree is more likely to decrease leaf water potential in water-stressed conditions to be able to continue transpiration and carbon assimilation. The similarity in environments makes ET and GPP almost equally sensitive to isohydricity and hydraulic conductivity. Hydraulic conductivity measures how easily water can pass through the plant and therefore impacts ET and indirectly GPP by regulating how much water can reach the leaves and can be used in photosynthesis/transpiration through canopy conductance.

2 Background

2.1 Worse droughts in the Anthropocene

Anthropogenic climate change-related droughts have been shown to be getting increasingly severe over past decades (Allen et al. 2010, Allen et al. 2015). In Sweden, warmer summer temperatures related to severe drought events have been frequent in recent decades, even though total annual precipitation has increased (Person 2015). As climate change leads to rising temperatures, drought-induced tree mortality can be accelerated (Adams et al., 2009). A combination of hotter temperatures and drought has been called “global-change-type drought” (Breshears et al. 2005). Increased stress and

mortality driven by warmer temperatures can be through physiological impacts or due to pests and pathogens (Allen et al. 2015). For the purpose of this study, the focus will be on the direct impacts of droughts. Drought stress in trees is caused by increasing atmospheric moisture demand or vapour pressure deficit (VPD). This amplifies evapotranspiration demand leading to drier soil (Jung et al. 2010), increasing trees' drought stress and associated tree mortality risk (Eamus et al. 2013). In the future, VPD is projected to become more extreme than today, leading to additional mortality risks due to drought stress (Williams et al. 2013). Extreme events, including severe drought compounded by unusually hot temperatures, are key drivers of climate-induced tree mortality (Allen et al. 2015). Drought impacts woody plants in various ways, e.g., on a local scale by decreasing leaf area and crown "dieback" (a portion of a tree`s canopy dies) (Carnicer et al. 2011), on a regional scale by higher background tree mortality (Phillips et al. 2010) and broader scale forest mortality events (Allen et al. 2010).

While to date, there have been only a few studies of drought-related tree mortality in northern Europe with increased warming, drought impact on trees in Northern Europe, including Sweden, is expected to increase in severity and frequency (Ruiz-Pérez & Vico 2020; Matkala et al. 2021). One example is a study of spruce in southeast Norway (Solberg 2004). Solberg (2004) monitored summer drought for Norway spruce for 14 years. Recent examples of hot droughts are the drought events in 2003 and 2018 (Schuldt et al. 2020). In 2018 central Europe experienced a long-lasting severe drought, and tree species in the temperate forest showed water deficit stress (Schuldt et al. 2020). The result of a study made by (Schuldt et al. 2020) showed low foliar water potentials beyond the threshold for xylem hydraulic failure, leaf discolouration and premature leaf shedding. Needle-leaved trees such as Scots pine and Norway spruce showed signs of discolouration. The 2018 drought event affected trees for a long time, and strong drought-legacy effects were detected a year after 2019. Secondary drought effects were higher, caused by insects or fungal pathogen attacks (Schuldt et al. 2020). As precipitation events in boreal forests have remained relatively stable, this ecosystem may be sensitive to more variability and drought events (Matkala et al. 2021). Norway spruce (Picea Abies) and Scots Pine (Pinus sylvestris) are two widespread species in North Europe. Scots pine is a dominating species in poor soils, but Norway spruce can outcompete Scots pine in richer soils (Matkala et al. 2021). Although Scots pine and Norway spruce respond differently to drought, studies have shown that Scots pine trees have a higher tolerance to drought conditions than Norway spruce (Matkala et al. 2021, Lévesque et al. 2013). Overall, the described drought and secondary drought-effects are expected to increase also in Sweden. This increases the necessity to have working models which resolve these drought-mechanisms for more accurate predictions.

2.2 Tree responses to drought

To understand tree responses to drought, it is essential to spend some time on water movement through the tree. The water flow follows a soil-plant-atmosphere continuum (Hartmann 2010). The water movement in the tree is influenced by hydraulic conductivity, isohydricity, and the water gradient in trees follows the gradient of negative water potential (Ψw, MPa). It moves from less negative (usually the soil) to more negative pressure (usually the air). More explicitly, water moves through a tree from high water potentials in the root via the xylem and further up to the leaves, where transpiration occurs in the stomata pores (Schulze et al. 2018). The xylem is a vascular tissue (the tree's vascular system) that transport water from the roots to the leaves (Hartmann 2010). The water potential is the amount of pressure required to remove water from a water-containing system, and more negative water potential means that more energy is needed to move water (Schulze et al. 2018).

Water loss from the leaves occurs mainly through stomata, and each stomata regulates the flow of water to the atmosphere and the inflow of carbon dioxide through two guard cells. (Martinez-Vilalta

et al. 2012). The concentration of water molecules lost is much greater than the carbon dioxide gain. Therefore, maintaining photosynthesis requires large fluxes of water through the plant. Therefore, water availability is vital in preserving productivity (Schulze et al. 2018). The turgor pressure follows potential water pressures and is essential for the guard cells building up the stomata's pores (Buckley 2005; Martinez-Vilalta et al. 2012). Hydraulic conductivity and the water potential gradient determine water transport from the soil to the root and further up along the tree. Hydraulic conductivity depends on tree tissue properties, soil texture and soil water content and is defined by how easily the water can pass through soil or a plant (Schulze et al. 2018).

For tree tissues, xylem, root, and leaf hydraulic conductivities have been measured in situ and in the laboratory for several decades (Markhart & Smit 1990; Knipfer & Steudle 2008; Melcher et al. 2012). Hydraulic conductivity measurements are useful for measuring responses for different tree species to environmental disturbance factors (drought and freezing), and they are important for parametrizations and evaluation of ecosystem models (Papastefanou et al. 2020). Hydraulic conductivity varies across species and environments and is dynamic depending on environmental conditions (Melcher et al. 2012). For example, hydraulic conductance decreases with more negative water potentials during soil dryness. However, soil and leaf potentials are affected differently depending on the air's moisture content (the atmospheric demand). Drier air creates a higher vapour pressure deficit (VPD), an important factor limiting plant transpiration, through stomatal closure to avoid excessive water loss (Zhang et al. 2017). The atmospheric demand is related to VPD and affects the leaf water change and transpiration (Gollan et al 1985; Zhang et al. 2017). Atmospheric aridity is quantified by VPD-controlled water demand that can passively drive water to move from plant to the atmosphere (Zhang et al. 2017).

Trees have different strategies to deal with drought stress caused by low soil moisture. The concept of isohydricity (Jones & Sutherland, 1991, Tardieu & Simonneau, 1998) describes such strategies and assumes that the plant's water potential and stomatal behaviour are coupled. Isohydricity concept (described in the introduction) is classical because recently this concept has been seen as continuous, with a range of strategies, rather than as a strict dichotomy (Klein 2014; Papastefanou et al. 2020). However, there are risks related to the strategies; a more isohydric strategy favoring earlier closure of stomata can cause early onset of a negative carbon balance or carbon starvation whereases a more anisohydric behaviour with open stomata combined with a decrease in water potential can result in hydraulic failure (Schulze et al. 2019). Hydraulic failure is caused when water needed for transpiration is much greater than the possible uptake of water by the roots, which leads to higher xylem water tension and cavitation of xylem vessels (McDowell et al. 2008). The stomata's guard cells respond to the water supply from the soil layer and the atmospheric water demand and close the stomata to prevent hydraulic failure (Martinez-Vilalta et al. 2012).

Mortality caused by drought events is related to drought intensity, duration, and frequency, all of which are thought to have increased in Sweden over the past few decades. Under extreme drought events, xylem hydraulic failure is common (Mantova et al. 2022). During a drought event, evaporative demand increases and/or soil water availability decreases (Li et al. 2022b, Noguera et al. 2022), leading to xylem tension causing cavitation (change from liquid water to water vapour under altered xylem tension) events in the xylem (McDowell et al. 2008; Mantova et al. 2022). The evaporative demand puts more pressure on the xylem vascular system to overcome the adhesive forces created between the water and the soil particles. Therefore, a negative pressure is needed in the xylem, and embolism occurs if it increases to critical levels (Hartmann 2010). Embolism is a water phase change due to cavitation that results in the formation of gas bubbles called “emboli” in the xylem (Hartmann 2010; Tyree & Sperry 1989). The cavitation can then be spread starting at the xylem conduit through

the xylem network, leading to decreased hydraulic conductance in the xylem. The resistance of water in xylem cavitated vessels increases until the water flow stops, leading to dehydration of the tree tissues, local cell death, and in the end, death of the tree (Mantova et al. 2022). Cavitation can occur due to freezing stress, and embolisms occur after the thaw phase when air bubbles cause cavitation (Tyree & Sperry 1989). At the species level, the risk of cavitation is extremely variable (Tyree & Sperry 1989; Mantova et al. 2022). One way to set cavitation thresholds is the percentage loss of hydraulic conductance (PLC). PLC links the loss of conductivity in xylem, root and leaves to water potentials and is caused by cavitation due to tension. Tyree & Sperry (1989) described the vulnerability curve to cavitation that links water tension to cavitation loss due to embolized cells. To normalize the cavitation loss along the water potential gradient, a vulnerability curve was made. From the vulnerability curve, species can be discriminated by the steepness of the curve and cavitation vulnerability of different plant parts can be described. Embolisms can occur in many cells and impact the conductance from the root to the leaves (Tyree & Sperry 1989). From the normalized vulnerability curve, different thresholds can be used. An important threshold is how much water can be taken out of the soil until the soil is unsaturated enough to cause a 50% decrease in conductivity in the plant. It is also referred to as runaway cavitation, a feedback process of amplified cavitation. This can occur when the atmospheric demand cannot be reached due to low soil water content (Tyree & Sperry 1989). PLC in trees can decrease 5-20% before reaching the state of runaway cavitation and quickly recover embolized cells (Tyree & Sperry 1989). Thresholds of ψ_{50} and ψ_{88} correspond to PLC's of 50% and 88% respectively and are commonly used in models to set thresholds for vulnerability to cavitation (Mantova et al. 2022). Both thresholds are associated with the capacity of the trees to recover from a drought event. For instance, ψ_{50} can be used to define vulnerability to cavitation or hydraulic safety margins and possible recovery thresholds for conifers, while ψ_{88} is set for angiosperms (Mantova et al. 2021). However, studies have shown that the value of PLC and possibility to recover can vary across individuals and species (Mantova et al. 2021, Hammond et al. 2019). For angiosperms the water potential at 88% is believed to represent a threshold of no return, while for coniferous trees, the threshold for no return is estimated to be at a 50% loss of hydraulic conductance (Schulze et al. 2019). Hydraulic conductivity is related to the cavitation processes; specifically, when cavitation reduces conductivity in different parts of the plant. Tracheid-bearing trees like spruce and pine species usually have lower non-water stressed sapwood conductivity and can therefore be less vulnerable to cavitation (Hickler et al. 2006). According to Choat et al. (2012), conifer species generally have higher hydraulic safety margins than angiosperms.

The section above describes processes related to water-stressed conditions, which can be linked to hydraulic failure, an irreversible xylem dysfunction. Carbon starvation (CS), a related mortality mechanism, is a commonly evaluated mechanism in available literature, often together with hydraulic failure. CS can be described as a process leading to a point when the plant supply of carbon is greater than the demand for both osmotic and metabolic functioning (Hartmann 2015). The two extreme (anisohydric/isohydric) conditions related to drought link to risks associated with either carbon starvation or hydraulic failure (see fig. 1). Among species that have a more nuanced response to the two extremes, it is more difficult to determine if CS or HF is the dominant mechanism causing tree mortality. Therefore, pure CS or HF may not exist, and a combination of both is more likely (Li et al. 2022b). While a few experimental studies show CS as the main mechanism of mortality, a majority of studies showed HF as the dominant condition (Li et al. 2022b). CS is much more difficult to identify, but HF can be assessed through percent loss of conductivity (Hartmann 2015). This is important for this study, because the new hydraulic model implemented here parameterizes safety margins (ψ_{50}), isohydrodynamic behaviour and hydraulic conductivity, which are key to the concept of HF. These

allow for the modelling of HF depending on environmental conditions (soil moisture, temperature, and precipitation).

2.3 Drought and ecosystem modelling

Ecosystem models incorporate ecosystem components (individual species, functional groups) and ecosystem processes (chemical, physical, and biological) into one model. The ecosystem model describes the interaction between processes (primary production, respiration, energy, water, carbon, and nutrient flow through food webs) and components (Geary et al. 2020). Ecosystem models are parameterized from field measurements, experiments, and expert elicited data (Peters & Okin 2017). The models are used to predict outcomes of complex interactions between components and processes in ecosystems under past, future, or novel scenarios (Geary et al. 2020). Drought affects both the water and carbon cycle, and many approaches have been developed to simulate water and carbon dioxide fluxes for different ecosystems (Keenan et al., 2009). Ecosystem models are constantly developed and model approaches from one model can be used in other models (BIOME3 model approaches are used in LPJ-GUESS). For example, early models predicting stomatal conductance (Collatz et al., 1991, Ball et al. 1987) and photosynthesis (Farquhar et al. 1980) were implemented in more recent land and climate models (Bonan et al. 2014). In addition, ecosystem models can be used to understand further the responses of the water and carbon cycles to drought events upon evaluation with observed data (Keenan et al., 2009; Krinner et al., 2005).

Based on several mechanisms or strategies previously mentioned related to how plants react to drought, ecosystem modellers mathematically include these processes in models. Models are essential to understanding ecosystem processes and making future projections (Hartmann et al. 2018). Still, current models need to be improved to integrate a better representation of tree mortality and the impacts of droughts on ecosystems. That is to enhance the performance of long-term forest dynamics and the regulation of C storage and water fluxes (Hartmann et al. 2018).

Based on the Lund-Potsdam-Jena-Dynamic-Global-Vegetation-Model (LPJ-DGVM) (coupled biogeography–biogeochemistry model), Hickler et al. (2006) incorporate a plant hydraulic architecture into their model along with an upgraded hydraulic architecture. The upgraded model contains the processes of water uptake by vegetation. The model is based on pressure gradients and water potential that drive water flow between the soil through the roots, xylem, and leaves (Hickler et al. 2006). The water supply for transpiration is based on Darcy`s law (Whitehead, 1998 as cited in Hickler et al 2006). It is an upgraded model formulation for calculating water supply to leaves; if the water supply is lower than the atmospheric demand then the canopy conductance is reduced until transpiration is at the same rate as the demand. When the water supply is lower than the demand, the diffusion of carbon dioxide into the leaf is decreased too, which in turn leads to lower photosynthesis (Hickler et al. 2006). This upgraded version made it possible to mechanistically address the effects of hydraulic variation for each PFT (Hickler et al. 2006).

Based on Hickler et al. (2006), Papastefanou et al. (in review) further developed this representation of plant hydraulics as well as a new representation of leaf water potential and different isohydric strategies based the isohydric spectra (Papastefanou et al. 2020) into the LPJ- GUESS model (this version will be referred to as LPJ-GUESS-HYD in this thesis). Papastefanou et al. (in prep.) use sapwood, root and leaf resistance based on the same equation in Hickler et al. (2006) but added several new equations to LPJ-GUESS. In the standard version of LPJ-GUESS, the maximum canopy conductance in the non-stressed condition is estimated, assuming fully open stomata Canopy conductance is then used for the estimation of photosynthetic carbon uptake (Papastefanou et al. in review).

2.4 Theoretical background

2.4.1 Model description of LPJ-GUESS

Hickler et al. (2012) developed a European version of LPJ-GUESS, where individual tree species are represented. Several common European tree species are represented through distinct parameterizations. All tree species in this study are based on Picea abies, Pinus silvestris, Betula pendula, and are represented by the European version of LPJ-GUESS. The European version of LPJ-GUESS differs from an older version of LPJ-GUESS (Smith et al. 2001) by representing individual species within a PFT. For instance, spruce (Picea abies) can be represented by several additional parameters and values represented by literature studies (see appendix for more details), instead of being more broadly classified as a BNE (Boreal needleleaved evergreen tree) PFT. (Hickler et al. 2012).

LPJ-GUESS version 4.1 simulates vegetation dynamics on both a regional and global scale. The model contains fast processes on a daily basis, slow processes on an annual basis and state variables. Input to the model is temperature, precipitation, radiation, CO_2, and soil physical properties (see figure 1). The rate of the processes is affected by input values. The output of the model contains current state variables and biogeochemical fluxes of H_2O and CO_2 (Smith et al. 2001). LPJ-GUESS uses PFTs to represent and simplify the structural and functional variety among a diverse range of plant species (Smith et al. 2001). The below section describes processes of soil hydrology, evapotranspiration, mortality, and photosynthesis (GPP).

2.4.2 Soil hydrology

LPJ-GUESS version 4.1 uses soil hydrology equations from Gerten et al. (2004), but instead of two soil layers, it uses fifteen. Soil water content is modelled for each layer individually, and each layer has a depth of ten centimetres. Each layer's physical properties (hydraulic porosity, thermal) are scaled between mineral and organic soil types and can be regulated by the user. Soil water content (SWC) is calculated considering daily precipitation, interception, percolation between the layers, evapotranspiration, and runoff. The water uptake rate of each PFT is independent of SWC (to a default wilting point threshold of -3.5 MPa soil water potential), but with fractional uptake from different layers according to prescribed root distribution (Gerten et al. 2004). The root distribution settings for the fifteen layers of soil are the same for all PFTs (see appendix for PFT settings).

The definition of the minimum fractional water uptake (Fw) for the soil layers is calculated by:

$$\boldsymbol{Fw = \frac{\min(wcont * awc * fpc_{rescale} * emax * r.dist)}{emax}} \quad (1)$$

where $wcont$ is water content in the soil, awc is available water holding capacity (mm), $fpc_{rescale}$ is a scaling factor for foliar projective cover (complement of patch summed FPC overlap), $emax$ is maximum evapotranspiration (mm/day) and $r.dist$ is root distribution. The root distribution that is used in this study (for both model versions) is parameterized following Jackson et al. (1996).

2.4.3 GPP and carbon biomass (standard and hydraulic version)

Photosynthesis (GPP), stomatal conductance, evapotranspiration and plant water uptake are modelled on a daily basis. In the standard version of LPJ-GUESS, photosynthesis is coupled with a soil water balance scheme adapted from the BIOME3 model (not the new hydraulic scheme in LPJ-GUESS-HYD) (Haxeltine & Prentice 1996; Sitch et al. 2003). Photosynthesis uses 50 % of incoming shortwave radiation, which is absorbed by particle active radiation (APAR), water availability,

temperature, and the maximum rate of carboxylation, V_{max} (Rubisco-activity limited photosynthesis rate). Photosynthesis is calculated according to Sitch et al. (2003), who refer to Haxeltine & Prentice (1996). For more details on the calculation of GPP are given by Haxeltine & Prentice (1996). Water-stressed photosynthesis results in a lower canopy conductance. Calculation of a numerical iteration procedure to find the level of stomatal aperture that is characterised by λmax (the ratio of leaf intercellular to ambient CO_2 concentrations). A lower λmax results in less canopy conductance and lower GPP. Carbon assimilation in water-stressed conditions is based on the hydraulics estimate for canopy conductance calculated within the hydraulic version of LPJ-GUESS. Assimilation is based on a non-foliar projective cover weighted canopy conductance value for each PFT under water-stress conditions (mm/s), and is calculated within the standard version.

LPJ-GUESS calculates growth by adding the current year's NPP of an average individual tree to its current year biomass. Then the available carbon divides among the living biomass tissues (leaves, fine roots and sapwood) such that four allometric constraints remain satisfied (Smith 2001).

2.4.4 Evapotranspiration (standard version)

Evapotranspiration is calculated by adding transpiration, interception, and soil evaporation. The standard LPJ-GUESS (version 4.1) uses a modified hydrological scheme from Gerten et al. (2004). Transpiration E_T is modelled through the minimum of the potential rate, which is determined by atmospheric demand (D) and a plant-controlled supply function (S) using the following formula: $E_T = min\ (D, S)f_v$, where f_v is the fraction of the gridcell covered by vegetation. S is estimated through the maximum transpiration rate (E_{max}) under non-stressed conditions and decreases with lower relative soil water content (wr) (weighted by the fraction of roots in the soil layers), and D is estimated the average maximum stomatal conductance of a cohort of trees. If S is smaller than D canopy conductance decreases, which limits both transpiration and GPP (Gerten et al 2004).

Evaporation (Es) from the soil is estimated through the fraction of a grid cell not covered by vegetation multiplied by the soil moisture. Interception loss is estimated through the prescribed precipitation rate (see fig. 2), and LAI (leaf area index, in m^2 leaves per m^2 ground) and f_v (Gerten et al 2004).

2.4.5 Mortality in LPJ-GUESS and LPJ-GUESS-HYD

The standard and hydraulic versions of LPJ-GUESS include several additive tree-mortality mechanisms; a patch destroying disturbance, a mortality mechanism associated with fire (not included in this study), bioclimatic limit mortality (based on minimum temperature thresholds a given plant type can survive, (see appendix table A1 for species specific settings), a background, longevity mortality, and a growth-efficiency based mortality (Smith 2007). Only the standard version's growth efficiency mortality can be dynamically linked to drought stress. Therefore, a new mortality related to hydraulic failure is added to the hydraulic version of LPJ-GUESS (Papastefanou in review) described in the model description below.

Carbon-stressed related mortality can affect growth efficiency and (annual process, see fig. 2) is defined as the ratio of individual annual NPP (in KgC m^{-2} $year^{-1}$) to individual LAI, averaged over five years. If the ratio is smaller than a PFT/species-specific threshold for growth efficiency, the individuals face a 30% likelihood of death each year. A lower growth efficiency occurs most likely due to severe shading by taller individuals but also due to drought, low temperatures, or a shortened growing season. Both model versions use the above carbon-related mortality mechanism (carbon starvation).

In the European version of LPJ-GUESS, where individual tree species are represented, parameters are associated with different shade tolerance classes (tolerant, intermediate and intolerant). In this study, spruce is assumed to be shade tolerant, pine is intermediate, and birch is intolerant to shading. Tree species use a trade-off between high growth efficiency (fast growth, see birch in table A2) and high maximum recruitment or survival at low growth rates from intense shading by neighbouring trees (Hickler et al. 2012).

Mortality related to shading is given by:

$$mort = \frac{mort_{\max}}{1 + (greff / greff_{species})^{c}} \quad (2)$$

Where $greff_{species}$ is the growth efficiency parameter (see table A2 in the Appendix), $mort_{max}$ being the maximum mortality rate caused by growth efficiency, $greff$ is the growth efficiency and *c* is a shape parameter (see table A2 in appendix).

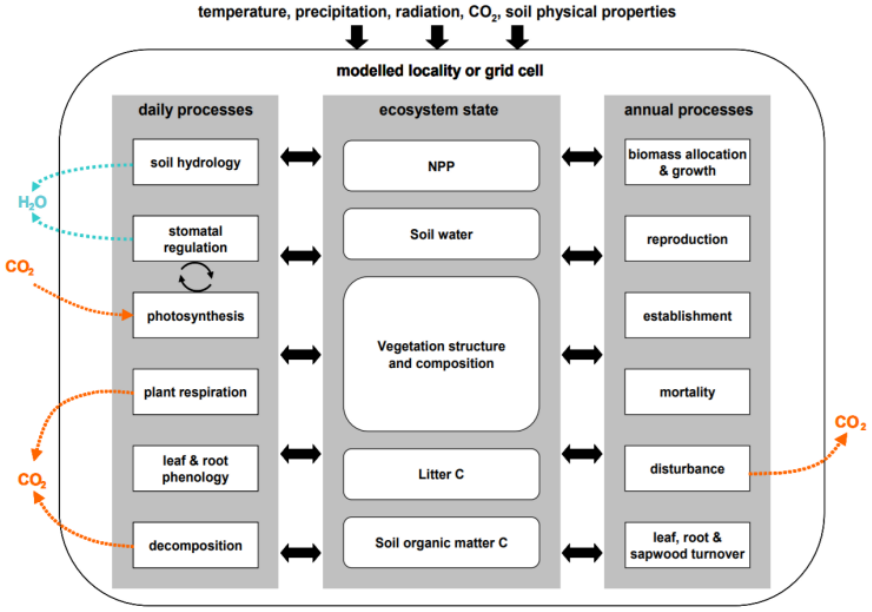

FIGURE 2. *Shows overview of the conceptual representation of LPJ-GUESS. The main processes, time steps (daily and annually), state variables and input environmental data for a grid cell are locally modelled.*

2.4.6 Model description of LPJ-GUESS-HYD

LPJ-GUESS uses PFTs in order to get structural and functional variation among plant species of the world (Smith et al. 2001). This is necessary to simplify the diversity species have and find the most important functional and structural variety. In LPJ-GUESS-HYD this concept extends to plant water-regulation strategies (PWS). This diversifies the existing PFTs to include more plant hydraulic traits (Papastefanou et al. in review). In this study, PFTs are replaced or parametrized by species, which Hickler (et al. 2012) introduced. The section below presents how the PWS`s are derived in the model. Soil water content changes are directly linked to soil water potential changes that control processes in the tree from the roots up to the canopy. Chosen values for isohydricity and other parameters (green boxes in fig. 3) related to water stresses activate different processes. For instance, isohydricity is directly linked to leaf water potential dynamics in water-stressed conditions with increasing negative soil water potential, which in turn affects xylem water potential depending on SWC. The parameter is directly linked to xylem water potential depending on the difference between leaf and soil water

potentials. If it is close to 1, xylem water potential follows the change of leaf water potential to a greater extent. See below for detailed equations for each changeable parameter and model component.

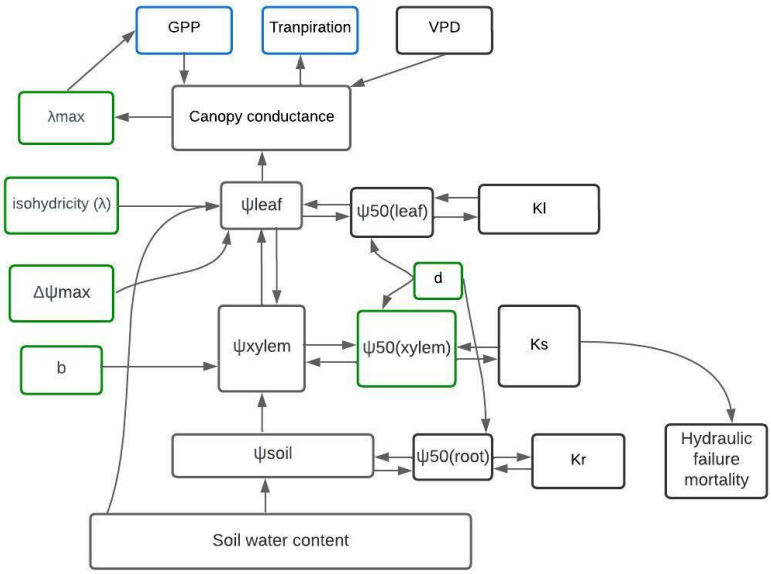

***FIGURE 3**: Conceptual diagram of the model components (black boxes), outputs (blue boxes), and parameters (green boxes). Changed parameters used in calibration and the sensitivity test are green boxes and outputs of the model for this study are blue boxes. Parameter definitions are in Table 1 and the model description bellow.*

The seven components of LPJ-GUESS-HYD are described below (Papastefanou et al. in review), alongside the description of λmax (shared across LPJ-GUESS-HYD and LPJ-GUESS). (1) describes the water potential (soil, leaf and xylem). Each (leaf, xylem and soil) water potential is estimated based on soil water content and a dynamic approach considering different hydraulic strategies (isohydricity). (2) The hydraulic resistance of roots, stem and leaves is derived from the loss of conductivity and maximum conductivity. (3) a polynomial response curve is used to calculate the loss of conductivity. (4) A new mortality plant probability, m_k is derived from the loss of sapwood conductivity from (3). (5) Following Darcy's law and the supply-demand theory a canopy conductivity g_C is derived using (1) and (2). (6) The total evapotranspiration flux E_Σ is estimated based on the Penman-Monteith equation using g_C from (5) and a simple energy-atmosphere-balance model including aerodynamic conductance and leaf temperature (7). λmax is calculated through the ratio of intercellular to ambient CO_2 partial pressures.

1. **The soil-, leaf- and xylem water potential.**
   For the soil water potential $\psi_{s,}$, individual soil layer water potential $\psi_{s,i}$ is estimated and weighed using a species-specific rooting depth parameter r_i and across the soil layers, *i*, is calculated using the following formula (Papastefanou in review):

$$\psi_s = \sum_i \psi_{s,i} \cdot r_i \quad (3)$$

   The change in leaf water potential, $\Delta\psi_L$ is calculated using the following dynamic formula (Papastefanou et al. 2020):

$$\frac{\Delta\psi_L}{\Delta t} = \alpha((1-\lambda)\,\psi_s - \psi_L - \Delta\psi_{max}) \quad (4)$$

Where λ is the isohydricity, the species leaf specific water potential regulation strategy, spanning -0.3 to 1 and $\Delta\psi_{max}$ is the plant water forcing potential under well-water condition and the difference of $\psi_s - \psi_L$ under non-water stress conditions. α is a rate parameter and describe the speed of ψ_L to changes in ψ_s. λ and $\Delta\psi_{ww}$ are plant water strategies used in sensitivity test. Leaf and soil water potentials updates daily.

Xylem water potential, ψ_x is calculated using the following empirical relationship (based on Fisher et al. 2006):

$$\psi_x = b(\psi_L - \psi_S) + \psi_S - w\rho * 9.81 * \frac{\text{ih}}{1.0E6} \quad (5)$$

b is the distribution of hydraulic resistance above and below ground (Fisher et al 2006) and is an empirical parameter and can normally be adjusted according to soil water conditions, but in this study changed regardless of soil water conditions (Fisher et al 2006). In this study b is changed from 0.1 – 0.9. It used to be from 0 to 0.2 under non-stressed conditions and from 0.5 to 0.9 under dry conditions. $w\rho$ is water density, ih is individual height. The parameter b is used in the sensitivity test.

2. **Hydraulic resistances of roots, stem, and leaves**

Hydraulic resistances are derived from water potentials and sapwood viscosity (Hickler et al. 2006).

Sapwood resistance is given by:

$$R_S = \frac{h \cdot \eta_S}{k_{Smax} \cdot (1 - \kappa_S) \cdot A_S} \quad (6)$$

Leaf resistance is calculated using following formula:

$$R_L = \frac{1}{k_{L,max} \cdot (1 - \kappa_L) \cdot fpc} \quad (7)$$

Root resistance is calculated using following formula:

$$R_R = \frac{\eta_R}{k_{R,max} \cdot (1 - \kappa_R)} \quad (8)$$

Where, $k_{S,max}$, $k_{L,max}$, and $k_{R,\,max}$ are maximum sapwood-, leaf-, and root conductivity. $k_{S,}$, k_L, and k_R are sapwood-, leaf-, and root loss of conductivity (0-1). A_S is sapwood area, h is tree height, η_S is viscosity of the sap flow. fpc: foliage projective cover and η_R is the conductivity of the root sap. $k_{S,max}$ is later used in the sensitivity test.

3. **Loss of conductivity:**

The loss of conductivity, K of each of sapwood, leaf and root (K_S, K_L, K_R) is calculated using following polynomial response curve (fraction loss of conductivity) (Santiago et al. 2018):

$$K(\psi) = \frac{1}{1 + \left(\frac{\psi L}{\psi_{50}}\right)^d} \quad (9)$$

where ψ_{50} is water potential at which 50% of the compartments (leaves, roots, xylems) conductivity is lost, ψL is leaf water potential and d is a slope parameter. It is assumed that K_S, K_L and K_R depend on ψ_x, ψ_L and ψ_s, respectively, and each slope d is parameterized based on ψ_{50} and ψ_{88} using the following formula:

$$d = \frac{\log(-1+1/0.88)}{\log\left(\frac{\psi_{88}}{\psi_{50}}\right)} \quad (10)$$

ψ_{50} and d is used in the sensitivity test.

4. Hydraulic failure mortality:
   A new mortality plant probability m_κ is implemented and based on hydraulic failure. A probability to mortality from loss of sapwood conductivity (Ks) is based on following formula:

$$m_K(K_S) = 1 - e^{-\left(\frac{\kappa_S}{f_\kappa}\right)^{d_\kappa}} \quad (11)$$

   Where $f_\kappa = 0.85$ and $d_\kappa = 8.0$ based on a wide range of loss-of-conductivity curves, K(ψ) .

5. Canopy conductance:

   Canopy conductance g_C is calculated via Darcy's law assuming that water flow J from soil via roots, shoot and leaves to the atmosphere balances the imposed transpiration flux E_{imp}.

   The water flow J is dependent on the differences between soil and leaf water potentials, water density (wp), gravitational pull (g), and tree height (h). J is estimated according to (Whitehead 1998):

$$J = \frac{\Delta\psi}{R_T} = \frac{\psi_s - \psi_L - w\rho \cdot g \cdot h}{R_L + R_S + R_R} \quad (12)$$

   and the imposed transpiration flux E_{imp} (water that comes from the soil induced by VPD) on foliage projective cover (FPC) basis:

$$E_{imp} = g_C * VPD \quad (13)$$

   Assuming $J = E_{imp}$:

$$g_C = J * \frac{1}{VPD} \quad (14)$$

   Non stressed canopy conductance $\widetilde{g_C}$ is based on fully open stomata and photosynthesis. This is calculated to avoid the overestimation of g_C under non-droughted conditions and estimate the final canopy conductivity as $min(g_C, \widetilde{g_C})$. The non –water stressed $\widetilde{g_C}$ only consider VPD affecting g_C, hence remove the effect of VPD on leaf water potential ψ_L. VPD is calculated from relative humidity and temperature inputs and non-water stressed $\widetilde{g_C}$ is denoted by:

$$\widetilde{g_C} \sim \frac{1}{VPD} \quad (15)$$

   If g_C is smaller than photosynthesis optimum, a minimum conductance not associated with photosynthesis, $gmin$ is used. $gmin$ is a PFT-specific minimum canopy conductance, that accounts for plant water loss not directly linked to photosynthesis (e.g., guttation).

$$if\ gc < gmin\ then\ gc = gmin \quad (16)$$

6. **Total evapotranspiration:**

The total evapotranspiration E_Σ uses both imposed- and equilibrium evapotranspiration fluxes, E_{imp} and E_{eql} using the instructive form of the Penn-Monteith-Equation (Köstner et al. 1992):

$$E_\Sigma = E_{eql}\,\Omega + E_{imp}(1 - \Omega) \quad (17)$$

where Ω is a dimensionless (0-1) factor that describes the coupling between the canopy and the atmosphere. Ω can be estimated as ref (Köstner et al. 1992):

$$\Omega = \frac{1+\epsilon}{1+\epsilon+\frac{g_A}{g_C}} \quad (18)$$

ϵ is the change of latent heat relative to the change in sensible heat of saturated air (~1.27), g_A is the aerodynamic conductance. The equilibrium evapotranspiration E_{eql} is an already established part of LPJ-GUESS and is used to calculate the water demand of the plant in the standard version and is the transpiration rate obtained in equilibrium with an extensive, homogeneous wet surface via the energy balance. E_{imp} is the transpiration rate imposed by the air saturation deficit (see Köstner et al. 1992 for detail description).

When gA >> gC, then $\Omega \sim 0$, and E approximates E_{imp} and stomatal control of canopy-level transpiration is regulated depending on isohydricity. E_{imp} increases i.e., if the atmosphere demands more water than the soil moisture would supply. When $gA << gC$, then $\Omega \sim 1$, and E approximates $E_{eql.}$ When E is equal to E_{eql}, a thick boundary layer isolates the canopy from the effects of air saturation deficit in the air above. Then the stomatal control on a canopy transpiration is negligible and Ω regulating the stomatal control over E (Köstner et al. 1992). E_{imp} can be lower as J allows, i.e., if the atmosphere wants less water than the soil moisture would supply.

Aerodynamic conductance g_A depends on several factors including wind speed and leaf temperature, roughness (z, zm, zh), windspeed height (d), molardensity ($molp$). Estimated g_A is based on following formula (mol/m^2/s):

$$gA = \frac{0.4*0.4 * molp*windspeed}{(log((z-d)/zm)*log((z-d)/zh)} \quad (19)$$

Total transpiration E_Σ, aerodynamic conductance g_A and leaf temperature T_L form a circular dependency (feedback loop).

7. **λmax:** A parameter that is also included in the standard LPJ-GUESS. The non-water-stressed ratio of intercellular to ambient CO_2 partial pressures is given by (Sitch et al 2003; Haxeltine & Prentice 1996):

$$\lambda max = \frac{pi}{pa} \quad (20)$$

λmax is a positive value. Under non-water-stressed conditions maximum values of λmax for C3 pathway (woody) plants is 0.8 by default.

3 Methods

3.1 Overview

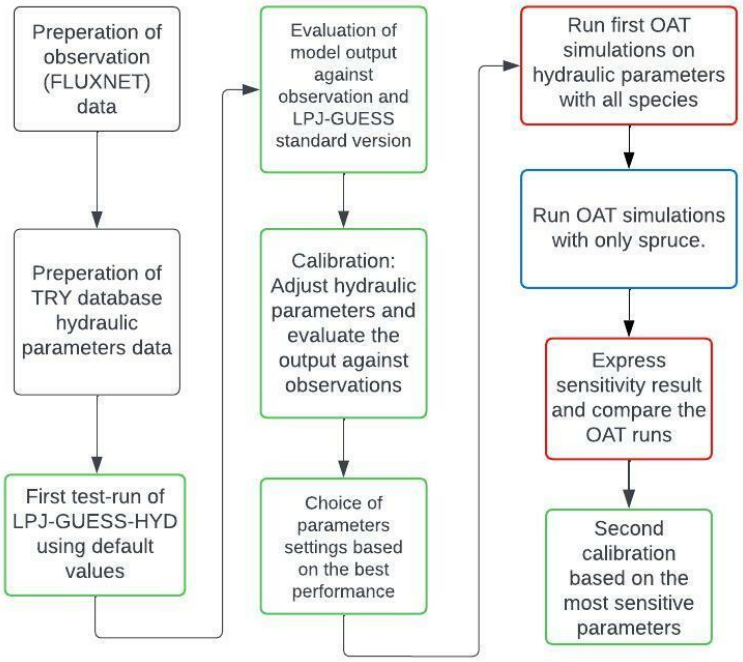

FIGURE 4: *Schematic overview of the methodology.*

A schematic overview of the methodological workflow which addresses the research questions is shown in Fig. 4. The first step includes the preparation of the observation data for the three sites in Sweden taken from FLUXNET (ICOS 2020). Default (initial "best-guess") parameters for this study were species-specific median trait values processed from trait data from the TRY-database (ICOS 2020). Species-specific maximum and minimum values from TRY provide the upper and lower ranges for the sensitivity analysis. To see how the model output of GPP and ET behaves with the default parameters (default run) against observation data, a test run was done. The default hydraulic model was compared with the standard version of LPJ-GUESS. Green boxes refer to **RQ1**. The test run was followed by calibration with adjusted parameters. The calibration results in a new set of parameter values used by an OAT sensitivity test. The sensitivity test was expressed with a yearly mean change of GPP and ET along with a parameter's percent change. The sensitivity test in the red boxes refers to **RQ2**. The sensitivity test was done twice, one with all species included and one with only spruce. This was done to answer **RQ3** in the blue box. The sensitivity test identifies parameters that could further be changed to minimize RRMSE (relative root mean square error). A second calibration of selected parameters was evaluated against the observed data using the same values from the selected parameters from the OAT simulations. The second calibration further evaluates **RQ1.**

3.2 Study areas

The study sites are all located in Sweden. The three sites are research stations from the integrated carbon observation system Sweden (ICOS-Sweden). The Norunda (NOR) research station (see table 1 for detailed information and fig. 5) is located in the southern part of the boreal forest zone (near the town of Uppsala), at an elevation of 45 meters above sea level. The site is flat with minor variation in elevation. The dominant trees are Norway spruce and Scots pine, with a small fraction of birch (around 10% birch) (ICOS 2022b). Effects from storms, thinnings and bark beetle attacks were reported to be seen from 2021- 2022 data (ICOS 2022b). The Hyltemossa (HTM) research station (see table 1 for information) is located in the northern part of Scania (a few kilometres south of the town of

Perstorp). The site is dominated by spruce (Picea abies, 98%), and a small fraction of birch (Betula sp.) (ICOS 2022a). The Svartberget (SVB) research station is located in northeast Sweden (60 km from Umeå). The forest is a mixed forest dominated by Norway spruce (Picea abies, 68 %), with less Scots pine (Pinus Sylvestris, 20%) and a small area of birch (Betula sp.) (ICOS 2022c).

TABLE 1. Three ICOS sites in Sweden (from south to north) taken from (ICOS 2020).

	Hyltemossa	**Norunda**	**Svartberget**
Lat./lon.	56°06′N, 13°25′E	60°05′N, 17°29′E	64°15′N, 19°46′E
Biome	Temperate	Hemi-boreal	Boreal
Dominating species	Picea abies	Picea abies and Pinus sylvestris	Picea abies and Pinus sylvestris
Mean tree height	19 m	25 m	20 m
Mean tree age	35 years	120 years	100 years
Ground vegetation	Mainly mosses.	Shrub layer is dominant.	Shrub layer is dominant.
Soil	Sandy till surrounded by glaciofluvial sediments.	Sandy-loamy tills with a with a thin organic layer on top. The area is rich in organic soils with surface peat cover and fens.	Moraine of various thicknesses.
Mean annual temperature	7.0 °C	5.6 °C	1.8 °C
Mean annual precipitation	830 mm	544 mm	614 mm

3.2.1 Map over study areas

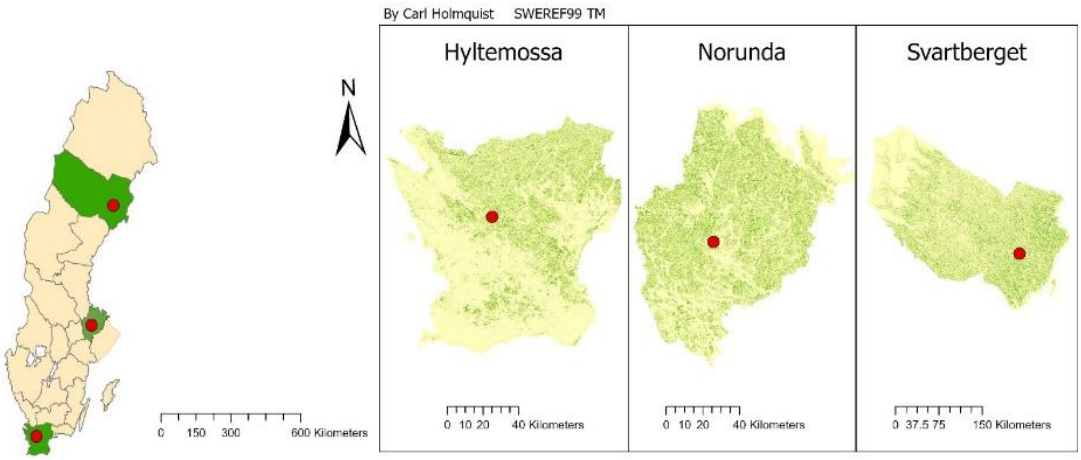

FIGURE 5: *Map of the study areas all located in Sweden. Green areas represent forest. (shapefiles obtained from Skogstyrelsen).*

3.3 Model inputs

LPJ-GUESS (hydraulic and standard version) was forced by (Climate Research Unit – Japanese Reanalysis) CRU-JRA (Friedlingstein et al., 2020) climate, CO_2, and N input data, spanning 2010-2019. A 500-year model-spin up was done to reach an initial equilibrium with respect to carbon pools and vegetation cover (Sitch et al., 2003). For this, the ten-year climate period was repeated. Inputs of temperature, precipitation, relative humidity, wind speed and short-wave radiation flux were from

Friedlingstein et al. (2020). The soil data was from the WISE dataset (Batjes 2009). Atmospheric nitrogen (N) deposition was from Lamarque et al. (2013).

3.4 Observational data

The observations used for validation of the output are taken from ICOS/FLUXNET. Data was available for the three Swedish sites covering the years 2014-2020 and 2015-2020 for HTM. Daily data of GPP (KgC m^{-2} day^{-1}) and latent heat (LE) (W/m^2) is taken and converted to monthly. A latent heat (LE) value corrected by an energy balance closure correction factor was taken for observation data (see Appendix A6). GPP was partitioned by the daytime (DT) and nighttime (NT) methods and filtered by a variable ustar threshold (VUT) and a constant ustar threshold (CUT) (Pastorello et al. 2020). For the NT method, ecosystem respiration (Reco) was estimated and GPP is estimated by the difference between NEE and Reco. For the DT method, GPP was estimated from incoming shortwave radiation. This may be more in agreement with how models such as LPJ-GUESS estimate GPP and thus better motivated to understand the differences between observation and models (Pastorello et al. 2020). VUT may be more unstable between years, while CUT has the advantage of being more realistic if there have been changes in the area, e.g., the height of trees (Pastorello et al. 2020). VUT and DT are chosen to validate model output. The uncertainty in the observations was calculated using the standard error for GPP and joint uncertainty for ET (more details see appendix A9).

3.5 Model set-up

Both LPJ-GUESS and LPJ-GUESS-HYD were run in cohort vegetation mode, which means that all individual trees belonging to the same age class and identical species/PFT (and PWS) are represented by an average individual. Cohort mode distinguishes age classes and patches, and vegetation is more detailed compared with population mode. New cohorts can grow and establish in a patch depending on when the climatic conditions are within species-prescribed bioclimate limits, and established cohorts can compete for light (PAR), water and even soil nitrogen (Smith et al. 2001; Smith et al. 2014).

A default run for both model versions was first done as described above. The number of patches was set to 50, which creates more stable simulations. The patches are assumed to be identical in terms of soil type and climate. The patch area was set to 1000 m^2. The species used in this study; spruce (Picea abies), pine (Pinus sylvestris) and birch (Betula pendula) were chosen because they are the three most dominant tree species at the sites modelled in this thesis. PFT settings were based on previous species-adopted values parametrized from the European version of LPJ-GUESS (see Hickler 2012: appendix S1). Birch was adopted from the shade-intolerant broadleaved summer green tree (IBS), spruce was from the shade-intolerant broadleaved summer green tree (BNE) and pine is from the intermediate shade tolerant boreal needle leaved tree (BNE). Water uptake was based on root distribution from fifteen soil layers. Root distribution across the soil profile is an array containing a fraction of roots in each of the soil layers. The root distribution was the same for all tree species used in this study (0.6 in the upper five layers and 0.4 in the lower layers). For more information on settings for the rest of the parameters (see Appendix table A1).

3.6 LPJ-GUESS-HYD parameters

LPJ-GUESS-HYD uses a range of hydraulic related functional traits that can be adjusted by the user (see model description section for detailed explanation). PWS are thus added to the original PFT/Species traits (see table 2 for detailed descriptions of each parameter). More parameters are included in the model at a static default value (see appendix fig. 1A). This study evaluates changes to λ, Ks_{max}, b, ψ_{50}, d and λmax (parameters also represented in the standard version of LPJ-GUESS). Kr_{max} and Kl_{max} was set by default and not changed.

TABLE 2: *PWS hydraulic parameters in LPJ-GUESS-HYD. λmax is previously used in the standard model. Used is referred to if the parameter is used/changed in the sensitivity test and the calibration.*

Parameters/Traits description	Abbreviations	Units	Used
Isohydricity is the stomatal behaviour *of the plant (Papastefanou et al. 2020).*	λ	-	YES
The water potential under non-water-stressed condition or the difference of $\psi_s - \psi_L$ *under non-stress conditions* ($\psi_s \approx 0$) *(Papastefanou et al. 2020).*	$\Delta\psi_{max}$	MPa	YES
Cavitation slope	d	-	YES
Water potential where 50% of xylem conductivity are lost (Papastefanou et al. in review).	ψ_{50}	MPa	YES
Max specific sapwood conductivity (Papastefanou et al. in review).	Ks_{max}	$kg\ m^{-1}\ s^{-1}\ MPa^{-1}$	YES
Max specific root conductivity (Papastefanou et al. in review).	Kr_{max}	$s^{-1}\ MPa^{-1}$	NO
Max specific leaf conductivity (Papastefanou et al. in review).	Kl_{max}	$mmol\ m^{-2}\ s^{-1}\ MPa^{-1}$	NO
The proportion of resistance located below ground and above ground (Fisher et al.2006).	b	-	YES
λ_{max} *is the ratio pa is the ratio of intercellular to ambient* CO_2 *partial pressures (Sitch et al. 2003).*	λ_{max}	-	YES

3.7 Parameter calibration

The default parameter values for the model tested against the observation data from FLUXNET gave an underestimation of ET for all sites. To obtain a better calibration result for both ET and GPP with lower RRMSE a trade-off between overestimated GPP and underestimated ET was needed. The default values represent the median values of each parameter recorded in the TRY (2022) database.

Therefore, a calibration process was needed before setting up the sensitivity test. The aim was to find a new nominal parameter (reference point) setting which results in a better agreement with the observation data. Plant water-regulation parameters (PWS) are chosen for calibration and sensitivity tests in regard to regulating the outputs ET and GPP in different environments. For instance, regulates isohydricity (λ) leaf water potential (ψL) in drier conditions which in turn regulates ET at the end. The parameters have never been tested for this Swedish site before and are therefore important to evaluate. Due to time limitations and range uncertainty, leaf- and root hydraulic conductivity was not changed in this study (see appendix table A1 for values).

For calibrating parameters, LPJ-GUESS-HYD was run multiple times (6 runs per parameter repeated for all species) with different sets of parameters, with a stepwise process. In total 7 parameters were changed from max to min and four of them (λ, $Ksmax$, $\Delta\psi_{max}$, Ψ_{50}) are new parameters included in the new model LPJ-GUESS-HYD (see table 3). The parameters are chosen because their impacts on ET and GPP. For example, λ reflects the trees water potential regulation mechanism, 1 represents no change in (ψL) and -0.3 the most change in (ψL) when the soil dries (Papastefanou et al. 2020). The value range for the rest of the parameters was set by the TRY database and are max and min recorded for tree species.

The first step was to calibrate the PWS parameters for spruce (see table 3). Since spruce was the dominated species for all three sites, it was crucial to get accuracy values compared to the observations. The second and third step, a calibration process was done with the same PWS parameters for pine and birch. A model comparison to the observational data for the years ranging from 2014-2018 (2015-2018 for HTM) was used for evaluation. For SVB observational data for year 2017, was missing and therefore removed to not impact the calibration. Root mean square error (RMSE) was stated in the same units of the original observation/model values. When two different model outputs RMSE needed to be compared, a metric with the same unit was preferred. So, for comparison with observational data a statistical test was done using relative root mean error (RRMSE) (see the section below). RRMSE was used to be able to compare output values with different units. ET with mm/year and GPP with KgC m^{-2} $year^{-1}$ converted to a relative unit (%). To find the lowest mean RRMSE, an aggregation was done using the outputs (GPP and ET), and all the sites. RRMSE is a metric Papastefanou et al. (2020) used to calibrate the parameters pairs $\lambda/\Delta\psi_{max}$. A benefit to use the mean RRMSE for both outputs ET and GPP can be that they are treated equally when choosing the lowest mean RRMSE. Isohydricity for spruce and pine ranges from 0.5 to 1.0 because needle-leaves are often classified to have a more isohydric drought strategy (Papastefanou et al 2020 supplementary, Tomasella et al. 2017) and from -0.3 to 0.5 for birch (Papastefanou et al 2020 supplementary). For each step, the best parameter values were taken with the lowest mean RRMSE when comparing observed and modelled ET and GPP.

The lowest mean RRMSE (%) aggregated using all sites and model outputs (GPP+ET), from each parameter range (6 runs/row) was taken to the next row with 6 new runs. For each PFT (6 * 7) 42 runs were made. One cell in table 3 represent one change in one parameter for one PFT. If the default value resulted in the lowest RRMSE this value was taken.

TABLE 3: *Parameter values used in the stepwise calibration process. Values varies from max to min species trait/parameter value ranges from the TRY database (except for λ and λmax).*

	Parameter	*Default*	*Calibration values / Run number*					
			Run1	Run 2	Run 3	Run 4	Run 5	Run 6
Step 1: Spruce	$\boldsymbol{\lambda}$	0.565	0.5	0.6	0.7	0.8	0.9	1.0
	$\boldsymbol{kS_{max}}$	0.57	0.195	2.094	3.993	5.892	7.791	9.690
	$\boldsymbol{\Delta\psi_{max}}$	0.7816	0.425	0.600	0.776	0.951	1.127	1.302
	$\boldsymbol{\psi_{50}}$	-3.68	-1.885	-3.050	-4.215	-5.380	-6.545	-7.710
	$\boldsymbol{d}$	-11.1929	-2.5	-7.09	-11.68	-16.27	-20.86	-25.85
	$\boldsymbol{b}$	0.5	0.1	0.26	0.42	0.58	0.74	0.9
	$\boldsymbol{\lambda_{max}}$	0.8	0.8	0.838	0.876	0.914	0.952	0.999
Step 2: Pine	$\boldsymbol{\lambda}$	0.442	0.5	0.6	0.7	0.8	0.9	1.0
	$\boldsymbol{kS_{max}}$	0.445	0.195	2.094	3.993	5.892	7.791	9.690
	$\boldsymbol{\Delta\psi_{max}}$	1.1237	0.425	0.600	0.776	0.951	1.127	1.302
	$\boldsymbol{\psi_{50}}$	-3.19	-1.885	-3.050	-4.215	-5.380	-6.545	-7.710
	$\boldsymbol{d}$	-4.7462	-2.5	-7.09	-11.68	-16.27	-20.86	-25.85
	$\boldsymbol{b}$	0.5	0.1	0.26	0.42	0.58	0.74	0.9
	$\boldsymbol{\lambda_{max}}$	0.8	0.8	0.838	0.876	0.914	0.952	0.999
Step 3: Birch	$\boldsymbol{\lambda}$	0.358	-0.3	-0.1	0.1	0.3	0.5	0.7
	$\boldsymbol{kS_{max}}$	3.07	1.320	2.552	3.784	5.016	6.248	7.480
	$\boldsymbol{\Delta\psi_{max}}$	1.1385	0.5436	0.8529	1.1624	1.4717	1.7811	2.0905

ψ_{50}	-2.05	-1.885	-3.050	-4.215	-5.380	-6.545	-7.710
d	-18.2276	-2.5	-7.09	-11.68	-16.27	-20.86	-25.85
b	0.5	0.1	0.26	0.42	0.58	0.74	0.9
λ_{max}	0.8	0.8	0.838	0.876	0.914	0.952	0.999

3.7.1 Statistical analysis

To determine the model runs with the lowest error the relative root mean square error (RRMSE) metric was used. All years that overlapped with the period of the observation data from FLUXNET are taken in a statistical analysis, spanning 2014-2019 for NOR and SVB and 2015-2019 for HTM. In addition, monthly values for the variables gross primary production (GPP) and evapotranspiration (ET) from the model are compared to observational data. For evaluating the time-series accuracy, RRMSE (%) are calculated by:

$$RRMSE = \frac{\left(\sqrt{\sum_{i=1}^{N}(Predicted_i - Actual_i)^2}\right)}{\sum_{i=1}^{N}(Actual_i)} * 100 \quad (21)$$

where $Predicted_i$ are the ith value from the model, $Actual_i$ are the ith value from the observation data, and N is the number of data points.

The mean RRMSE of GPP and ET for all sites (HTM, NOR and SVB), was calculated by taking the RRMSE to mean for all sites, for GPP and then the same for ET. Then an overall RRMSE mean was aggregated using all sites and model outputs (GPP+ET). The lowest mean RRMSE was taken for each parameter that was changed from its lowest to its highest value. So, the lowest mean RRMSE from each varied parameter was chosen in each table row in table 3. If one calibrated value in table 3 gave a higher mean RRMSE, the default value was taken to the next row of parameters.

3.7.2 Calibrated model and observation comparison

To be able to visualize the monthly change of ET and GPP, time-series are used to see how the calibrated, the non-calibrated (default) hydraulic model, and the standard model relate to the observations. The first calibrated model was further compared to the observation using a *fit metric* related to a 1:1 reference line when the model is in perfect agreement with the observations. From the *fit metric* value of 1 indicates that the model perfectly fits the observations and 0 indicates no fit to the observations. A *fit metric* can be used to calculate goodness to fit or how well the model predicts the output against the observation (Turney 2022). The benefit to use residuals to 1:1 line was that the calculation was based on the 1:1 line and not the regression line, that may overestimate the result. The mean bias of the model was calculated to estimate the tendency for the simulated values of ET and GPP to underestimate or overestimate the corresponding model values (Smith & Smith 2007).

The mean bias in the difference was calculated by (Smith & Smith 2007):

$$mean\ bias = \sum_{i=0}^{N}\left(\frac{Actual_i - Predicted_i}{N}\right) \quad (22)$$

where, $actual_i$ is the ith measured value, $predicted_i$ is the ith simulated value, and N is the total number of values being compared.

The *fit metric* was denoted by (Turney 2022):

$$fit\ metric = 1 - \frac{\sum_{i=0}^{N}(Predicted_i - Actual_i)^2}{\sum_{i=0}^{N}(Predicted_i)^2} \quad (23)$$

where, $actual_i$ is the ith measured value, $predicted_i$ is the ith simulated value, and N is the total number of values being compared.

3.8 Sensitivity test

In order to assess the sensitivity of ET and GPP to various hydraulic and non-hydraulic parameters at the Swedish sites, a sensitivity analysis was done. Sensitivity analysis (SA) is a study of the relative important of each input or parameter in determining the variability of output. SA can be divided into global and local methods (Hamby 1994, Smith & Smith 2007). A local SA is often referred to a One At a Time (OAT) method (Smith & Smith 2007). OAT is a common approach what the name refers to, thus, to changing one factor at a time and keep the other factors fixed to a default value (Smith & Smith 2007). In this study a SA to hydraulic traits was performed on LPJ-GUESS-HYD (see table 3 for hydraulic traits values). Every parameter was changed from its nominal value, with a change of 2.5-20% steps around the nominal value. The nominal value was taken from the first calibration referring to the best parameter value creating the lowest mean RRMSE. The steps of the percent change of each parameter depend on the range of each parameter. λmax with the smallest range was changed by 2.5% around the nominal value, λ was changed by 20%, Ks_{max} was changed by 10%, $\Delta\psi_{max}$ was changed by 10%, d was changed by 20%, b was changed by 10% and ψ_{50} was changed by 10% around the nominal value. In the first sensitivity test, only parameters for spruce are changed and the birch and pine were static at the nominal values. The second sensitivity test using the same change settings but without birch and pine is described below.

The sensitivity was expressed through an actual yearly mean change of ET and GPP against the percent change of each parameter, consolidated to show many parameters variables on one chart. This type of consolidated chart is called a spider plot. At the centre of the spider plot is the nominal value of the parameter. The yearly mean change was taken from the simulation years (2014-2019).

3.8.1 Second calibration

A second calibration was based on the same metric as the first calibration. It was done to further try to improve the hydraulic model related to the first question, if the hydraulic model version can be improved. A mean RRMSE of GPP and ET are calculated by using the same parameter values used in the sensitivity test. The most sensitive parameters and parameters that most likely could be used to improve the model further which means lower mean RRMSE, aggregated using all sites and model outputs (GPP+ET).

3.8.1 Competition effect

When all species (Spruce, Pine and Birch) are included a competition effect may influence each species' survival, depending on shade tolerant classes (see appendix, table A2). The shading classes are based on minimum light (PAR) to grow and establish, and grow efficiency and maximum establish the rate. The competition may affect below ground referring to available soil water. The competition effect in turn may also influence the parameter sensitivity test. To avoid competition and to see its effect, spruce was run in isolation and a second sensitivity test with the same parameter change was done. The monthly mean change of ET and GPP with changed parameter values with only spruce and the same but with all species included could then be compared.

4 Results

4.1 Parameter calibration:

A1: Spruce parameter values

Parameters	run1	run2	run3	run4	run5	run6	default
λ	0.5	0.6	0.7	0.8	0.9	1	0.565
ksmax	0.195	2.094	3.993	5.892	7.791	9.69	0.57
ΔΨ_max	0.425	0.6	0.776	0.951	1.127	1.302	0.782
Ψ_50	-1.885	-3.05	-4.215	-5.38	-6.545	-7.71	-3.68
d	-2.5	-7.09	-11.68	-16.27	-20.86	-25.85	-11.193
b	0.1	0.26	0.42	0.58	0.74	0.9	0.5
λmax	0.8	0.876	0.838	0.914	0.952	0.999	0.8

Runs

A2: Spruce mean RRMSE

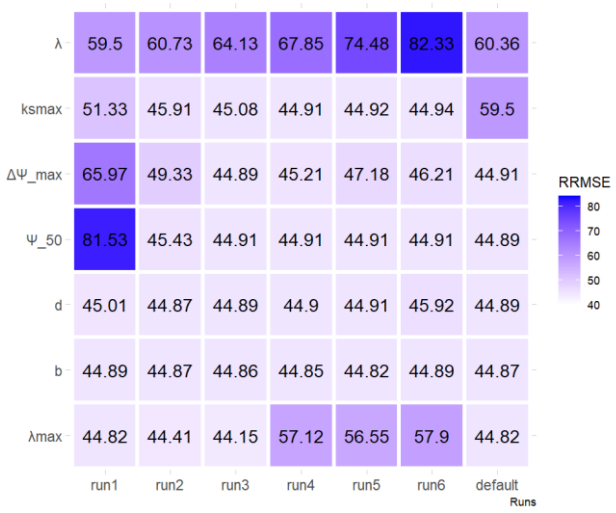

B1: Pine parameter values

Parameters	run1	run2	run3	run4	run5	run6	default
λ	0.5	0.6	0.7	0.8	0.9	1	0.442
ksmax	0.195	2.094	3.993	5.892	7.791	9.69	0.445
ΔΨ_max	0.425	0.6	0.776	0.951	1.127	1.302	1.1237
Ψ_50	-1.885	-3.05	-4.215	-5.38	-6.545	-7.71	-3.19
d	-2.5	-7.09	-11.68	-16.27	-20.86	-25.85	-4.7462
b	0.1	0.26	0.42	0.58	0.74	0.9	0.5
λmax	0.8	0.876	0.838	0.914	0.952	0.999	0.8

Runs

B2: Pine mean RRMSE

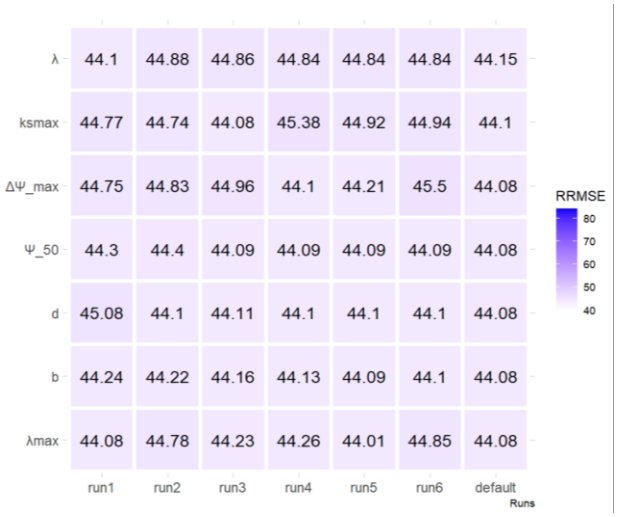

C1: Birch parameter values

C2: Birch mean RRMSE

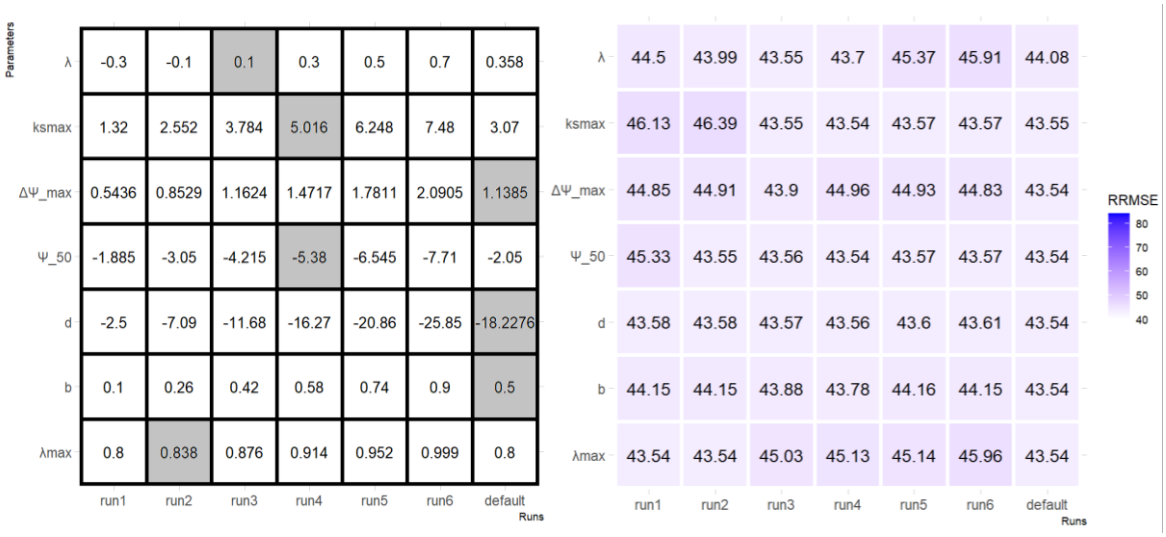

FIGURE 6: A1, B1 and C1: *Spruce, pine and birch parameter values are tested from run 1 to run 6. The grey boxes represent the chosen parameter value with the corresponding lowest mean RRMSE in the colored heat map (A2, B2 and C2) used for the next parameter row.* ***A2, B2 and C2:*** *Mean RRMSE (%) was aggregated using all sites and model outputs (GPP+ET). Rows are tested parameters, columns are the runs and the values represent the RRMSE of the modelled data in relation to the observed data, with parameter combinations reported in A1, B1 and C2. The parameter combinations that lead to the lowest mean RRMSE were taken from each row (corrsponding to the grey boxes), starting with λ (top-left) for spruce (A2) and ending with λmax (C2) (down-right) for birch. The lowest mean RRMSE per row should decrease as you go down the rows, starting with λ for run 1. Default means no change of the parameter (initial state).*

To answer the first research question**,** a parameter calibration was done. After the first calibration, new settings of parameter values represent the lowest mean RRMSE. The best parameter settings for all species are presented in table 4 and are related to fig. 6 with the lowest mean RRMSE when all sites and species are included in the RRMSE calculation. The lowest mean RRMSE was taken for each run; 1-6 and the run with default parameter values starting from run 1, λ (top-left) to run 6 in fig. 6 A2. The grey boxes in fig.6 A1 represent the chosen values that correspond to the lowest mean RRMSE. The calibration was an iterative process that results in a decreasing mean RRMSE starting with spruce and ending with birch. So, the parameter sets with the lowest mean RRMSE progressively feed into each new iteration. For each species 42 (6*7) runs were made. One cell in fig. 6 represents one parameter change for one species. If the default value resulted in the lowest mean RRMSE this value was taken. The calibration starts with the most dominant tree, which was spruce. After the calibration with all parameters the model was found to perform best for birch in SVB, with a mean RRMSE of 43.54%. The most dominant species spruce results in the greatest change in mean RRMSE because of the high biomass of spruce. Spruce dominates over birch and pine because spruce outcompetes the other species for light, space, and water. Thus, the mean RRMSE change was low for birch and pine because of the strong competition effect (see fig. 6). Spruce was dominant for all sites (74% HTM, 85% NOR and 98% SVB of carbon mass) and thus contributes to the greatest change of ET and GPP when parameters are changed.

Table 4 represents the best parameter values with the lowest mean RRMSE. Spruce results in parameter changes for λ, kS_{max}, $\Delta\psi_{max}$, d, b and λmax. Only ψ_{50} was not changed because the default value gives a slightly lower mean RRMSE (see fig. 6A). The calibration values for spruce results in the lowest λ of 0.5, higher kS_{max} than the default, a slightly lower $\Delta\psi_{max}$, a lower cavitation slope (d), a higher b value and a higher λmax. Calibrated parameters for spruce are used in the sensitivity test. Due to an error, the default value of 0.565 for λ was used instead in the sensitivity test. The default parameter values for pine and birch gives the lowest RRMSE.

TABLE 4: *The best parameter values from the calibration compared to the default value. The calibrated value for spruce was used as a nominal value in the sensitivity test.*

Parameter	PFT					
	Spruce (Calibrated)	**Spruce (Default)**	**Pine (Calibrated)**	**Pine (Default)**	**Birch (Calibrated)**	**Birch (Default)**
$\boldsymbol{\lambda}$	0.5	0.565	0.50	0.442	0.1	0.358
$\boldsymbol{kS_{max}}$	5.892	0.57	3.993	0.445	5.016	3.07
$\boldsymbol{\Delta\psi_{max}}$	0.776	0.7816	1.1237	1.1237	1.1385	1.1385
$\boldsymbol{\psi_{50}}$	-3.68	-3.68	-3.19	-3.19	-5.380	-2.05
d	-7.09	-11.1929	-4.7462	-4.7462	-18.2276	-18.2276
b	0.74	0.5	0.5	0.5	0.5	0.5
$\boldsymbol{\lambda max}$	0.876	0.8	0.8	0.8	0.838	0.8

4.2 Calibrated, default and standard model

4.2.1 Time-series of GPP and ET

To evaluate and compare the outputs from the hydraulic model before and after calibration to observed data from FLUXNET, time-series were done for ET and GPP. Fig. 7-8 shows the model result before and after the calibration process with the overall lowest mean RRMSE for each site when comparing the model with the observed data. The mean combined RRMSE (ET + GPP) for the default runs was 59.53%. The calibration improves the model by decreasing the mean RRMSE by 16%. This was mostly due to increased ET for the calibrated model compared to the default model, which results in a lower mean RRMSE of 50.21%, (table 6) for ET (see table 5-6 for site-specific RRMSE). The default model gives a large underestimation of the model ET (table 6, fig. 8), which was most clear for SVB. However, the default model performs better than the calibrated model for GPP at HTM and NOR, with lower mean GPP RRMSE (table 5, fig. 7).

After the calibration, the site HTM shows the lowest combined output mean RRMSE (38.76%) for ET and GPP. If only one output (ET or GPP) was compared with the observation, site SVB shows the lowest GPP RRMSE (31.93%) result after the calibration, and site HTM shows the lowest RRMSE (34.12%) for ET (see table 5-6). After the calibration of the parameters, the model slightly overestimates GPP for HTM and NOR (see table 5 and fig. 7), but at the same time, it underestimates ET for all sites (see table 6, fig. 8). However, the calibrated model outperforms the default model, and does not underestimate ET as strongly, so the overall calibrated mean RRMSE result was lower. The site SVB shows the largest decrease in mean RRMSE for GPP from the default to calibrated model (82.62% - 31.93 %).

The LPJ-GUESS standard model gives a mean combined RRMSE for ET and GPP at 39.76%, which indicates a slightly lower mean RRMSE than the calibrated hydraulic version. The standard version predicted ET much better than the hydraulic version (see table 6), due to lower RRMSE for all sites and especially for SVB. According to Li et al. (2013), model accuracy was considered excellent when RRMSE <10%, good if RRMSE was between 10% - 20%, fair if RRMSE was between 20-30% and poor if RRMSE was bigger than 30%. The lowest mean RRMSE (%) aggregated using all sites and model outputs (GPP+ET) of 43.54% was then still a poor representation of the observed values. Even the standard model the mean RRMSE of 39.76% was a poor representation of GPP. However, the standard model the mean RRMSE for ET and the default hydraulic model the mean RRMSE of GPP are a fair representation the of observation flux.

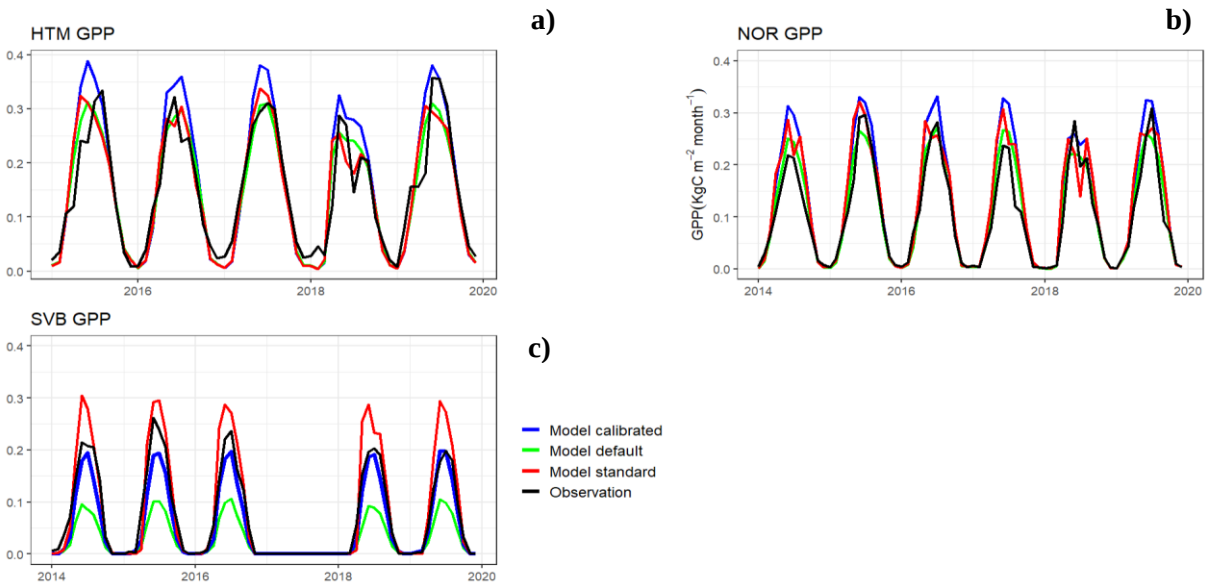

FIGURE 7: *Monthly timeseries comparison over GPP for a) HTM, b) NOR and c) SVB with observation, LPJ-GUESS-HYD: (model default, model calibrated) and LPJ-GUESS: (standard model). No data for observation for year 2017 SVB.*

TABLE 5: *GPP RRMSE (%) values for each site and model version.*

GPP	RRMSE HTM	RRMSE NOR	RRMSE SVB	Mean RRMSE
Calibrated	43.41	35.24	31.93	36.86
Default	23.32	24.87	82.62	43.60
Standard	41.42	29.47	48.37	39.76

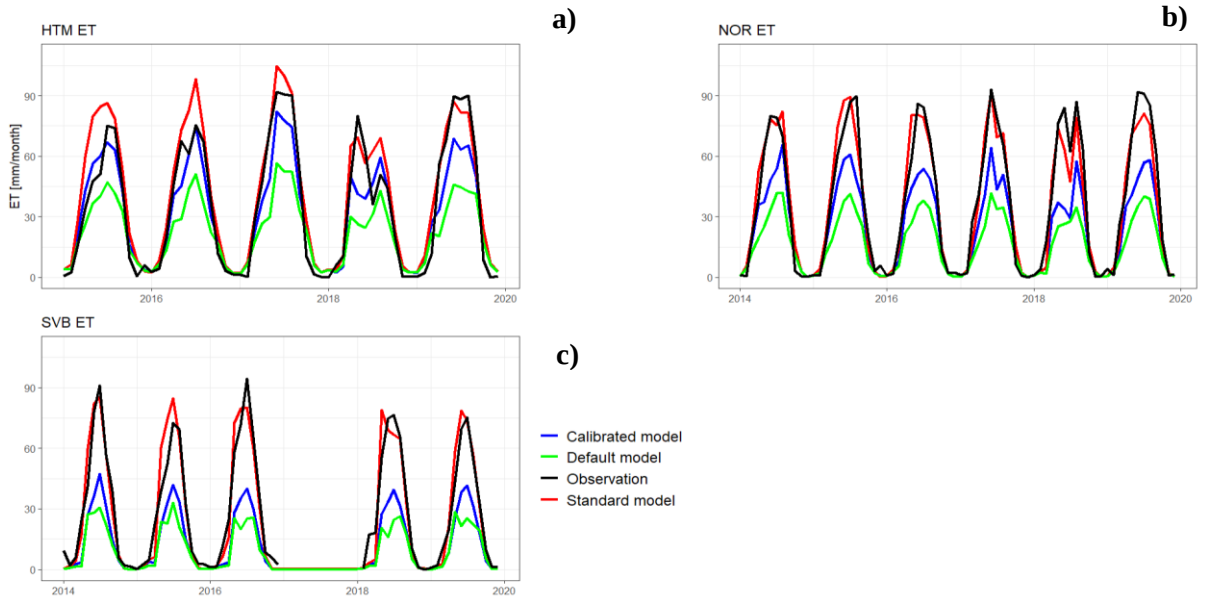

FIGURE 8: *Monthly timeseries comparison over ET for a) HTM, b) NOR and c) SVB with observation, LPJ-GUESS-HYD: (default model, calibrated model) and LPJ-GUESS: (standard model). No data for observation for year 2017 SVB.*

TABLE 6: *ET RRMSE (%) values for each site and model version.*

ET	RRMSE HTM	RRMSE NOR	RRMSE SVB	Mean RRMSE

Calibrated	34.12	46.50	70.05	50.21
Default	61.90	76.53	92.86	77.10
Standard	22.21	32.98	29.14	28.11

4.2.2 Calibrated model and observation linear regression

a) ET:

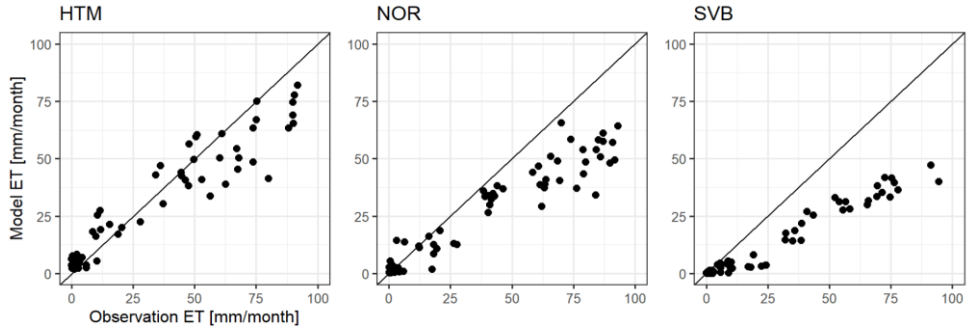

b) GPP:

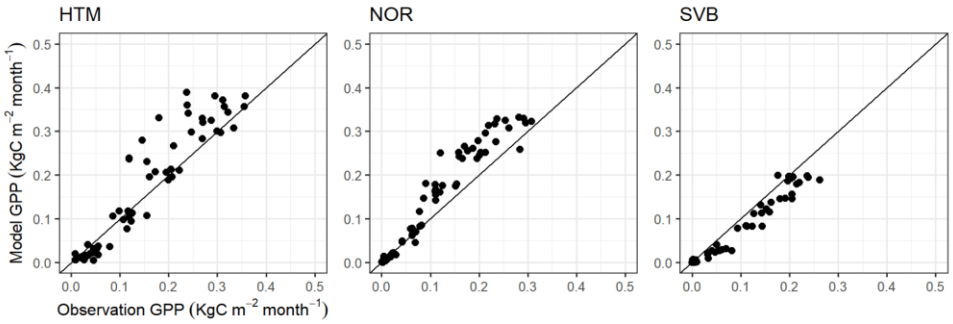

FIGURE 9. *Modelled (calibrated values) and observed a) ET and b) GPP for the tree sites. The solid line represents 1:1 line (perfect agreement).*

The linear regression analysis to 1:1 line with the calibrated data set revealed a highly significant relationship between modelled and observed ET and GPP values (Fig. 9). For ET, the best fit metric to the perfect agreement line (1:1) was 0.91 for HTM. HTM model shows the best association (trend) and lowest coincidence (difference) with observation. For ET, the mean bias of the model indicates an overall underestimation (mean bias, HTM: 3.27, NOR: 11.84, SVB: 14.96) of the model. SVB ET (fit metric: 0.039) shows the lowest agreement with observation. NOR ET (fit metric: 0.68) shows a higher agreement with the line (1:1) compared to SVB, but the underestimation of the model for almost every value, indicates a better association than coincidence (Fig. 9).

For GPP, the model against observed values results in an overall better agreement with the observation and low mean bias. HTM (fit metric: 0.93, mean bias: 0.017), NOR (fit metric: 0.94, mean bias: 0.028), and SVB (fit metric: 0.93, mean bias: 0.018) showed similar results for the coefficient of determination and mean bias (Fig. 9). Overall, the results show that the calibrated model performs better to predict GPP than ET.

4.3 Sensitivity test

To answer the second research question, a sensitivity test was done using 7 parameters. The calibration gave a more suitable reference point (nominal value) from which to start the sensitivity test. In the first sensitivity test all species/PFTs were included, but only the most dominated tree, and

spruce parameters were changed. Carbon mass, GPP and ET were too low for the two other tree species at all the tree sites, to be able to detect any changes from them with altered parameters.

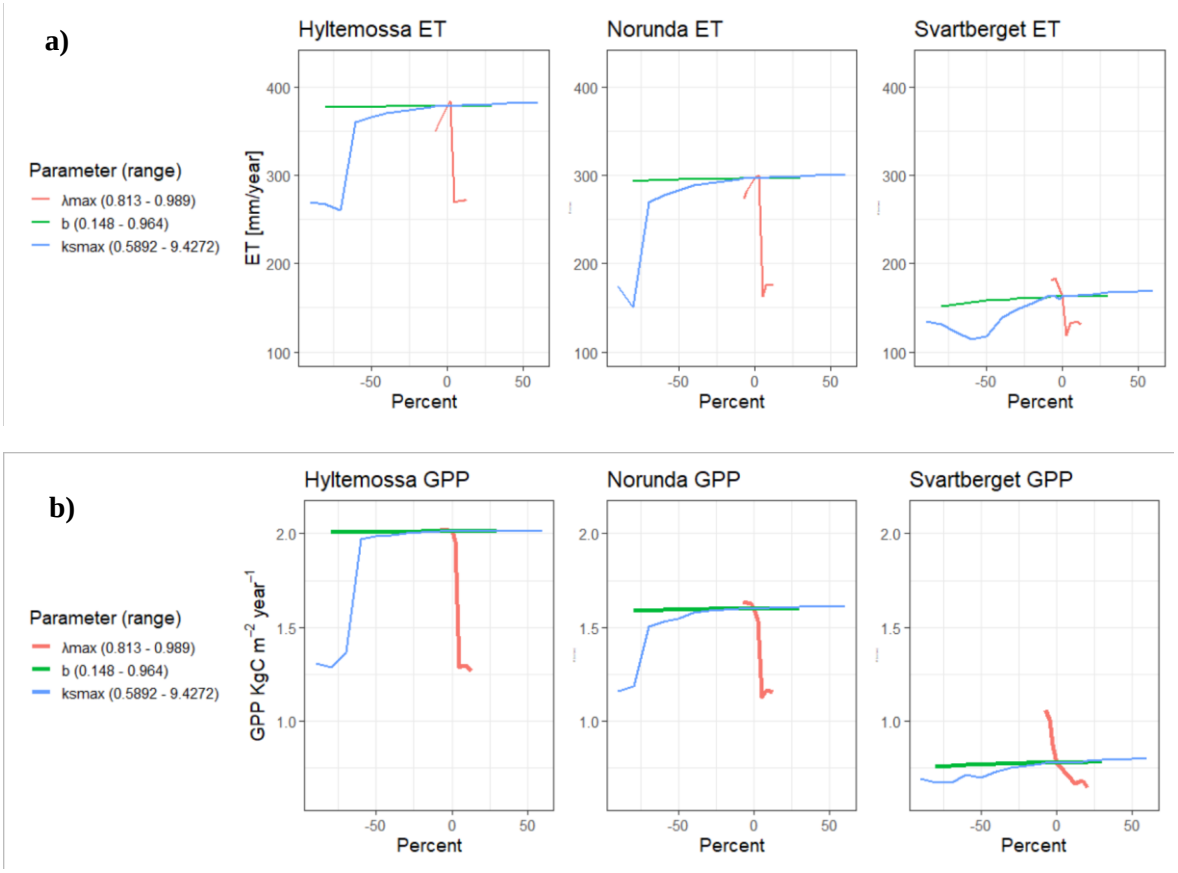

***FIGURE 10**: Percent change of three parameters effect on a) ET and b) GPP. Yearly average of the years (2014-2015). Only spruce was changed from its nominal value (0%). Nominal value for λmax was 0.8796, b was 0.5 and Ks_{max} was 5.892.*

The percentage parameters change from the nominal value and the corresponding yearly mean ET and GPP change (fig. 10-11), shows the sensitivity of each parameter. Only one parameter (for spruce) was changed each run in OAT sensitivity test and rest are set to constant values. The general pattern of change of the parameters in fig. 10 are similar for HTM and NOR. Lowest sensitivity from the nominal value was it for the parameter *b*. Ks_{max} shows a positive trend for GPP and ET with higher conductivity for the sapwood for spruce. λmax values higher than ~0.9 results in lower GPP and ET. General negative trend for higher λmax. For SVB the minimum λmax value resulted in the highest GPP and ET.

When the parameters $\Delta\Psi_{max}$, λ, Ψ_{50} and *d* are changed from each nominal value a reaction in ET and GPP was visible (fig. 11). Cavitation slope (*d*) shows a low sensitivity for both ET and GPP. Isohydricity (λ) values result in maximum values of GPP and ET around -50% to -100% (0-0.226) of the nominal value. Lower λ values than -0.133-0.133 result in lower ET and GPP at all sites, while the spruce-dominated forest at HTM tolerates more anisohydric behaviour with ET and GPP decreasing at lower anisohydric values than at the other sites. GPP and ET at HTM remains high above -120% of the nominal value, while both fluxes decrease at -100% and -80% at NOR and SVB, respectively. $\Delta\Psi_{max}$ (optimal forcing pressure to maintain max canopy conductance) shows a positive trend in ET and GPP over the range of the parameter. Ψ_{50} (water potential where 50% of xylem conductivity was lost) was reached at a threshold of -2.208 MPa where ET and GPP decreases in relatively wetter

conditions, while a Ψ_{50} of -7.36 MPa at the driest conditions does not negatively affect either flux. Therefore, Ψ_{50} was found to only be sensitive to high SWC. The threshold was reached first at SVB, where both fluxes decline at 0% of the nominal values, while the thresholds at NOR and HTM are both at 20%.

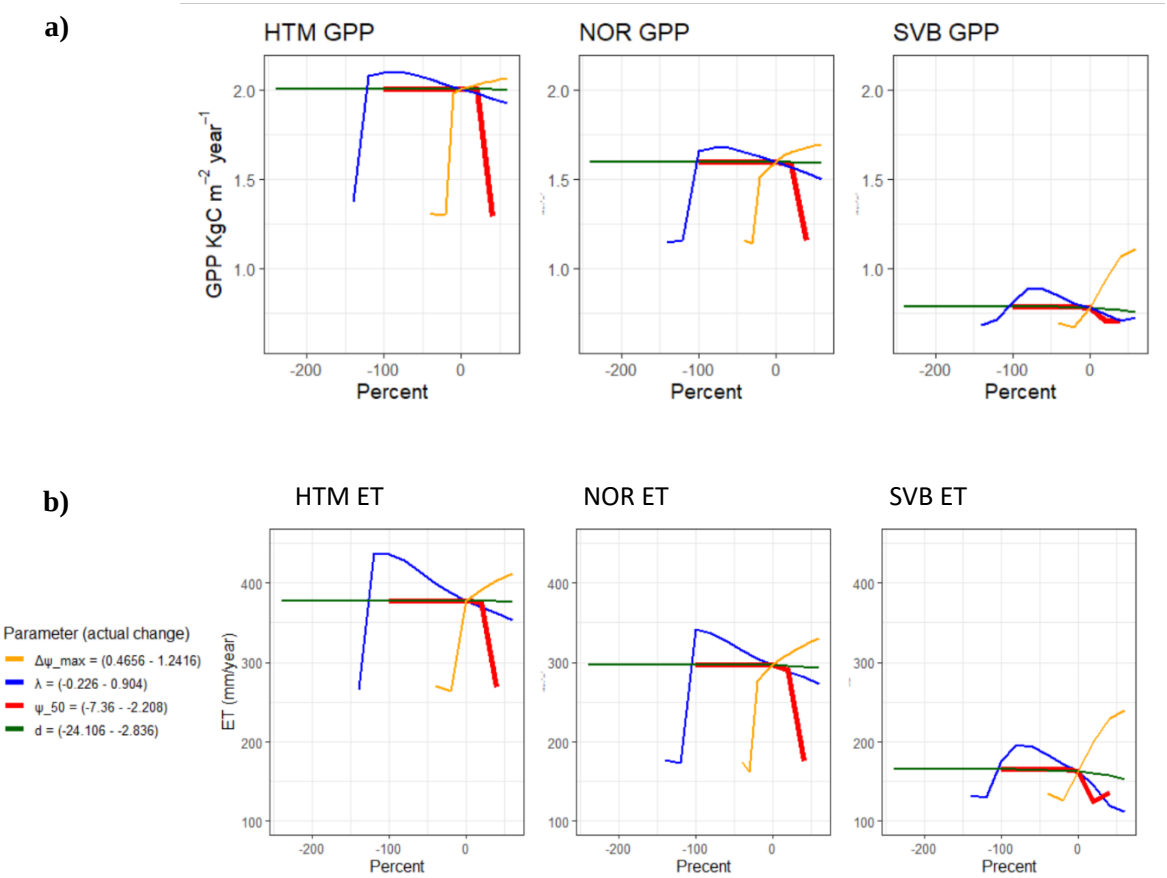

***FIGURE 11**: Percentual change of four parameters effect on a) GPP and b) ET. Yearly average of the years (2014-2015). Only spruce was changed from its nominal value (0%). Nominal value for $\Delta\Psi max$ was 0.776, λ was 0.565, Ψ_{50} was -3.68* and *d was -7.09*

4.4 Sensitivity for isohydrodynamic parameter (all PFT included):

A) GPP

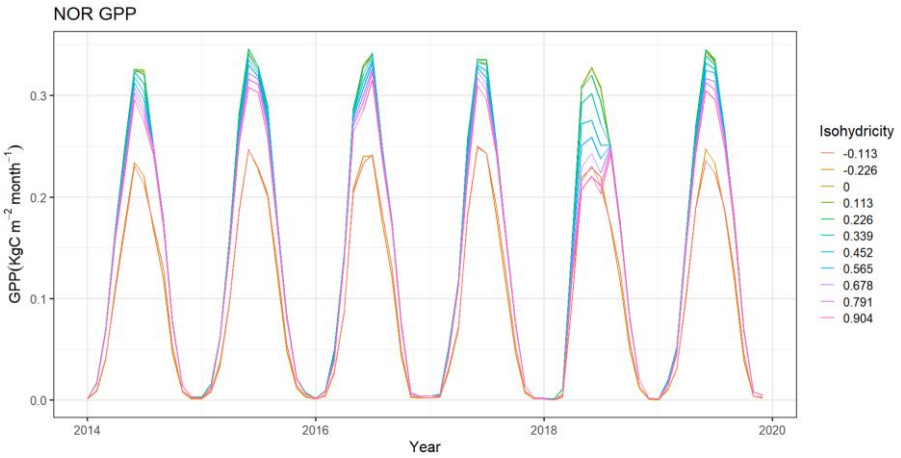

B) ET

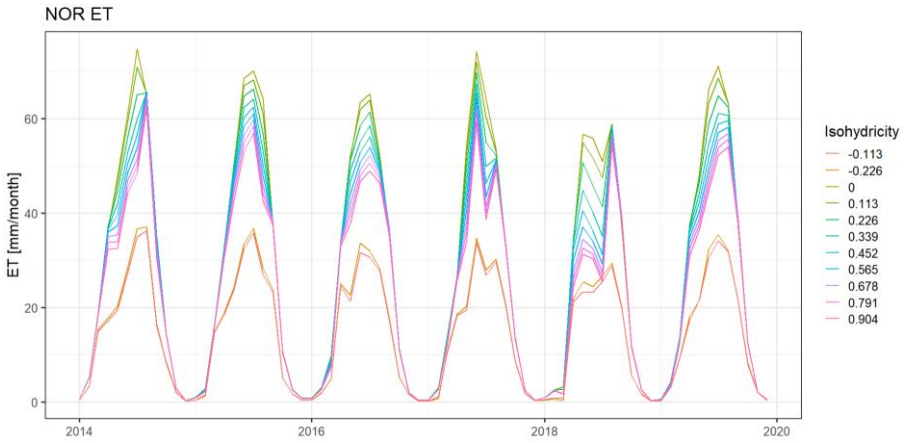

FIGURE 12. *Isohydricity spectra (λ) for NOR with a range of (-0.3 – 1); 1 meaning extreme isohydric behaviour and -0.3 extreme anisohydric behaviour. A) Seasonal GPP change with isohydric change. B) Seasonal ET change with isohydric change.*

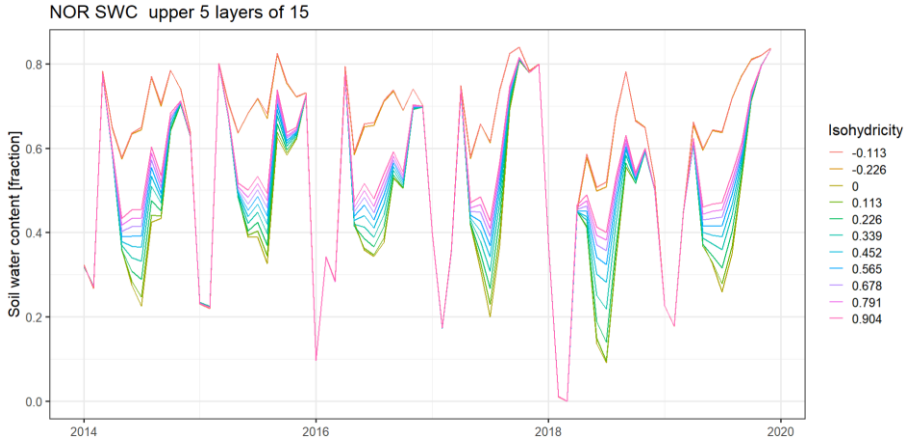

FIGURE 13. *Soil water content (SWC) for the isohydricity spectra (λ) for NOR with a range (-0.226 – 0.904); 1 meaning extreme isohydric behaviour and -0.3 extreme anisohydric behaviour.*

To further evaluate parameter sensitivity on a seasonal scale, the parameter λ was chosen. Instead of yearly mean ET and GPP used in the sensitivity test above, a monthly change of the fluxes depending on λ for the simulation period (2014-2020) was taken for the site NOR. Note that the same parameter range for λ was used in the yearly mean sensitivity test. A monthly sensitivity test (fig. 12) shows an increase in ET and GPP with more anisohydric behaviour. The largest magnitude of ET occurs at a λ of 0. The decrease of ET in the year 2018 (during the summer months) due to a drought event was apparent for λ between 0 – 0.904, with an earlier decline also evident at more isohydric SWC, which means that the leaf water potential was kept nearly constant with a closure of the stomata in drier soil. GPP correlates well with ET changes, but with some exceptions. For instance, GPP seems to not react strongly to severe SWC decreases. A constant leaf water potential under more negative soil water potentials associated with a λ of 1 and a lower canopy conductance led to overall lower transpiration. λ values of -0.133 - -0.226 led to lower ET, just like fig. 11 shows. This decline was due to lower transpiration rates for pine and birch, while spruce was more tolerant to lower SWC. Fig. 13 shows the monthly SWC along with the isohydricity spectra. SWC decreases during summer depending on the isohydricity values, and due to the transpiration rates. As in fig. 12, a chosen λ at 0 results in the lowest SWC due to the highest transpiration rate during the summer months. SWC and transpiration flux correlates depending on isohydricity. SWC drops in the winter months due to soil freezing.

4.5 Sensitivity test – competition effect

To be able to answer if competition effect the sensitivity a second sensitivity test was done with only spruce included. For the runs in which all PFTs (spruce, pine birch) are included, and only spruce parameters are changed, the competition effect by the other PFT/species can impact the sensitivity. To exclude the competition effect and compare the result with all PFT/species included, the model was run with only spruce included. From fig. A1 (see appendix) λ_{max} values higher than 0.8796, Ks_{max} values at 0.5892 and $\Delta\Psi_{max}$ values lower than 0.4656, spruce GPP was reduced to 0 and ET was reduced due to lower transpiration. Also, higher Ψ_{50} values create decreases in GPP and ET, although HTM spruce can tolerate even higher Ψ_{50} than the sensitivity range maximum. A comparison between the model runs with all PFTs included (fig. 1-2 see the result) and those with only spruce (fig. A1-A2 see appendix), shows that GPP decreases to 0 with a spruce monoculture forest, but other PFT/species takes over in a mixed forest. Less annual GPP/NPP leads to lower biomass and lower growth rate each year. In a monoculture forest the ET and GPP sensitivity along the parameter change was now directly linked to the parameter change and has no indirect effect on other PFT/species. The sensitivity when competition was included primarily impacts near the minimum and maximum (the edges) of the parameter range when the spruce PFT reaches a threshold for mortality. For NOR and HTM the competition effects influence ET and GPP as λ changes (compare fig 5-6 with fig. A1-A2 in appendix) to a more anisohydric behaviour. The spruce monoculture forest reaches higher ET and GPP at more anisohydric λ than with all species included and higher Ψ_{50} can be tolerated at HTM. For the monoculture forest a faster increase of ET and GPP with a higher Ks_{max} occurs than for the mixed forest. The monoculture forest at SVB generally shows higher ET and GPP fluxes than the mixed forest.

4.6 Second calibration

To further evaluate if the hydraulic model can be improved a second calibration was done. From the spider plots (fig. 10-11) it was clear that ET and GPP show a large sensitivity to λ and $\Delta\Psi_{max}$. To utilize the result in the sensitivity test, the same parameter values used in the sensitivity test are used in a second calibration. The second calibration was calculated using the metric RRMSE in relation to the observed data. A calibration was different from a sensitivity test in that it helps to show which parameter values bring the model closer to observed values. The site-specific calibration shows that SVB was mostly improved with a more anisohydric behaviour (λ) or a higher forcing pressure to maintain canopy conductance ($\Delta\Psi_{max}$) (see fig. A4-A5 in appendix).

4.6.1 All PFT RRMSE

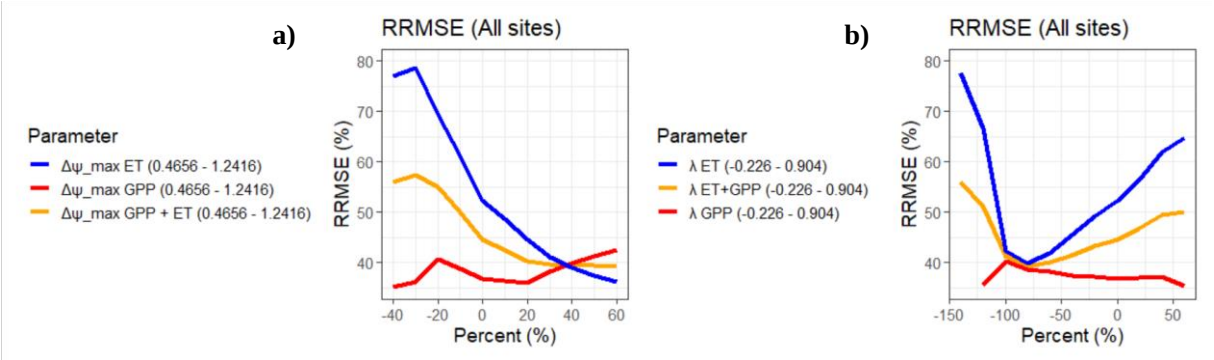

FIGURE 14: *The variation of the mean RRMSE for all sites against changed parameters a) $\Delta\Psi$ max, b) λ and the output ET and GPP. Yellow shows the mean RRMSE of both GPP and ET. 0% represents 0.565 for λ and 0.776 for $\Delta\Psi$ max.*

Fig. 14 shows the RRMSE variation against the changed parameters. The blue line shows the mean RRMSE in ET for all sites, red shows the mean RRMSE in GPP and yellow shows the combined mean in RRMSE for GPP and ET. The mean RRMSE from the nominal value can be improved by using 40-60% (1.086-1.2416) higher $\Delta\Psi_{max}$ or 80% (0.1) lower λ. Mean RRMSE in GPP was improved with more isohydric λ (higher λ than 0.5), while mean RRMSE in ET was improved with more anisohydric λ. Extreme anisohydric behaviour gives high combined mean RRMSE for all sites, which was also found by the sensitivity test (fig. 12 and fig. 11).

The calibration shows an overall lower RRMSE for higher $\Delta\Psi_{max}$ values, but GPP RRMSE increases with the parameter change. The trade-off between ET and GPP model accuracy was shown in yellow (see fig. 5A in the appendix). The site specific RRMSE for λ shows that the modelling of the SVB forest benefits the most from lower λ values (more anisohydric behaviour), with lower mean RRMSE for also both ET and GPP.

4.6.2 Spruce RRMSE

The same procedure was done but now with only spruce.

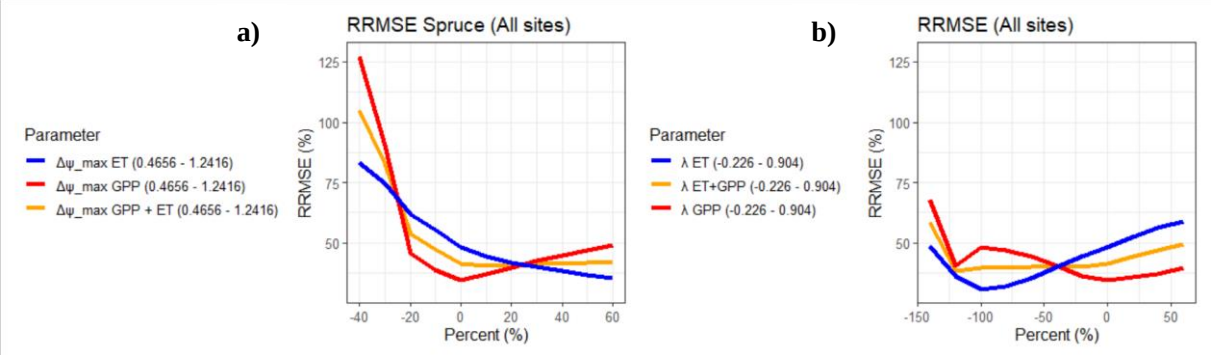

FIGURE 15: *The mean RRMSE for all sites variation against changed parameters a) $\Delta\Psi$ max, b) λ and the output ET and GPP. Yellow shows the mean RRMSE of both GPP and ET.*

When spruce was run in isolation (without the competition effect), the second calibration shows less improvement from the nominal value (0%). Fig. 15 shows that the accuracy of modelled ET can be improved with higher $\Delta\Psi_{max}$, although this also results in an overestimation of GPP and therefore higher mean RRMSE with higher $\Delta\Psi_{max}$ from the nominal value (0%). For both fig. 14-15, it was a trade-off between lower mean RRMSE for ET and higher mean RRMSE for GPP.

5 Discussion

5.1 Major findings

The aim of this study was to evaluate a new version of the dynamic global vegetation model LPJ-GUESS with an upgraded hydraulic implementation. Even though LPJ-GUESS-HYD includes an upgraded hydraulic architecture, it still underestimated ET for all three sites. The parameter calibration improved the hydraulic model`s performance in estimating ET and GPP compared with the observations, although the standard version modelled the fluxes with smaller mean RRMSE. One possible reason for the underestimation of ET by the hydraulic model was that the uptake of water from the soil was limited. The next section discusses this in more detail.

The OAT sensitivity test showed low sensitivity in the fluxes ET and GPP to the parameters *b* and *d*. By contrast, the fluxes showed high sensitivity to the parameters λ and $\Delta\psi_{max}$ for all sites. Generally,

ET and GPP showed sensitivity to all parameters that may cause hydraulic failure or carbon starvation (Ks_{max}, λ, ψ_{50}, λ_{max} *and* $\Delta\psi_{max}$).

5.2 Uncertainties in the FLUXNET observations

The calibration is based on the assumption that the flux data observations are correct, but the flux data is generally noisy, and uncertainties can be largely due to random measurement error (Hollinger & Richardson 2005). It is important to have knowledge of uncertainties in the observations, for statistical evaluation of measured and modelled fluxes. The knowledge of the measurement's uncertainty is vital to determine if the model can be accepted or rejected with some level of confidence. In this study water and carbon fluxes from the hydraulic model are evaluated against the FLUXNET observation data from ICOS.

The estimation of uncertainty can be quantified in several ways, and a common way is through standard error. In this study GPP was estimated through a daytime partitioning method Lasslop et al. (2009). GPP flux is estimated from incoming shortwave radiation (Pastorello et al. 2020). Standard Error for GPP see appendix, eq. 4. A more detail description the uncertainty estimation can divide into random error (RE) (stochastic or instrumental) and systematic error (SE) (Mauder et al. 2013). RE classified as instrumental noise and measurement error is estimated through the standard deviations (SD). RE and SE cannot be compensated or eliminated completely. LE (W/m^2) used for this study is a corrected version (LE_{corr}) as it is corrected for energy balance closure (EBC), and this is supposed to be better when comparing with models (Pastorello et al. 2020). The estimated uncertainty for the corrected version is the join uncertainty that combines the EBC correction factor and random uncertainty (see appendix A.9, eq. 5). According to Hollinger & Richardson (2005) latent heat (LE) uncertainty is positively correlated with net radiation flux and CO^2 flux uncertainty is negatively correlated with wind speed. The random uncertainty-based Hollinger & Richardson (2005) is calculated as the standard deviation of the measured fluxes. The uncertainty for ET_{corr} is larger than for GPP and probably because join uncertainty includes the EBC factor and the random uncertainty. EBC corrects the imbalance in the energy budget within EC measurements and assumes that the Bowen ratio is correct (Pastorello et al. 2020).

The calibration assumes that the observations are fixed, and errors (RRMSE) are based on the fixed values. The calibration is based on RRMSE to compare with the standard model. The values for the RRMSE are important to answer the research question. Uncertainties in the flux data make the answering the research question; if the new hydraulic model can be calibrated against the observations and perform better than the standard version, more complicated and with large uncertainties especially for the observed ETcorr raise the question if the calculated RRMSE is acceptable or can be trusted.

For the three sites (HTM, NOR and SVB) used in this study, wind speed and net radiation are two important factors that may have caused the error in the water and carbon fluxes. Measurement error varies depending on the time of the day, day of the year, net radiation and wind speed or the magnitude of the measured flux (Holinger & Richardson 2005). The last one mentioned (magnitude) makes large uncertainties at the summer months. The uncertainty in the EBC factor used for LE_{corr} is classified as a systematic error, and the estimated error is in the measurement of available energy at the surface. The error appears to vary with different weather conditions, e.g., with the development of the boundary layer, cloud cover and wind direction (Mauder et al. 2013). There are possible uncertainties in the conversion from LE_{corr} to ET_{corr} (see appendix A.7). The conversion equation assumes that the density of water is equal to 1000 kg/m^2. Latent heat of vaporisation varies also with temperature, even if the equation provides a solution to include these variations.

5.3 Standard versus hydraulic LPJ-GUESS

5.3.1 Soil water and VPD

This section discusses possible causes why LPJ-GUESS-HYD underestimated ET fluxes for all sites, related to **RQ1** (if the model can be improved) and **RQ2 (**if ET and GPP sensitive to hydraulic parameters in these environments). The default run using parameter values from the TRY database led to a lot of water not being absorbed by the trees. Calibrating to higher conductivity (only xylem conductivity Ks_{max} was changed) partly solved the issue that led to low ET by increasing the amount of water taken up from the soil to the trees, especially for sapwood. Increasing maximum hydraulic conductivity for sapwood alone was responsible for the greatest increase of ET in the calibration process. However, after calibration of LPJ-GUESS-HYD, ET still remained lower than the observed values especially for the northern site SVB. After calibrating model parameters, the modelled GPP at HTM and NOR were overestimated compared to observed data, because ET and GPP are connected e.g., a more anisohydric behaviour (lower λ values) or higher optimal forcing pressures are required to maintain maximum canopy conductance ($\Delta\psi_{max}$), which leads to more water being transpired and more carbon being assimilated.

One reason that the standard version estimated much higher ET than the hydraulic version was that the standard version allowed for the plants to take up more water from the soil. The standard model version let the trees take up more water which allowed more water to reach the leaves for transpiration. The SWC in the five upper soil layers was much lower during the summer months, indicating that the trees were taking up more water from these soil layers (see fig. A3 in the appendix). For all sites the SWC for the summer months was higher than for the summer months in the standard version. The evaporation from the soil was only slightly higher in the hydraulic version (calibrated) than the standard version, leading to an overall underestimated ET. In the first calibration process maximum hydraulic specific conductivity for sapwood (Ks_{max}) led to lower mean RRMSE due to an increase of ET (fig. 6). Higher sapwood conductivity allowed more water to pass through the sapwood and reach the leaves where transpiration occurs. As described by Eq. 6 in the model description, if Ks_{max} increases the sapwood resistance can be lower, but only if no loss of conductivity occurs due to more negative water potentials. It was shown in fig. A3 in the Appendix that the calibration led to lower SWC, indicating that a higher max sapwood conductivity in combination with other calibrated parameters values led to increased soil water uptake. But also, the stomatal conductance during the summer months had effects on transpiration. When the spruce stomata were calibrated to be open for a longer time (with more anisohydric behaviour), continuous tree transpiration and photosynthesis increased. Another reason was the competition between the species in the hydraulic model. Spruce outcompetes birch and pine trees. NOR and SVB are more mixed forests with broadleaves trees that account for around 9-12 % of the area (ICOS 2022b, ICOS 2022c). Birch trees can account for a higher rate of transpiration than needle-leaved trees due to larger leaf areas (Oltchev et al. 2002; Wang et al. 2019). However, HTM was a spruce-dominated forest (97%) ICOS (2022a) and therefore may be more in agreement with the model species composition. This site showed the best mean RRMSE (38.5%) for ET and GPP, including fit metrics of 0.91 for ET and 0.93 for GPP. The third reason that can explain the underestimation of ET has to do with vapour pressure deficit (VPD), which influences the transpiration rate of plants. High VPD can decrease transpiration through decreased canopy conductance (gc) (see Eq. 14-15). In non-water-stressed conditions, the model assumes that gc was directly related to VPD. Studies have shown that VPD has a strong influence on hydraulic conductivity, especially during drought due to drier air leading to decreased hydraulic conductivity and increased canopy temperature (Zhang et al. 2017). The hydraulic model calculates VPD through temperature and relative humidity inputs. If VPD was higher (atmospheric drought), this decreases *gc* depending on the stomatal behaviour of the plant (isohydricity). If the SWC was low, this

can in turn increase imposed transpiration (the transpiration rate imposed by the effects of the air saturation deficit, E_{imp} due to the atmosphere demanding more water than the soil water can supply with a more anisohydric behaviour (higher water flow, J). Further studies could compare temperature and relative humidity inputs with observations, to detect any differences that may affect the overall transpiration rates for all sites.

5.3.2 Standard and hydraulic model ET and GPP

As already described above, the standard version performed better than the hydraulic version in representing the ET fluxes even after two calibrations. The standard version of the model using an ET calculation derived from Gerten et al. (2006), modelled an overall higher ET compared with the hydraulic model, however seasonal GPP was similar for both models (see fig. 7-8). The calculation of ET based on an atmospheric demand and soil water supply for the standard version predicted higher ET than the hydraulic version based on imposed and equilibrium ET fluxes (Papastefanou in review). Equilibrium ET was the transpiration rate received in equilibrium with an extensive, homogeneous wet surface via the energy balance and was not imposed by the air deficit (VPD) (Köstner et al. 1992). In the standard version, water supply was most likely not limited and was able to reach the atmospheric demand of transpiration. In the hydraulic version, ET was derived differently depending on non-water-stressed (equilibrium ET play a bigger role) or water-stressed conditions (imposed ET play a bigger role). The SWC for the hydraulic version was higher than for the standard version (see fig. A3 in the Appendix). The hydraulic model avoided overestimation of ET in non-water stressed conditions, $\widetilde{g_C}$ only considering VPD affecting g_C (and water flow, $J \sim 1$), hence removing the effect of VPD on leaf water potential ψ_L (Papastefanou in review). Therefore, *VPD* was the most important factor that may limit ET for all sites. The possible overestimation of ET during well-watered conditions may have happened if J was allowed to affect gc, because J increases with higher $\Delta\psi_{max}$ (see model description, Eq. 12). However, for the three sites ET for the hydraulic version was never overestimated compared to the observations; only GPP was overestimated at HTM and NOR.

After calibration, the hydraulic model performed better at estimating seasonal GPP than ET, attaining a lower mean RRMSE. Associating canopy conductance with photosynthesis à la Sitch et al. (2001) estimated GPP with a good fit to the observations even before calibration (default model, fig. 7-8) for NOR and HTM. The hydraulic model was less likely to represent a decrease in GPP due to a long dry period during 2018 in HTM (fig. 7) compared to the standard version. This may indicate that the hydraulic version`s representation of ET was more sensitive to SWC decreases than the representation of GPP.

5.4 Sensitivity test

5.4.1 Parameter effects on ET and GPP

The calibrated parameters used in the sensitivity test led to changed ET and GPP. Several parameters were important for improved representations of ET and GPP. In the section below the improved performance is discussed in light of tree physiological understanding to offer explanations for the calibrated model`s behaviour regarding water and carbon fluxes.

5.4.2 Hydraulic safety margins parameters

The sensitivity test visualized the change in the annual mean ET and GPP when a parameter was gradually changed. Water potential where 50% of xylem conductivity is lost, ψ_{50} was varied from -7.36 - -2.208 in the OAT sensitivity test. ψ_{50} is a common hydraulic parameter threshold used in many studies to define a species hydraulic safety margin (Mayr & Cochard 2003). Higher ψ_{50} (less negative values) indicates a lower safety margin due to the threshold 50% loss of xylem conductivity reaches in relatively wetter conditions than lower ψ_{50}. By changing this parameter, the vulnerability to

cavitation along the xylem water potential gradient can be changed. The sensitivity test indicates a decrease in ET and GPP when changing ψ_{50} to its max value (-2.208 MPa) for all the sites when all PFT is included (see red line in fig. 11) and for the sites NOR and SVB for the spruce monoculture (see fig. A2 in appendix). For HTM in the monoculture spruce forest ET and GPP do not decrease by a ψ_{50} at -2.208 but may drop by a further increase ψ_{50}. When ψ_{50} reaches over 20% (-2.944) from the nominal value (-3.68), the threshold of 50% lost conductivity reaches in relatively wetter conditions (0 MPa means total saturated soil) than if ψ_{50} is set to lower than 20% from the nominal value or more negative pressures. From -100% - 20% of nominal value of ψ_{50}, water potential may not reach the threshold because the threshold is at higher negative pressures. Red line in fig. 16 indicates high vulnerability to cavitation and blue line indicates low vulnerability. The xylem water potential is usually lower (more negative pressure) than soil water potential (~ 0 well-watered) this makes water move from lower to higher water potentials (McElrone 2013). LPJ-GUESS-HYD assume that xylem cavitation only can be repaired during the allocation process, which means once at the end of each calendar year (Papastefanou in review). For the sensitivity test a yearly mean change of ET and GPP is compared to percent change of the parameter, and for ψ_{50} at -2.208, GPP, ET is low or at 0 indicating that cavitation may occur every year (2010 – 2019) the model is run. The model assumes that ψ_{88} (88% loss of conductivity) is a threshold for trees to survive and this threshold is most likely reached for ψ_{50} at -2.208. In addition to xylem, also root and leaf can be cavitated and LPJ-GUESS-HYD assumes that leaves are approximately half as much vulnerable as the xylem ($\psi_{50,leaf} = 2\,\psi_{50,xylem}$, equal slope parameter). So, if the threshold for cavitation occurs at -2.08 for the xylem, leaves cavitation occurs at -4.16. Root cavitation is assumed to occur equally to xylem cavitation, which means that roots are equally vulnerable to hydraulic failure compared to the xylem. Both roots and leaves cavitation can be repaired on a daily level.

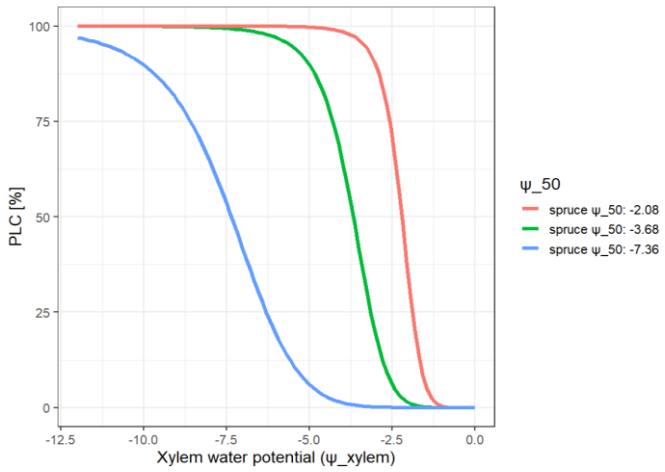

FIGURE 16: *The percent loss of conductivity (PLC) for nominal ψ_{50} (green), max and min of the range for ψ_{50} in red and blue. Cavitation slope (d) is 7.09 for all lines.*

LPJ-GUESS-HYD is run on a daily time step, but the output was only for a monthly time step for this study, but to identify if cavitation occurs and if so which days of the year the model was run a daily timestep is needed. The model was run twice with a changed $\psi_{50,xylem}$ from -2.994 - -2.208. The result can be seen in the appendix fig. A6-A7. Result showed conductivity loss of over 88% occur for the xylem for mostly of the years at $\psi_{50,xylem}$ at -2.208. The cavitation occurs due to very low water potential in the xylem and the root during the winter month, most likely due to the freezing of the soil at the time when evapotranspiration is still actively demanding water. Drought and freeze-thaw cycles related to embolism has been reported for spruce (Picea abies) by Mayr, Schwienbacher, & Bauer

(2003) and Mayr et al. (2006) in Alpine timberline. During winter month, water uptake was blocked by frozen soil and frozen stems while increasingly warmer atmosphere and solar radiation amplified the evaporate demand leading to frost related drought (Mayr et al. 2006). Spruce losses >88% of conductivity during the winter month ψ_{50} at -4.34 (Mayr et al. 2006) and this may indicate that thresholds of critical low conductivity for spruce are normally at more negative water potentials than what the sensitivity test shows.

Cavitation slope, d is a parameter related to the safety margins of a plant due to its effect on the steepness of the PLC along the xylem water potential gradient. Higher values indicate higher steepness and thus fast PLC in water-stressed conditions. In water-stressed condition, the highest value of d indicates a fast process of lost conductivity, from 50 % lost conductivity to 88% in the root, stem and xylem. In the model the user can change both parameters ($\psi_{50},\ d$) and the ψ_{88} is calculated using the parameters according to the equation:

$$\psi 88 \ = \ \psi 50 * \left(\frac{1}{0.88} - 1\right)^{\left(\frac{1}{d}\right)} \tag{24}$$

If cavitation occurs due to higher negative soil water potential, a higher d can amplify the cavitation process by utilizing the difference between ψ_{50} and ψ_{88} is smaller. In the OAT sensitivity test, only one parameter was changed each run, so any amplified effect on lost conductivity due to cavitation could not be seen. The model assumes a threshold of over 12% loss of cavitation for the detection of any damage. The parameter d showed low sensitivity and the reason for that can be simple, no cavitation occurs or a change in the output due to changed d cannot be seen in an average yearly output of ET and GPP. To be able to detect any sensitivity (ET, GPP) with changed d a daily timescale can be useful.

5.4.3 Isohydrodynamic parameter

Isohydrodynamic parameter (λ) is an important parameter in LPJ-GUESS-HYD previously used and defined in Papastefanou et al. (2020). λ is important because it links drought driven specific behaviour of degree of stomatal closure or increases of leaf water potential. λ is a parameterization of the hydraulic model to represent the continuum of the isohydrodynamic spectra, to go beyond the older definition seen as a dichotomy (Klein 2014, Martínez-Vilalta & Garcia-Forner 2017, Ratzmann et al. 2019). From Eq. 4, λ regulates the leaf water potential in water-stressed conditions $\Delta\psi_{leaf}$. In water stresses conditions $\Delta\psi_{leaf}$ can then increases when choosing a λ less than 1. When $\Delta\psi_{leaf}$ is more negative than the $\Delta\psi_{soil}$ water flow (J), gc and transpiration can continue depending on safety margin settings ($\psi_{50},\ d$).

The OAT sensitivity test resulted in a max GPP and ET around -80 – -100% (0 - 0.133) from the nominal value (0.565) and this is the case both when only spruce λ is changed in a mixed forest (all species) and in a monoculture forest (fig. 11 and fig. A2). More anisohydric representing (0 - -0.3) include a maximum opening of the stomata and maintain transpiration and photosynthesis under increasingly dry conditions, resulted in a decrease of ET and GPP. As the OAT sensitivity shows (fig. 11), a lower λ values (-0.133 - -0.266) results in carbon mass of around 0 for spruce (see appendix fig. A8) and therefore very low transpiration. When the soil water potential decreases, a chosen λ value of 0 letting the $\Delta\psi_{leaf}$ to decrease more than if the λ is 0.565 MPa (see Eq. 4 in model description).

The chosen λ at -0.133 to -0.266 most likely starting processes causing hydraulic failure, and this is driven by critical low leaf- and xylem water potentials, which in turn increases canopy conductance at the expense of increasingly drier soil (see fig. 11 in the result). Drier soil means more negative pressure which leads to the feedback of more negative pressure in the leaf and xylem. As previously

mentioned, the xylem reaches a water potential of -3.68 MPa and runaway cavitation, ψ_{88} (hydraulic failure) reaches around -5 MPa. Most likely runaway cavitation for the xylem reached for chosen $\lambda <$ 0, due to too low pressure of the xylem. This is possible due to a calibrated b at 0.74, which means that xylem water potential is closer to leaf water potential change and with an anisohydric decrease of leaf negative pressure spills over to xylem pressure.

Parameter b (ranging from 0 to 1) is defined by Fisher et al. (2006) as the ratio of (leaf-specific) hydraulic resistance below ground (roots and soil), and resistance located above ground (soil to leaf). In other words, if b varies from 0 to 1 the difference between leaf- and soil potentials is more or less important for deriving xylem potentials (see model description). Simplified in water-stressed conditions; if b is low, then xylem water potentials are more dependent on soil potentials change and if b is high leaf water potentials change influence more (see eq. 5). The parameter b is then directly linked to λ. The parameter λ, regulates leaf potential change and if λ is more (-0.3 - 0) anisohydric, leaf potential decreases more than soil potential. If high b (with a more leaf water influence) combines with anisohydric λ, runaway cavitation can occur due to very low xylem potential in water-stressed conditions. If then low b combines with anisohydric λ, xylem potential followed soil potential that decreases less fast. Parameter b through λ can then be linked to hydraulic failure caused by runaway percent loss of cavitation (ψ_{88}) by altering how xylem tensions react to leaf tensions.

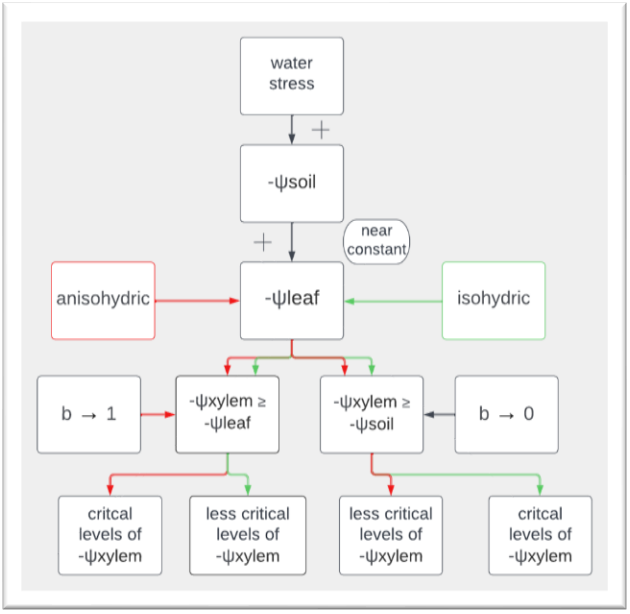

FIGURE 17: *Simplified water stress feedback on isohydric/anisohydric behaviour and parameter b.*

The calibrated value of b and λ for spruce (0.5 respective 0.5) indicates that 22% more of the resistance was located above ground and a more isohydric behaviour of leaf potentials change. Each change of parameter b results in negligible change of ET and GPP (see fig. 10 in result). It is most likely that a more isohydric behaviour ($\lambda = 0.5$) limit any critical levels of xylem-leaf water potentials to changed soil potentials and lower transpiration rate, which resulted in higher soil water content in soil (see fig. 11 in result). Fisher et al. (2006) suggested a value of b at 0.8 during dry season and 0.2 during the wet season for isohydric species in an Amazonian Forest. In Fisher et al. (2006), b is treated as a dynamic parameter depending on wetness in the soil, but for this study b is a fixed value over the simulation period and manually changed for each run of the model. Followed by fig. 17 more isohydric λ at 0.5 (green box) means that soil water potential decreases faster than leaf water potential when soil water drops, therefore soil water potential can be more negative than leaf water potential (see fig. A6-A7, in the appendix and Fisher et al. 2006) then to keep b at high values means that b is more dependent on leaf water potential, that is nearly constant depending on the degree of isohydric behaviour. Lower b with a combination of more isohydric can cause critical xylem tensions if soil potentials are bigger than leaf potentials. If more anisohydric (red box) λ, leaf

potentials decrease faster and then a higher b value means critical levels of xylem tensions. Fig. 17 assumes that soil water decreases, and trees are water stressed. For this study b changes around the nominal b value and resulted in a small change in the fluxes (ET and GPP) for all sites, most likely due to stable water conditions. However, this is a simplification of how b connects to λ, xylem water potential depends also on the height of the tree, water density and indirect also on $\Delta\psi_{max}$ (see model description). Tree height is not further evaluated in this study, impact xylem tension by increasing tensions along with the increasing height. Taller trees increase the risk of cavitation (McDowell et al. 2002).

5.4.4 λmax

λmax change resulted in the highest sensitivity to both GPP and ET. The parameter is different from the others because it has influence even in the absence of water stress. Just like the hydraulic (PWS) parameters, this parameter has never been calibrated for this region for LPJ-GUESS-HYD. λmax was previously calibrated to 0.8 (Haxeltine & Prentice 1996), which is for this study used as a default value to see if higher values can represent the carbon and water fluxes closer to observations. The calibrated value for spruce is 0.876 indicating a higher intercellular CO_2 rate than ambient CO_2 rate than the default value at 0.8. However, SVB showed a higher ET and GPP with a default λmax value at 0.8 and a negative trend with higher λmax. According to Haxeltine & Prentice (1996), trees have a constant λmax value of 0.6-0.8 under non-water-stressed conditions based on observations. When a too high λmax or *pi/pa* ratio (the ratio of partial to ambient pressure of CO2), where *pi* is λmax*pa, creating decreasing amount of ET and GPP. The optimal *pi* is 87.6% of *pa* for all sites and higher λmax creating fast drop in carbon mass for all sites (see the Appendix fig. A9). The ratio λmax is a trade-off between the rates of inward CO_2 diffusion and CO_2 assimilation (Ehleringer & Celring 1995). Most likely the hydraulic model could not further increase the CO_2 assimilation with extremely high λmax values or extreme high ambient pressure of CO_2.

5.4.5 Forcing pressure to maintain canopy conductance

$\Delta\psi_{max}$ is an optimal forcing pressure to maintain maximum canopy conductance and higher values impact how much ψ_{leaf} are allowed to decrease. Another definition is the difference in soil water- and leaf water potential under non-water stressed (well water condition) conditions (Papastefanou et al. 2020; Papastefanou in review). When this parameter increases the difference between the soil and the leaf potentials increases in a non-water stressed condition. This further means that the water flow increases (J) (see Eq.12) in a water-stressed condition which have an increasing effect on canopy conductance and transpiration (Whitehead et al. 1984).

The result showed that $\Delta\psi_{max}$ is sensitive to ET and GPP, with a positive trend for the fluxes with increasing forcing pressure to maintain canopy conductance. ET increases due to increased transpiration rate most likely due to increase water flow (J). Higher transpiration leads to drier soil and decreasing soil water potential. $\Delta\psi_{max}$ is directly linked to λ and when $\Delta\psi_{max}$ was changed λ as fixed at 0.5. Due to rather isohydric λ at 0.5, the ψ_{leaf} and ψ_{xylem} may not reach critically low levels when increasing $\Delta\psi_{max}$, due to isohydric behaviour means lower decreasing levels of ψ_{leaf}. In water-stressed conditions ψ_{leaf} are allowed to increase even more with higher $\Delta\psi_{max}$, which leading to higher transpiration, with higher J. Water flow is dependent on the differences between soil and leaf water potentials and if ψ_{leaf} increase more than ψ_{soil}, the water flow increases (see model description).

The sensitivity to ET and GPP with higher $\Delta\psi_{max}$, means that water stress may occur during the simulation years for all sites. Under a non-stressed water condition, ET rate only depend on $\widetilde{g_C}$ consider that VPD only affecting g_C, hence remove the effect of VPD on leaf water potential ψ_L.

Under water-stress conditions $\left(g_C = J\frac{1}{VPD} \right)$, J impact and higher J due to higher $\Delta\psi_{max}$ means higher g_C and transpiration.

It is a trade-off especially for more anisohydric species to maintain high g_C during drought on one hand and loss of conductance on the other hand. Therefore, a combination of high $\Delta\psi_{max}$ and more anisohydric λ, can lead to critical loss of conductance. Papastefanou et al. (2020), calibrated $\Delta\psi_{max}$ and λ parameters but used three cluster groups. An anisohydric cluster group used low $\Delta\psi_{max}$, λ to avoid critical levels of ψ_{leaf}. An more isohydric group with higher $\Delta\psi_{max}, \lambda$ (mean $\lambda = 0.48$ and $\Delta\psi_{max} = 2.15$) and as described above higher $\Delta\psi_{max}$, means that the trees operate at lower levels of ψ_{leaf} relative to ψ_{soil}, but with a more isohydric behaviour adjusting ψ_{leaf} to decreases in ψ_{soil} is limited by λ. This may suggest that the calibrated $\Delta\psi_{max}$ at 0.776, is underestimated for spruce. The second calibration on $\Delta\psi_{max}$, suggested a 40-60% higher $\Delta\psi_{max}$, value at 1.0864 - 1.2416 (see fig. 15-16) with lower RRMSE (mean with GPP and ET included) for all sites and species included. Because of the trade-off between higher GPP and lower ET compared to the observation, the RRMSE could not be lower with even higher $\Delta\psi_{max}$. The second calibration on λ suggested an 80% lower λ, indicating that a more anisohydric strategy decreases the overall site mean RRMSE.

5.4.6 Environmental factors and sensitivity

In general, the environmental factors are crucial for determining the degree of isohydricity variation and similar environmental conditions is needed to compare the degree of isohydricity (Ratzmann et al. 2019). However, the three sites, HTM (south Sweden), NOR (middle Sweden) and SVB (north Sweden) differ in sensitivity in carbon and water fluxes with changed parameters (see fig. 10-11 and fig. A1- A2 in the Appendix). HTM and NOR showed similarity in sensitivity around the local nominal value, and higher magnitude of ET and GPP than SVB. The two southern Swedish sites NOR and HTM general change in the reaction of the percentual parameters change are similar apart from the magnitude. Similar SWC (see appendix fig. A3), bioclimatic and climate variables (temperature, precipitation, and light conditions) affect the water and carbon fluxes nearly equally. Therefore, higher temporal resolution in the sensitivity test is needed to discriminate any change in ET and GPP from the two sites. The parameters change can also be smaller to detect for instance an earlier decrease of ET and GPP with changes of the ψ_{50} parameter.

The carbon and water fluxes sensitivity for SVB was overall smaller compared to NOR and HTM, due to the lower magnitude of ET and GPP for SVB, especially for ET. Even though the model runs with only spruce, ET for SVB was smaller than the rest of the sites. The SWC (see fig. A3 appendix) and soil temperature (freezing of the soil) for SVB can partly explain why the sensitivity differ mostly for SVB compared to the other sites. Soil water drops to zero in the upper layers due freezing of soil water. Winter cavitation due to high negative soil water potential is likely a higher limiting factor for tree growth in SVB. To be able to assimilate carbon and transpire the hydraulic safety margins (ψ_{50}) needed to be lower than for the other sites (see red line in fig. 11).

5.4.7 Competition effect

To try to answer the RQ3, two sensitivity tests were made, one without competition and one with competition included. Competition effects above soil based on shading categorisation (tolerant, intermediate, and intolerant) were visible through a comparison of the yearly mean OAT sensitivity test (see fig. 10-11 and fig A1-A2 in appendix) with all species/PFTs and with only spruce. The shading-related mortality described in the method is based on how fast the tree grows (growth efficiency) and how low light conditions (PAR) the tree needs to be able to grow. For all sites, spruce had the advantage to be shade tolerant (surviving lower PAR levels but with lower growth efficiency) and therefore may out-competed birch and pine. The competition effects also below soil, related to the

soil water and the root distribution. With competition species compete for soil water to be able to grow and transpire. Generally, all parameters that may causes hydraulic failure or carbon starvation (Ks_{max}, λ, ψ_{50}, λmax and $\Delta\psi_{max}$) was affected by competition effects (shading or soil water) that may amplify these effects.

The first calibration result in spruce mean carbon mass of 75% for HTM ~98% for NOR and 97% for SVB for the simulation period. Because spruce was already a dominated tree species for all sites the competition effect made by pine and birch at the max and min of parameters related to the safety margins and isohydricity mainly. When altered spruce hydraulic parameters, especially λ and ψ_{50}, HTM and NOR in fig. 11**,** showed a large decrease in ET and GPP at nearly extreme anisohydric λ and at high values of ψ_{50}, when all species was included. This decrease (in GPP and ET) was not visible for the sensitivity range of λ in HTM and NOR and not for ψ_{50} in HTM, with only spruce included (see fig. A1. in the Appendix). Without competition, spruce can tolerate higher ψ_{50} values in HTM than with competition included. With competition for soil water, the spruce threshold for cavitation may reach faster when changing the safety margin (ψ_{50}) and this is most likely reached for spruce in HTM. Spruce trees can also tolerate more anisohydric behaviours in especially in HTM and in NOR without competition (see fig. A2 in the Appendix).

The decrease in ET and GPP with changed ψ_{50}, λ for NOR and HTM for could be a competition effect of shading mortality and soil water, but also by changing isohydric behaviour for spruce to nearly anisohydric can be the limiting factor or by changing spruce vulnerability to cavitation (ψ_{50}) to lower safety margins. Anisohydric behaviour of spruce in combination with competition effects may have caused spruce hydraulic failure, with critical levels of xylem water potential. This effect may have been enhanced by the fact that the other tree species utilized the situation of critical levels of hydraulic conductivity for spruce. Fig. 13 in result showed decreasing levels of soil water content (mean upper 5 layers of 15) for the summer month with more anisohydric λ to a threshold when spruce may have reached a threshold of hydraulic failure, driven by decreasing levels of leaf- and xylem water potentials. Critical levels of xylem-leaf potentials/loss of conductance are also enhanced by the calibrated value of *b* at 0.74, which in turn makes xylem potential higher (more negative) if soil potential is less negative than leaf water potentials. So, what may a caused the large decrease in ET and GPP in HTM and NOR for λ (all PFT included, see fig. 11) is a combination of critical xylem water potentials/loss of conductivity, enhanced by high chosen *b* value, amplified by a competition effect. However, when comparing soil water content with changed λ for both mixed and monoculture forest, the competition effect may be the main reason for a drastic drop in ET and GPP for more anisohydric behaviour (compare fig. 13 and fig. A11 in the Appendix). Without competition spruce can tolerate low soil water content with anisohydric behaviour (λ: -0.226) and carbon mass drastically decreases for spruce with competition (see fig. A8 in the Appendix) indicating that competition related disturbance is the main reason for the suddenly decrease in ET and GPP. There is a possibility that the taller height of the spruce trees in the monoculture forest may have caused spruce more resistant to cavitation.

5.5 Parameter values according to the literature:

Hydraulic regulation is important in predicting different tree species' responses to drought. LPJ-GUESS-HYD representation on hydraulic regulation, the PWS parameters made it possible to discriminate plant strategies on the species level. PWS parameters are a prediction of a species or ecosystem reaction to different soil water conditions. These parameters and the unique combination of several parameters are difficult to predict due to limited measurements in different ecosystems and species (Lu et al. 2022). Hydraulic parameters can vary interspecific but also intraspecific, depending on environmental conditions and can be measured in situ or in a laboratory (Haberstroh et al. 2022, Lu

et al. 2022, Ratzmann et al. 2019). Several parameters used in this study are derived from previous specific literature, including the parameters *d*, $\Delta\psi_{max}$ and *b*. The parameter *d* derived from Santiago et al. (2018) define each slope on Amazonian species, $\Delta\psi_{max}$ and λ is derived from Papastefanou et al. (2020) and *b* on Fisher et al. 2006. Papastefanou et al. (2020) have listed $\Delta\psi_{max}$ and λ for conifers and broadleaves trees. A wide range of λ (-0.3-0.8) and $\Delta\psi_{max}$ (0.26 – 1.65) is reported for pine species, but 0.8 for Pinus sylvestris (Papastefanou et al. 2020).

The hydraulic safety margin parameters and hydraulic conductivity are widely used in the literature. As mentioned earlier the chosen default value for Ks_{max} was low compared to the calibrated, which in turn gave higher sapwood resistance. The calibrated value of Ks_{max} for spruce was 5.892 and this is ten times bigger than the default value of 0.570. The question is if this large change in Ks_{max} is reasonable for a spruce dominated forest or if this value compensates for other possible error or parameter values (chosen changed parameter or parameters that was not changed). Hickler et al. (2006) use Ks_{max} for boreal needle leaves trees like spruce and pine 0.008 m^2 s^{-1} MPa^{-1}. This is a different unit Ks_{max} is used through this study which is kg m^2 $s^{-1}MPa^{-1}$. A laboratory study measuring hydraulic conductivity in stem showed a result of 0.4 - 0.8 kg m^2 $s^{-1}MPa^{-1}$ in a sampling of Norway spruce (Paljakka et al. 2020). If that result can be used as a benchmark, the calibrated value of spruce Ks_{max} is probably overestimated to represent a mean value of a spruce forest in relatively wet conditions. Sapwood resistance also depends on sapwood area and a higher sapwood area decreases resistance. For further studies it can be necessary to vary leaf to sapwood area ratio (*SA:LA*) to see if a lower resistance led to higher ET. According to Togashi et al. (2015) *SA:LA* is a key parameter that links photosynthesis to transpiration. An overestimated Ks_{max} is partly due to a chosen narrow range of λ (0.5 – 1.0) used in the calibrating process for spruce. A lower λ for spruce minimizes the error between the observation and modelled ET (see fig. 14-15 in the result) due to higher transpiration rate by higher carbon mass for spruce, but still using high values of Ks_{max} and lower λ the model underestimated ET. However, needle leaves trees like spruce and pine have studies that suggest having a more isohydric stomatal behaviour in isohydric spectra (Pretzsch, Schütze & Biber 2018, Leo et al. 2014).

The calibrated Ψ_{50} resulted in the same value as the default value for spruce (-3.68 MPa). A measurement study of Norway spruce vulnerability to cavitation resulted in -3.6 - -3.2 MPa for 50 % loss of cavitation in twigs, depending on where in the stem the measurement is taken (compression and opposite wood) (Mayr & Cohard 2003). Mayr et al. (2014) estimated Ψ_{50} for several species and for spruce (picea abies) in boreal biome and it was measured at -3.98 MPa. Ψ_{50} or Ψ_{88} is used to define "the point of no return" and had been suggested to be reached for conifers trees at 50 - 88 % loss conductivity (Brodribb & Cochard, 2009, Urli et al., 2013), but it also depends on how species will recover from a drought event (embolism reversal) (Klein et al. 2018). A global study showed that conifers species have higher safety margins (Ψ_{50}) than angiosperms (Choat et al. 2012).

5.6 Limitations

5.6.1 Calibration limitation

The calibration process was meant to vary one parameter OAT, starting with the most dominated species. Just like the OAT sensitivity test the calibration had limitations. The aim of the calibration process was to find the local lowest RRMSE for ET and GPP for each parameter and the order of calibrated parameter (which parameter you start with, and which go next with), how many values the parameter was varied in between the range (now 6 values/parameter) can impact the result. How much the calibrating order of the parameters affects the result of RRMSE is unclear. To improve the calibration, cluster groups of two parameters affecting each other can be tested. Papastefanou et al.

(2020) used cluster groups of λ and $\Delta\psi_{max}$, two parameters that are linked to each other through $\Delta\psi_{leaf}$ that both affecting. The aim of cluster group is to vary one parameter with increasing value of the other parameters. For instance, if you vary λ from max to min (6 runs) with a stepwise higher $\Delta\psi_{max}$, then you need 36 runs. It is a time-consuming process if you do it manually and therefore not suitable for this study. A R Package (rLPJ-GUESS) could also be used to perform a Bayesian calibration with a Markov-Chain Monte Carlo (MCMC) algorithm **(**Bagnara et al. 2018).

The calibration was done using all species but was limited by representing birch and pine. The calibration method favour spruce trees and pine and birch were strongly limited. Therefore, the calibration values birch and pine may not be the optimal parameter values.

Calibration used RRMSE metric for the cost function for the calibration. Other calibration metric could be used in the calibration process, for instance a R^2 value. Precisely as RRMSE (%), a R^2 (fraction) is a value that can be used to compare two outputs with different units. However, it is not clear if a R^2 cost function can result in different calibration result with a different parameter setting for the lowest R^2, which is a commonly used metric used in linear regression calibration (Sanchez 2021). According to Sanchez (2021) the use of R^2 should be avoided for assessing the goodness of fit of a calibration and other metrics performed better to accuracy represent the goodness of fit. A large value of R^2 is not always ensure a good fit neither the model predict well and proof of linearity. Instead, relative error (%RE) is a better metric to use in any type of linearity evaluation (non-linear and linear regression) (Raposo 2016).

It was mentioned before that the environmental factors are important to determine the degree of iso/anisohydry and other parameters related to this study. Therefore, a site-specific calibration may result in different optimal parameters values across the sites, especially for the northers site SVB.

5.6.2 Model limitation

All models are a simplification of the reality (Smith & Smith 2007). However, the simplification is necessary because all complex interactions cannot be considered, even if the hydraulic modification of LPJ-GUESS is a more complex and upgraded model which integrates tree species responses to cope with different soil water deficits. Model limitation and simplification for LPJ-GUESS-HYD are incorporated in the parameter's assumptions and parameters uncertainty. This model assumes that the leaves are half as much vulnerable to cavitation compared to the xylem and the roots are equally vulnerable to cavitation compared to the xylem. If the xylem is more or less vulnerable to cavitation compared to the roots is highly uncertain (Li et al. 2022b). Xylem equal to root conductivity assumption is most likely a compromise according to the literature, which suggested that the xylem is more vulnerable than the roots (Johnson et al. 2016, Wason et al. 2018), or roots are more vulnerable (Rodriguez-Dominguez et al., 2018, Peters et al., 2020). Overall, a lack of hydraulic parameter values measured for different tree species in different environments makes it difficult to evaluate whether the calibrated values suggested by the model are reasonable. More studies on how vulnerable roots are relative to other parts of the plants are needed. Some studies on hydraulic traits have worked by measuring traits in combination with modelling to evaluate how close the model predicted the chosen hydraulic traits (Li et al. 2022b). However, measuring techniques have developed and more recently it has been shown that isohydricity gradient can be calculated through remote sensed vegetative optical depth, which is directly related to leaf water potential and measured from the AMSR-E satellite (Konings & Gentine 2016).

The model assumes that xylem recovery time or the time for xylem cavitation to be repaired is on a daily level for roots and leaves but on a yearly level for the xylem. This is a simplification of the model, and according to studies, recovery time may depend on species level and degree of isohydricity

(Kannenberg et al. 2019), but it is uncertain if vessels that have embolized can recover after drought (Li et al. 2022b).

5.6.3 Sensitivity limitation

The OAT sensitivity test visualization of the local sensitivity around the nominal value limited a broader view of the sensitivity. The OAT sensitivity is a simplistic approach because of its negligible parameter interactions. The parameters used in this study are related to each other through variations in soil water content and atmospheric demand. In the relative wet sites (NOR, HTM, SVB), ET and GPP showed a low local sensitivity when changing the parameter *b*. However, this non-sensitive behaviour is not necessarily insensitive to other sites, that are more characterized by drought. The above discussion on parameter *b* links to visualize the problematic issues related to a local OAT sensitivity. The links between *b* change to λ change cannot be evaluated through an OAT sensitivity test. Another interesting interaction is between the λ and $\Delta\Psi_{max}$ because both are directly affecting the change of leaf water potentials ($\Delta\Psi_{leaf}$) along the soil water potential gradient (see eq. 4). $\Delta\Psi_{max}$ acts like an amplifier to decrease the leaf water potentials when the soil water potential drops depending on chosen λ, but a chosen λ of 1 disconnects the soil water potential and leaf water potential change and the leaf water potential is only changing according to the initial $\Delta\Psi_{max}$.

The concept of an OAT is just changing one parameter at once and never several connected parameters are changed each time, common in global analysis (Zhou, Lin & Lin 2008). For instance, can a variance based (Sobol method) be applied to evaluate the model sensitivity and interactions between the parameters (Sobol 2001).

5.7 Further studies

5.7.1 Additional parameters/traits

Hydraulic functional traits belong to leaf, stem, or root levels and the traits related to each level determine the tree species ability to acquire, circulate, and use water (Matheny, Mirfenderesgi & Bohrer 2017). The hydraulic version of LPJ-GUESS upgraded each woody PFT/species (spruce, pine and birch) hydraulic strategy based on hydraulic functional traits that occur at all three levels. For this study selected hydraulic parameters are changed and for further studies, additional parameters can be evaluated to understand to whole plant hydraulic strategy. For instance, specific root may alter the outputs of ET and GPP depending on each sensitivity. Root hydraulic conductivity is the ability of the roots to absorb water from the soil and is important for the water uptake (Nguyen, Joshi & Kant 2017). Specific root conductivity is by default 0.00112 (s-1 MPa-1), taken from the TRY database for all species. However, below ground traits are difficult to study and determine from remote sensing and measurement. Therefore, root system traits are underrepresented in the traits database and in the literature (Matheny, Mirfenderesgi & Bohrer 2017). The uncertainty related to the specific root conductivity is bigger than for the xylem conductivity. Root traits in LPJ-GUESS-HYD including root distribution and specific root conductivity. Two parameters that can further develop the sensitivity and calibration result. However, a test run of the hydraulic model with higher specific root conductivity and leaf conductivity resulted only in slightly higher ET for the sites.

Root distribution is an important factor to further evaluate and include in a calibration. Deeper roots increase drought resistance and are important for mitigating the impacts of drought stress (Li et al. 2022a). There are also parameters that are related to traits for the stem and the leaves. For instance, leaf conductivity, sapwood, and heartwood density (*wooddens*), leaf area index (LAI), leaf longevity, and tree leaf to sapwood cross-sectional area ratio. Wood density is an important plant trait and has been shown to be a good predictor of xylem vulnerability to embolism. Higher wood density makes the tree more resistant to drought related to decreases in xylem potential (Li et al. 2022b). Species

having dense wood and anisohydric behaviour were more likely to root at shallower depths (Hoffmann et al. 2011). The parameters listed above are important to further study to evaluate how hydraulic parameters correlated with non-hydraulic parameters.

Further studies include also to calculate leaf-xylem-soil water potentials. This would make it easier to explain the processes in the sensitivity test. For instance, when cavitation and when thresholds on chosen $\Delta\psi_{50}$ and if thresholds of no return $\Delta\psi_{88}$ reach. Water potentials may further explain why parameter *b* showed low sensitivity for ET and GPP for all three Swedish environments. This may require daily output of soil water and water potentials instead of monthly.

Further studies can be to test how sensitive the hydraulic model version is to modified inputs (precipitation, temperature, CO2 – levels). But an improved calibration and sensitivity test of the parameters to improve the model against the observation and a better understanding of the model behaviour is probably needed. The underestimation of ET for all sites in Sweden, the question arises if an improved calibration is needed, with additional parameters tested or if errors in the model structure cause the underestimation.

6 Conclusion

While drought events are predicted to increase in strength and frequency, a new model was developed to include upgraded hydraulic implementation in LPJ-GUESS. This study aimed to evaluate this model in simulating carbon and water fluxes in three Swedish boreal sites. The hydraulic model was improved in simulating land-atmosphere exchanges of carbon and water at the three sites by two calibrations, but when the hydraulic model was compared to the standard version, the hydraulic model performed less well to represent ET. The calibration process with altered parameter values resulted for all sites a lower combined mean RRMSE for ET and GPP compared to the default (not changed) chosen parameters. However, large uncertainties in the observation data especially for the ET flux complicate answering the question if the hydraulic model is better than the standard version and if the model can be improved by calibration.

The hydraulic parameters representing the tree species' strategies to cope with drought were tested through an OAT sensitivity test. The sensitivity test resulted in an overall site, high sensitivity to ET and GPP for λmax, λ, Ψ_{50}, $\Delta\Psi_{max}$ *and* Ks_{max}. These four parameters resulted in a clear visible change in the water and carbon fluxes when the parameter value was changed around a nominal value. The sensitivity test showed low sensitivity to the water and carbon fluxes for parameters *b* and *d*.

The hydraulic model species/PFT compete for light and water. Spruce had an advantage in adapting to a low growth rate but was established in low light conditions and then survived a lot of shading of other tree species. This strategy (shade tolerant) was successful for all sites resulting in an almost spruce monoculture forest. The competing effect, when including all tree species (spruce, birch and pine), impacted the sensitivity test when spruce was reaching thresholds for hydraulic failure. The competition effect may have amplified the variations in the fluxes mainly when the parameters was at the extreme values. Competition may amplify hydraulic failure/carbon starvation for spruce due to light shading and soil-water competition.

Hypothesis (1), if a higher sensitivity to soil water change for the hydraulic model improves the model performance of ET and GPP, is partly true because the hydraulic model was improved by predicting GPP and ET in the calibration, but the underestimation of ET magnitude during the summer month resulted in a higher RRMSE. The combined mean RRMSE (ET and GPP) was still higher than

compared to the standard version. The second hypothesis (2), if both carbon and water fluxes will prove sensitive to isohydricity and sapwood hydraulic conductivity changes for the chosen sites, is partly true, ET and GPP were relatively sensitive to parameter changes of isohydricity and hydraulic conductivity for sapwood, but not equally sensitive across the sites. HTM and NOR environments showed similar sensitivity changes for ET and GPP, but for SVB the sensitivity change is generally lower due to the lower magnitude of both fluxes. This different model behaviour for the fluxes is mostly due to different climate forcing and SWC.

For future studies, additional parameters are important to study to evaluate how hydraulic parameters are correlated with non-hydraulic parameters and their interactions. For instance, specific leaf- and root conductivity, root distribution, sapwood-, heartwood density and leaf to sapwood area ratio can be evaluated in an improved sensitivity test. Even the calibration needs to be improved by additional parameters included and with an improved method.

7 References

Adams, H. D., Guardiola-Claramonte, M., Barron-Gafford, G. A., Villegas, J. C., Breshears, D. D., Zou, C. B., Troch, P. A., & Huxman, T. E. (2009). Temperature sensitivity of drought-induced tree mortality portends increased regional die-off under global-change-type drought. *Proceedings of the National Academy of Sciences*, *106*(17), 7063-7066. https://doi.org/doi:10.1073/pnas.0901438106

Allen, C. D., Macalady, A. K., Chenchouni, H., Bachelet, D., McDowell, N., Vennetier, M., Kitzberger, T., Rigling, A., Breshears, D. D., Hogg, E. H., Gonzalez, P., Fensham, R., Zhang, Z., Castro, J., Demidova, N., Lim, J.-H., Allard, G., Running, S. W., Semerci, A., & Cobb, N. (2010). A global overview of drought and heat-induced tree mortality reveals emerging climate change risks for forests. *Forest Ecology and Management*, *259*(4), 660-684. https://doi.org/10.1016/j.foreco.2009.09.001

Bagnara, M., Van Oijen, M., Cameron, D., Gianelle, D., Magnani, F., & Sottocornola, M. (2018). Bayesian calibration of simple forest models with multiplicative mathematical structure: A case study with two Light Use Efficiency models in an alpine forest. *Ecological Modelling*, *371*, 90-100. https://doi.org/10.1016/j.ecolmodel.2018.01.014

Ball, J., Woodrow, I., & Berry, J. (1987). A Model Predicting Stomatal Conductance and Its Contribution to the Control of Photosynthesis Under Different Environmental Conditions. *Progress in Photosynthesis Research*, *4*, 221–224. https://doi.org/10.1007/978-94-017-0519-6_48

Batjes, Niels H. (2009). ISRIC-WISE - Global Soil Profile Data (ver. 3.1). World Data Centre for Soils, Wageningen, The Netherlands, PANGAEA, https://doi.org/10.1594/PANGAEA.858569

Bonan, G. B. (2014). Connecting mathematical ecosystems, real-world ecosystems, and climate science. *New Phytologist*, *202*(3), 731-733. https://doi.org/10.1111/nph.12802

Breshears, D., Cobb, N., Rich, P., Price, K., Allen, C., Balice, R., Romme, W., Kastens, J., Floyd, M., Belnap, J., Anderson, J., Myers, O., & Meyer, C. (2005). Regional vegetation die-off in response to global-change-type drought. *Proceedings of the National Academy of Sciences of the United States of America*, *102*, 15144-15148. https://doi.org/10.1073/pnas.0505734102

Brodribb, T. J., & Cochard, H. (2009). Hydraulic Failure Defines the Recovery and Point of Death in Water-Stressed Conifers. *Plant Physiology*, *149*(1), 575-584. https://doi.org/10.1104/pp.108.129783

Buckley, T. N. (2005). The control of stomata by water balance. *New Phytologist*, *168*(2), 275-292. https://doi.org/10.1111/j.1469-8137.2005.01543.x

Carnicer, J., Coll, M., Ninyerola, M., Pons, X., Sánchez, G., & Peñuelas, J. (2011). Widespread crown condition decline, food web disruption, and amplified tree mortality with increased climate change-type drought. *Proceedings of the National Academy of Sciences*, *108*(4), 1474-1478. https://doi.org/doi:10.1073/pnas.1010070108

Choat, B., Brodribb, T. J., Brodersen, C. R., Duursma, R. A., López, R., & Medlyn, B. E. (2018). Triggers of tree mortality under drought. *Nature*, *558*(7711), 531-539. https://doi.org/10.1038/s41586-018-0240-x

Choat, B., Jansen, S., Brodribb, T., Cochard, H., Delzon, S., Bhaskar, R., Bucci, S., Feild, T., Gleason, S., Hacke, U., Jacobsen, A., Lens, F., Maherali, H., Martinez Vilalta, J., Mayr, S., Mencuccini, M., Mitchell, P., Nardini, A., Pittermann, J., & Zanne, A. (2012). Global convergence in the vulnerability of forests to drought. *Nature*, *491*. https://doi.org/10.1038/nature11688

Christmann, A., Weiler, E. W., Steudle, E., & Grill, E. (2007). A hydraulic signal in root-to-shoot signalling of water shortage. *The Plant Journal*, *52*(1), 167-174. https://doi.org/10.1111/j.1365-313X.2007.03234.x

Collatz, G. J., Ball, J. T., Cyril, G., & Joseph, A. B. (1991). Physiological and environmental regulation of stomatal conductance, photosynthesis and transpiration: a model that includes a laminar boundary layer. *Agricultural and Forest Meteorology*, *54*(2), 107-136. https://doi.org/10.1016/0168-1923(91)90002-8

Eller, C. B., Rowland, L., Oliveira, R. S., Bittencourt, P. R. L., Barros, F. V., & Da Costa, A. C. L. (2018). Modelling tropical forest responses to drought and El Niño with a stomatal optimization model based on xylem hydraulics. *Philos. Trans. R. Soc. B Biol*. Sci. 373:20170315. https://doi.org/10.1098/rstb.2017.0315

Eamus, D., Boulain, N., Cleverly, J., & Breshears, D. D. (2013). Global change-type drought-induced tree mortality: vapor pressure deficit is more important than temperature per se in causing decline in tree health. *Ecology and Evolution*, *3*(8), 2711-2729. https://doi.org/10.1002/ece3.664

Ehleringer, J. R., & Cerling, T. E. (1995). Atmospheric CO_2 and the ratio of intercellular to ambient CO_2 concentrations in plants. *Tree Physiology*, *15*(2), 105-111. https://doi.org/10.1093/treephys/15.2.105

Farquhar, G. D., von Caemmerer, S., & Berry, J. A. (1980). A biochemical model of photosynthetic CO2 assimilation in leaves of C 3 species. *Planta*, *149*(1), 78–90. https://doi.org/10.1007/BF00386231

Fisher, R. A., Williams, M., Do Vale, R. L., Da Costa, A. L., & Meir, P. (2006). Evidence from Amazonian forests is consistent with isohydric control of leaf water potential. *Plant, cell & environment*, *29*(2), 151–165. https://doi.org/10.1111/j.1365-3040.2005.01407.x

Friedlingstein, P., O'Sullivan, M., Jones, M. W., Andrew, R. M., Hauck, J., Olsen, A., Peters, G. P., Peters, W., Pongratz, J., Sitch, S., Le Quéré, C., Canadell, J. G., Ciais, P., Jackson, R. B., Alin, S., Aragão, L. E. O. C., Arneth, A., Arora, V., Bates, N. R., & Zaehle, S. (2020). Global Carbon Budget 2020. *Earth Syst. Sci. Data*, *12*(4), 3269-3340. https://doi.org/10.5194/essd-12-3269-2020

Garcia-Forner, N., Biel, C., Savé, R., & Martínez-Vilalta, J. (2017). Isohydric species are not necessarily more carbon limited than anisohydric species during drought. *Tree Physiol*, *37*(4), 441-455. https://doi.org/10.1093/treephys/tpw109

Geary, W. L., Bode, M., Doherty, T. S., Fulton, E. A., Nimmo, D. G., Tulloch, A. I. T., Tulloch, V. J. D., & Ritchie, E. G. (2020). A guide to ecosystem models and their environmental applications. *Nature Ecology & Evolution*, *4*(11), 1459-1471. https://doi.org/10.1038/s41559-020-01298-8

Gerten, D., Schaphoff, S., Haberlandt, W., Lucht, W. & Sitch, S. 2004. Terrestrial vegetation and water balance—hydrological evaluation of a dynamic global vegetation model. *Journal of Hydrology 286*, 249-270.

Gollan, T., Turner, N. C., & Schulze, E.-D. (1985). The responses of stomata and leaf gas exchange to vapour pressure deficits and soil water content. *Oecologia*, *65*(3), 356–362. https://doi.org/10.1007/bf00378909

Haberstroh, S., Lobo-do-Vale, R., Caldeira, M. C., Dubbert, M., Cuntz, M., & Werner, C. (2022). Plant invasion modifies isohydricity in Mediterranean tree species. *Functional Ecology*, *36*(9), 2384.

Hammond, W. M., Yu, K., Wilson, L. A., Will, R. E., Anderegg, W. R. L., & Adams, H. D. (2019). Dead or dying? Quantifying the point of no return from hydraulic failure in drought-induced tree mortality. *New Phytologist*, *223*(4), 1834-1843. https://doi.org/10.1111/nph.15922

Hartmann, H. (2015). Carbon starvation during drought-induced tree mortality – are we chasing a myth? *Journal of Plant Hydraulics*, *2*(0), e005. https://doi.org/10.20870/jph.2015.e005

Hartmann, H., Moura, C. F., Anderegg, W. R. L., Ruehr, N. K., Salmon, Y., Allen, C. D., Arndt, S. K., Breshears, D. D., Davi, H., Galbraith, D., Ruthrof, K. X., Wunder, J., Adams, H. D., Bloemen, J., Cailleret, M., Cobb, R., Gessler, A., Grams, T. E. E., Jansen, S., & O'Brien, M. (2018). Research frontiers for improving our understanding of drought-induced tree and forest mortality. *New Phytologist*, *218*(1), 15-28. https://doi.org/10.1111/nph.15048

Haxeltine, A., & Prentice, I. C. (1996). BIOME3: An equilibrium terrestrial biosphere model based on ecophysiological constraints, resource availability, and competition among plant functional types. *Global Biogeochemical Cycles*, *10*(4), 693-709. https://doi.org/10.1029/96GB02344

Hickler, T., Vohland, K., Feehan, J., Miller, P. A., Smith, B., Costa, L., Giesecke, T., Fronzek, S., Carter, T. R., Cramer, W., Kühn, I., & Sykes, M. T. (2012). Projecting the future distribution of European potential natural vegetation zones with a generalized, tree species-based dynamic vegetation model. *Global Ecology and Biogeography*, *21*(1), 50-63. https://doi.org/10.1111/j.1466-8238.2010.00613.x

Hickler, T., Prentice, I. C., Smith, B., Sykes, M. T., & Zaehle, S. (2006). Implementing plant hydraulic architecture within the LPJ Dynamic Global Vegetation Model. *Global Ecology and Biogeography*, *15*(6), 567-577. https://doi.org/10.1111/j.1466-8238.2006.00254.x

Hoffmann, W. A., Marchin, R. M., Abit, P., & Lau, O. L. (2011). Hydraulic failure and tree dieback are associated with high wood density in a temperate forest under extreme drought. *Global Change Biology*, *17*(8), 2731-2742. https://doi.org/10.1111/j.1365-2486.2011.02401.x

Hollinger, D., & Richardson, A. (2005). Uncertainty in eddy covariance measurements and its application to physiological models. *Tree Physiol*, *25*, 873-885. https://doi.org/10.1093/treephys/25.7.873

IPCC (2021). Summary for Policymakers. In: Climate Change 2021: The Physical Science Basis. Contribution of Working Group I to the Sixth Assessment Report of the Intergovernmental. Panel on Climate Change [Masson-Delmotte, V., P. Zhai, A. Pirani, S. L. Connors, C. Péan, S.Berger, N. Caud, Y. Chen, L. Goldfarb, M. I. Gomis, M. Huang, K. Leitzell, E. Lonnoy, J.B.R. Matthews, T. K. Maycock, T. Waterfield, O. Yelekçi, R. Yu and B. Zhou (eds.)]. *Cambridge University Press*. In Press.

Jackson, R. B., Canadell, J., Ehleringer, J. R., Mooney, H. A., Sala, O. E., & Schulze, E. D. (1996). A global analysis of root distributions for terrestrial biomes. *Oecologia*, *108*(3), 389-411. https://doi.org/10.1007/BF00333714

Johnson, D. M., Wortemann, R., McCulloh, K. A., Jordan-Meille, L., Ward, E., Warren, J. M., Palmroth, S., & Domec, J.-C. (2016). A test of the hydraulic vulnerability segmentation hypothesis in angiosperm and conifer tree species. *Tree Physiology*, *36*(8), 983-993. https://doi.org/10.1093/treephys/tpw031

Jones, H. G., & Sutherland, R. A. (1991). Stomatal control of xylem embolism. *Plant, Cell & Environment*, *14*(6), 607-612. https://doi.org/https://doi.org/10.1111/j.1365-3040.1991.tb01532.x

Kannenberg, S. A., Guo, J. S., Novick, K. A., Anderegg, W. R. L., Feng, X., Kennedy, D., Konings, A. G., Martínez-Vilalta, J., & Matheny, A. M. (2022). Opportunities, challenges and pitfalls in characterizing plant water-use strategies. *Functional Ecology*, *36*(1), 24-37. https://doi.org/https://doi.org/10.1111/1365-2435.13945

Kannenberg, S. A., Novick, K. A., & Phillips, R. P. (2019). Anisohydric behavior linked to persistent hydraulic damage and delayed drought recovery across seven North American tree species. *The New phytologist*, *222*(4), 1862–1872. https://doi.org/10.1111/nph.15699

Keenan, T., García, R., Friend, A. D., Zaehle, S., Gracia, C., & Sabate, S. (2009). Improved understanding of drought controls on seasonal variation in Mediterranean forest canopy CO^2 and water fluxes through combined in situ measurements and ecosystem modelling. *Biogeosciences*, *6*(8), 1423-1444. https://doi.org/10.5194/bg-6-1423-2009

Klein, T. (2014). The variability of stomatal sensitivity to leaf water potential across tree species indicates a continuum between isohydric and anisohydric behaviours. *Functional Ecology*, *28*(6), 1313-1320.

Klein, T., Zeppel, M. J. B., Anderegg, W. R. L., Bloemen, J., De Kauwe, M. G., Hudson, P., Ruehr, N. K., Powell, T. L., von Arx, G., & Nardini, A. (2018). Xylem embolism refilling and resilience against drought-induced mortality in woody plants: processes and trade-offs [article]. *Ecological Research*(5).

Knipfer, T., & Steudle, E. (2008). Root hydraulic conductivity measured by pressure clamp is substantially affected by internal unstirred layers. *Journal of Experimental Botany*, *59*(8), 2071-2084. https://doi.org/10.1093/jxb/ern064

Konings, A. G., & Gentine, P. (2017). Global variations in ecosystem-scale isohydricity. *Global Change Biology*, *23*(2), 891-905. https://doi.org/https://doi.org/10.1111/gcb.13389

Krinner, G., Viovy, N., de Noblet-Ducoudré, N., Ogée, J., Polcher, J., Friedlingstein, P., Ciais, P., Sitch, S., & Prentice, I. C. (2005). A dynamic global vegetation model for studies of the coupled atmosphere-biosphere system. *Global Biogeochemical Cycles*, *19*(1), 1015-1015. https://doi.org/10.1029/2003GB002199

Köstner, B. M. M., Schulze, E. D., Kelliher, F. M., Hollinger, D. Y., Byers, J. N., Hunt, J. E., McSeveny, T. M., Meserth, R., & Weir, P. L. (1992). Transpiration and canopy conductance in a pristine broad-leaved forest of Nothofagus: an analysis of xylem sap flow and eddy correlation measurements. *Oecologia*, *91*(3), 350-359. https://doi.org/10.1007/BF00317623

Lamarque, J. F., Dentener, F., McConnell, J., Ro, C. U., Shaw, M., Vet, R., Bergmann, D., Cameron-Smith, P., Dalsoren, S., Doherty, R., Faluvegi, G., Ghan, S. J., Josse, B., Lee, Y. H., MacKenzie, I. A., Plummer, D., Shindell, D. T., Skeie, R. B., Stevenson, D. S., & Nolan, M. (2013). Multi-model mean nitrogen and sulfur deposition from the Atmospheric Chemistry and Climate Model Intercomparison Project (ACCMIP): evaluation of historical and projected future changes. *Atmos. Chem. Phys.*, *13*(16), 7997-8018. https://doi.org/10.5194/acp-13-7997-2013

Lasslop, G., Reichstein, M., Papale, D., Richardson, A. D., Arneth, A., Barr, A., Stoy, P., & Wohlfahrt, G. (2010). Separation of net ecosystem exchange into assimilation and respiration using a light response curve approach: critical issues and global evaluation. *Global Change Biology*, *16*(1), 187-208. https://doi.org/https://doi.org/10.1111/j.1365-2486.2009.02041.x

Leo, M., Oberhuber, W., Schuster, R., Grams, T. E. E., Matyssek, R., & Wieser, G. (2014). Evaluating the effect of plant water availability on inner alpine coniferous trees based on sap flow measurements. *European Journal of Forest Research*, *133*(4), 691-698. https://doi.org/10.1007/s10342-013-0697-y

Lévesque, M., Saurer, M., Siegwolf, R., Eilmann, B., Brang, P., Bugmann, H., & Rigling, A. (2013). Drought response of five conifer species under contrasting water availability suggests high vulnerability of Norway spruce and European larch. *Global Change Biology*, *19*(10), 3184-3199. https://doi.org/10.1111/gcb.12268

Li, B., Zhang, X., Morita, S., Sekiya, N., Araki, H., Gu, H., Han, J., Lu, Y., & Liu, X. (2022a). Are crop deep roots always beneficial for combating drought: A review of root structure and function, regulation and phenotyping. *Agricultural Water Management*, *271*, 107781. https://doi.org/https://doi.org/10.1016/j.agwat.2022.107781

Li, M.-F., Tang, X.-P., Wu, W., & Liu, H.-B. (2013). General models for estimating daily global solar radiation for different solar radiation zones in mainland China. *Energy Conversion and Management*, *70*, 139-148. https://doi.org/10.1016/j.enconman.2013.03.004

Li, X., Xi, B., Wu, X., Choat, B., Feng, J., Jiang, M., & Tissue, D. (2022b). Unlocking Drought-Induced Tree Mortality: Physiological Mechanisms to Modeling. *Frontiers in Plant Science*, *13*, 1-15. https://doi.org/10.3389/fpls.2022.835921

Matheny, A. M., Mirfenderesgi, G., & Bohrer, G. (2017). Trait-based representation of hydrological functional properties of plants in weather and ecosystem models. *Plant Diversity*, *39*(1), 1-12. https://doi.org/10.1016/j.pld.2016.10.001

Mantova, M., Herbette, S., Cochard, H., & Torres-Ruiz, J. M. (2022). Hydraulic failure and tree mortality: from correlation to causation. *Trends in Plant Science*, *27*(4), 335-345. https://doi.org/10.1016/j.tplants.2021.10.003

Mantova, M., Menezes-Silva, P. E., Badel, E., Cochard, H., & Torres-Ruiz, J. M. (2021). The interplay of hydraulic failure and cell vitality explains tree capacity to recover from drought. *Physiologia Plantarum*, *172*(1), 247-257. https://doi.org/10.1111/ppl.13331

Markhart, A., H., & Smit, B. (1990). Measurement of root hydraulic conductance. *HortScience*, *25*(3), 282-287.

Martínez-Vilalta, J., Lloret, F., & Breshears, D. D. (2012). Drought-induced forest decline: causes, scope and implications. *Biology Letters*, *8*(5), 689-691. https://doi.org/doi:10.1098/rsbl.2011.1059

Martínez-Vilalta, J., & Garcia-Forner, N. (2017). Water potential regulation, stomatal behaviour and hydraulic transport under drought: deconstructing the iso/anisohydric concept. *Plant, Cell & Environment*, *40*(6), 962-976. https://doi.org/10.1111/pce.12846

Martin-StPaul, N., Delzon, S., & Cochard, H. (2017). Plant resistance to drought depends on timely stomatal closure. *Ecology Letters*, *20*(11), 1437-1447. https://doi.org/10.1111/ele.12851

Matkala, L., Kulmala, L., Kolari, P., Aurela, M., & Bäck, J. (2021). Resilience of subarctic Scots pine and Norway spruce forests to extreme weather events. *Agricultural and Forest Meteorology*, *296*, 108239. https://doi.org/10.1016/j.agrformet.2020.108239

Mauder, M., Cuntz, M., Drüe, C., Graf, A., Rebmann, C., Schmid, H. P., Schmidt, M., & Steinbrecher, R. (2013). A strategy for quality and uncertainty assessment of long-term eddy-covariance measurements. *Agricultural and Forest Meteorology*, *169*, 122-135. https://doi.org/https://doi.org/10.1016/j.agrformet.2012.09.006

Mayr, S., & Cochard, H. (2003). A new method for vulnerability analysis of small xylem areas reveals that compression wood of Norway spruce has lower hydraulic safety than opposite wood. *Plant, Cell & Environment*, *26*(8), 1365-1371. https://doi.org/10.1046/j.0016-8025.2003.01060.x

Mayr, S., Hacke, U., Schmid, P., Schwienbacher, F., & Gruber, A. (2006). Frost drought in conifers at the alpine timberline: xylem dysfunction and adaptations. *Ecology*, *87*(12), 3175–3185. https://doi.org/10.1890/0012-9658(2006)87[3175:fdicat]2.0.co;2

Mayr, S., Schwienbacher, F., & Bauer, H. (2003). Winter at the Alpine Timberline. Why Does Embolism Occur in Norway Spruce But Not in Stone Pine? *Plant Physiology*, *131*(2), 780-792. https://doi.org/10.1104/pp.011452

McDowell, N. G., Phillips, N., Lunch, C., Bond, B. J., & Ryan, M. G. (2002). An investigation of hydraulic limitation and compensation in large, old Douglas-fir trees. *Tree Physiology*, *22*(11), 763-774. https://doi.org/10.1093/treephys/22.11.763

McDowell, N., Pockman, W. T., Allen, C. D., Breshears, D. D., Cobb, N., Kolb, T., Plaut, J., Sperry, J., West, A., Williams, D. G., & Yepez, E. A. (2008). Mechanisms of plant survival and mortality during drought: why do some plants survive while others succumb to drought? *New Phytologist*, *178*(4), 719-739. https://doi.org/10.1111/j.1469-8137.2008.02436.x

McDowell NG. (2011). Mechanisms linking drought, hydraulics, carbon metabolism, and vegetation mortality. *Plant Physiology 155*, 1051–1059.

Melcher, P. J., Michele Holbrook, N., Burns, M. J., Zwieniecki, M. A., Cobb, A. R., Brodribb, T. J., Choat, B., & Sack, L. (2012). Measurements of stem xylem hydraulic conductivity in the laboratory and field. *Methods in Ecology and Evolution*, *3*(4), 685-694. https://doi.org/10.1111/j.2041-210X.2012.00204.x

Nguyen, G. N., Joshi, S., & Kant, S. (2017). Chapter 13 - Water availability and nitrogen use in plants: effects, interaction, and underlying molecular mechanisms. In M. A. Hossain, T. Kamiya, D. J. Burritt, L.-S. P. Tran, & T. Fujiwara (Eds.), *Plant Macronutrient Use Efficiency* (pp. 233-243). Academic Press. https://doi.org/10.1016/B978-0-12-811308-0.00013-2

Noguera, I., Vicente-Serrano, S. M., & Domínguez-Castro, F. (2022). The Rise of Atmospheric Evaporative Demand Is Increasing Flash Droughts in Spain During the Warm Season. *Geophysical Research Letters*, *49*(11), e2021GL097703. https://doi.org/10.1029/2021GL097703

Olchev, A., Cermák, J., N, N., Tatarinov, F., A, T., Ibrom, A., & Gravenhorst, G. (2002). Transpiration of a mixed forest stand: Field measurements and simulation using SVAT models. *Boreal Environment Research*, *4*, 389-397.

Paljakka, T., Rissanen, K., Vanhatalo, A., Salmon, Y., Jyske, T., Prisle, N. L., Linnakoski, R., Lin, J. J., Laakso, T., Kasanen, R., Bäck, J., & Hölttä, T. (2020). Is Decreased Xylem Sap Surface Tension Associated With Embolism and Loss of Xylem Hydraulic Conductivity in Pathogen-Infected Norway Spruce Saplings?. *Frontiers in plant science*, *11*, 1090. https://doi.org/10.3389/fpls.2020.01090

Papastefanou, P., Zang, C. S., Pugh, T. A. M., Liu, D., Grams, T. E. E., Hickler, T., & Rammig, A. (2020). A Dynamic Model for Strategies and Dynamics of Plant Water-Potential Regulation Under Drought Conditions [Original Research]. *Frontiers in Plant Science*, *11*. https://doi.org/10.3389/fpls.2020.00373

Pastorello, G., Trotta, C., Canfora, E., Chu, H., Christianson, D., Cheah, Y.-W., Poindexter, C., Chen, J., Elbashandy, A., Humphrey, M., Isaac, P., Polidori, D., Reichstein, M., Ribeca, A., van Ingen, C., Vuichard, N., Zhang, L., Amiro, B., Ammann, C., . . . Papale, D. (2020). The FLUXNET2015 dataset and the ONEFlux processing pipeline for eddy covariance data. *Scientific Data*, *7*(1), 225. https://doi.org/10.1038/s41597-020-0534-3

Person, G. (2015). *Sveriges klimat 1860-2014: Underlag till Dricksvattenutredningen*. Stockholm: SMHI. http://www.diva-portal.org/smash/get/diva2:948139/FULLTEXT01.pdf

Peters, J. M. R., Gauthey, A., Lopez, R., Carins-Murphy, M. R., Brodribb, T. J., & Choat, B. (2020). Non-invasive imaging reveals convergence in root and stem vulnerability to cavitation across five tree species. *Journal of Experimental Botany*, *71*(20), 6623-6637. https://doi.org/10.1093/jxb/eraa381

Phillips, O. L., van der Heijden, G., Lewis, S. L., López-González, G., Aragão, L. E. O. C., Lloyd, J., Malhi, Y., Monteagudo, A., Almeida, S., Dávila, E. A., Amaral, I., Andelman, S., Andrade, A., Arroyo, L., Aymard, G., Baker, T. R., Blanc, L., Bonal, D., de Oliveira, Á. C. A., . . . Vilanova, E. (2010). Drought–mortality relationships for tropical forests. *New Phytologist*, *187*(3), 631-646. https://doi.org/10.1111/j.1469-8137.2010.03359.x

Pretzsch, H., Schütze, G., & Biber, P. (2018). Drought can favour the growth of small in relation to tall trees in mature stands of Norway spruce and European beech. *Forest Ecosystems*, *5*(1), 20. https://doi.org/10.1186/s40663-018-0139-x

Raposo, F. (2016). Evaluation of analytical calibration based on least-squares linear regression for instrumental techniques: A tutorial review. *TrAC Trends in Analytical Chemistry*, *77*, 167-185. https://doi.org/10.1016/j.trac.2015.12.006

Ratzmann, G., Meinzer, F. C., & Tietjen, B. (2019). Iso/Anisohydry: Still a Useful Concept. *Trends in Plant Science*, *24*(3), 191-194. https://doi.org/10.1016/j.tplants.2019.01.001

Rodriguez-Dominguez, C. M., Carins Murphy, M. R., Lucani, C., & Brodribb, T. J. (2018). Mapping xylem failure in disparate organs of whole plants reveals extreme resistance in olive roots. *The New phytologist*, *218*(3), 1025–1035. https://doi.org/10.1111/nph.15079

Ruiz-Pérez, G., & Vico, G. (2020). Effects of Temperature and Water Availability on Northern European Boreal Forests [Original Research]. *Frontiers in Forests and Global Change*, *3*. https://doi.org/10.3389/ffgc.2020.00034

Salazar-Tortosa, D., Castro, J., Villar-Salvador, P., Viñegla, B., Matías, L., Michelsen, A., Rubio de Casas, R., & Querejeta, J. I. (2018). The “isohydric trap”: A proposed feedback between water shortage, stomatal regulation, and nutrient acquisition drives differential growth and survival of European pines under climatic dryness. *Global Change Biology*, *24*(9), 4069-4083. https://doi.org/10.1111/gcb.14311

Sanchez, J. M. (2021). The inadequate use of the determination coefficient in analytical calibrations: How other parameters can assess the goodness-of-fit more adequately. *Journal of Separation Science*, *44*(24), 4431-4441. https://doi.org/10.1002/jssc.202100555

Santiago, L. S., De Guzman, M. E., Baraloto, C., Vogenberg, J. E., Brodie, M., Hérault, B., Fortunel, C., & Bonal, D. (2018). Coordination and trade-offs among hydraulic safety, efficiency and drought avoidance traits in Amazonian rainforest canopy tree species. *New Phytologist*, *218*(3), 1015-1024. https://doi.org/10.1111/nph.15058

Schulze, E-D., Beck, E., Buchmann, N., Clemens, S., Müller-Hohenstein, K., & Scherer-Lorenzen, M. (2019). *Plant Ecology.* https://doi.org/ 10.1007/978-3-662-56233-8

Schuldt, B., Buras, A., Arend, M., Vitasse, Y., Beierkuhnlein, C., Damm, A., Gharun, M., Grams, T., Hauck, M., Hajek, P., Hartmann, H., Hilbrunner, E., Hoch, G., Holloway-Phillips, M., Körner, C., Larysch, E., Luebbe, T., Nelson, D.,

Rammig, A., & Kahmen, A. (2020). A first assessment of the impact of the extreme 2018 summer drought on Central European forests. *Basic and Applied Ecology*, *45*. https://doi.org/10.1016/j.baae.2020.04.003

Seidl, R., Thom, D., Kautz, M., Martin-Benito, D., Peltoniemi, M., Vacchiano, G., Wild, J., Ascoli, D., Petr, M., Honkaniemi, J., Lexer, M. J., Trotsiuk, V., Mairota, P., Svoboda, M., Fabrika, M., Nagel, T. A., & Reyer, C. P. O. (2017). Forest disturbances under climate change. *Nature Climate Change*, *7*(6), 395-402. https://doi.org/10.1038/nclimate3303

Sitch, S., Smith, B., Prentice, I. C., Arneth, A., Bondeau, A., Cramer, W., Kaplan, J. O., Levis, S., Lucht, W., Sykes, M. T., Thonicke, K., & Venevsky, S. (2003). Evaluation of ecosystem dynamics, plant geography and terrestrial carbon cycling in the LPJ dynamic global vegetation model. *Global Change Biology*, *9*(2), 161-185. https://doi.org/10.1046/j.1365-2486.2003.00569.x

Smith, B, Prentice, IC & Sykes, M. (2001). Representation of vegetation dynamics in modelling of terrestrial ecosystems: comparing two contrasting approaches within European climate space, *Global Ecology and Biogeography*, *10*, 621-637

Smith, B., Wårlind, D., Arneth, A., Hickler, T., Leadley, P., Siltberg, J., & Zaehle, S. (2014). Implications of incorporating N cycling and N limitations on primary production in an individual-based dynamic vegetation model. *Biogeosciences*, *11*(7), 2027-2054. https://doi.org/10.5194/bg-11-2027-2014

Smith, J., & Smith, P. (2007). *Environmental Modelling: An Introduction*. OUP Oxford.

Sobol′, I. M. (2001). Global sensitivity indices for nonlinear mathematical models and their Monte Carlo estimates. *Mathematics and Computers in Simulation*, *55*(1), 271-280. https://doi.org/10.1016/S0378-4754(00)00270-6

Solberg, S. (2004). Summer drought: a driver for crown condition and mortality of Norway spruce in Norway. *Forest Pathology*, *34*(2), 93-104. https://doi.org/10.1111/j.1439-0329.2004.00351.x

Tardieu, F., & Simonneau, T. (1998). Variability among species of stomatal control under fluctuating soil water status and evaporative demand: modelling isohydric and anisohydric behaviours. *Journal of Experimental Botany*, *49*(Special_Issue), 419-432. https://doi.org/10.1093/jxb/49.Special_Issue.419

Togashi, H., Prentice, I., Evans, B., Forrester, D., Drake, P., Feikema, P., Brooksbank, K., Eamus, D., & Taylor, D. (2015). Morphological and moisture availability controls of the leaf area-to-sapwood area ratio: Analysis of measurements on Australian trees. *Ecology and Evolution*, *5*. https://doi.org/10.1002/ece3.1344

Tomasella, M., Beikircher, B., Häberle, K.-H., Hesse, B., Kallenbach, C., Matyssek, R., & Mayr, S. (2017). Acclimation of branch and leaf hydraulics in adult Fagus sylvatica and Picea abies in a forest through-fall exclusion experiment. *Tree Physiology*, *38*(2), 198-211. https://doi.org/10.1093/treephys/tpx140

Tyree, M., & Sperry, J. (1989). Vulnerability of xylem to cavitation and embolism. *Ann. Rev. Plant Biology*, *40*, 19-36.

Urli, M., Porté, A., Cochard, H., Guengant, Y., Burlett, R., & Delzon, S. (2013). Xylem embolism threshold for catastrophic hydraulic failure in angiosperm trees. *Tree Physiology*, *33*. https://doi.org/10.1093/treephys/tpt030

Wang, C., He, J., Zhao, T.-H., Cao, Y., Wang, G., Sun, B., Yan, X., Guo, W., & Li, M.-H. (2019). The Smaller the Leaf Is, the Faster the Leaf Water Loses in a Temperate Forest [Original Research]. *Frontiers in Plant Science*, *10*. https://doi.org/10.3389/fpls.2019.00058

Wason, J. W., Anstreicher, K. S., Stephansky, N., Huggett, B. A., & Brodersen, C. R. (2018). Hydraulic safety margins and air-seeding thresholds in roots, trunks, branches and petioles of four northern hardwood trees. *The New phytologist*, *219*(1), 77–88. https://doi.org/10.1111/nph.15135

Whitehead, D., Edwards, W. R. N., & Jarvis, P. G. (1984). Conducting sapwood area, foliage area, and permeability in mature trees of Piceasitchensis and Pinuscontorta. *Canadian Journal of Forest Research*, *14*(6), 940-947. https://doi.org/10.1139/x84-166

Xu, X., Medvigy, D., Powers, J. S., Becknell, J. M., & Guan, K. (2016). Diversity in plant hydraulic traits explains seasonal and inter-annual variations of vegetation dynamics in seasonally dry tropical forests. *New Phytologist*, *212*(1), 80-95. https://doi.org/10.1111/nph.14009

Yuan, W., Zheng, Y., Piao, S., Ciais, P., Lombardozzi, D., Wang, Y., Ryu, Y., Chen, G., Dong, W., Hu, Z., Jain, A. K., Jiang, C., Kato, E., Li, S., Lienert, S., Liu, S., Nabel, J. E. M. S., Qin, Z., Quine, T., . . . Yang, S. (2019). Increased atmospheric vapor pressure deficit reduces global vegetation growth. *Science Advances*, *5*(8), eaax1396. https://doi.org/doi:10.1126/sciadv.aax1396

Zhang, D., Du, Q., Zhang, Z., Jiao, X., Song, X., & Li, J. (2017). Vapour pressure deficit control in relation to water transport and water productivity in greenhouse tomato production during summer. *Scientific Reports*, *7*(1), 1-11.

Zhou, X., Lin, H., & Lin, H. (2008). Global Sensitivity Analysis. In S. Shekhar & H. Xiong (Eds.), *Encyclopedia of GIS* (pp. 408-409). Springer US. https://doi.org/10.1007/978-0-387-35973-1_538

A. Appendix

A.1 Only spruce sensitivity test

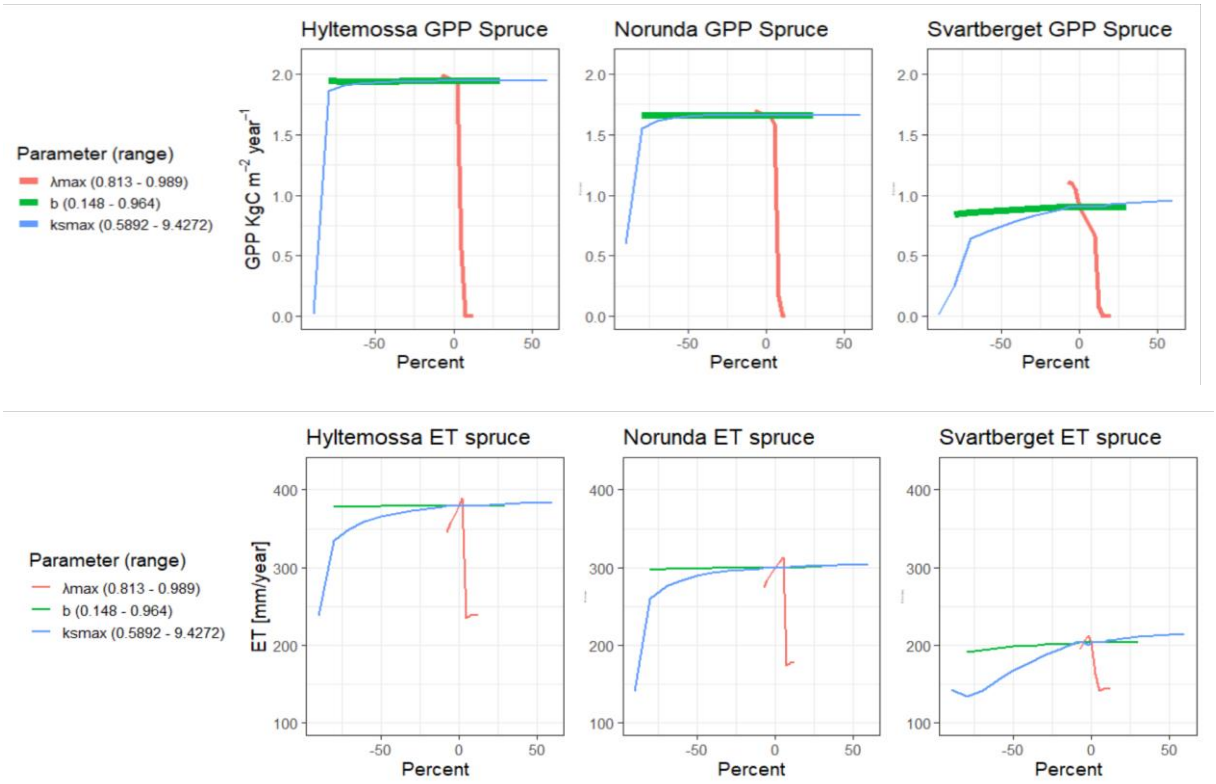

FIGURE A1: *Percentual change of three parameters effect on ET and GPP. Yearly average of the years (2014-2015) for ET and GPP in a monoculture spruce forest.*

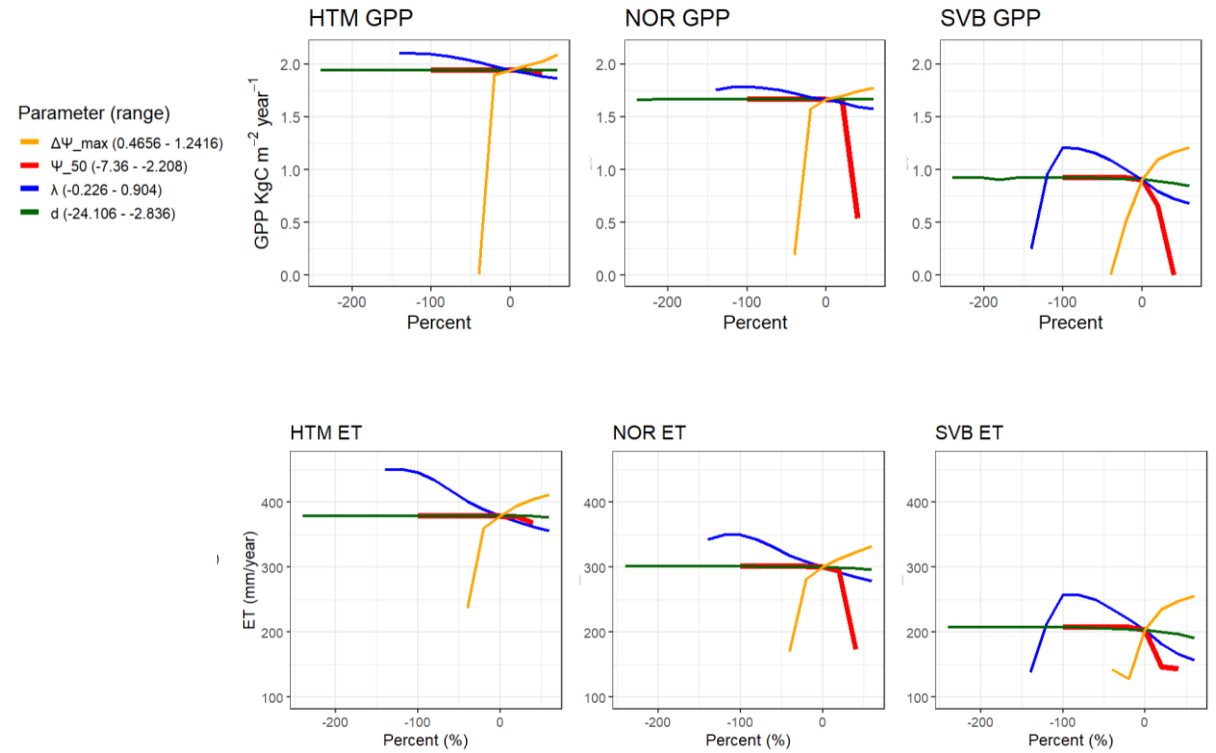

FIGURE A2: *Percentual change of four parameters effect on ET and GPP. Yearly average of the years (2014-2015) for ET and GPP in a monoculture spruce forest.*

A.2 Soil water

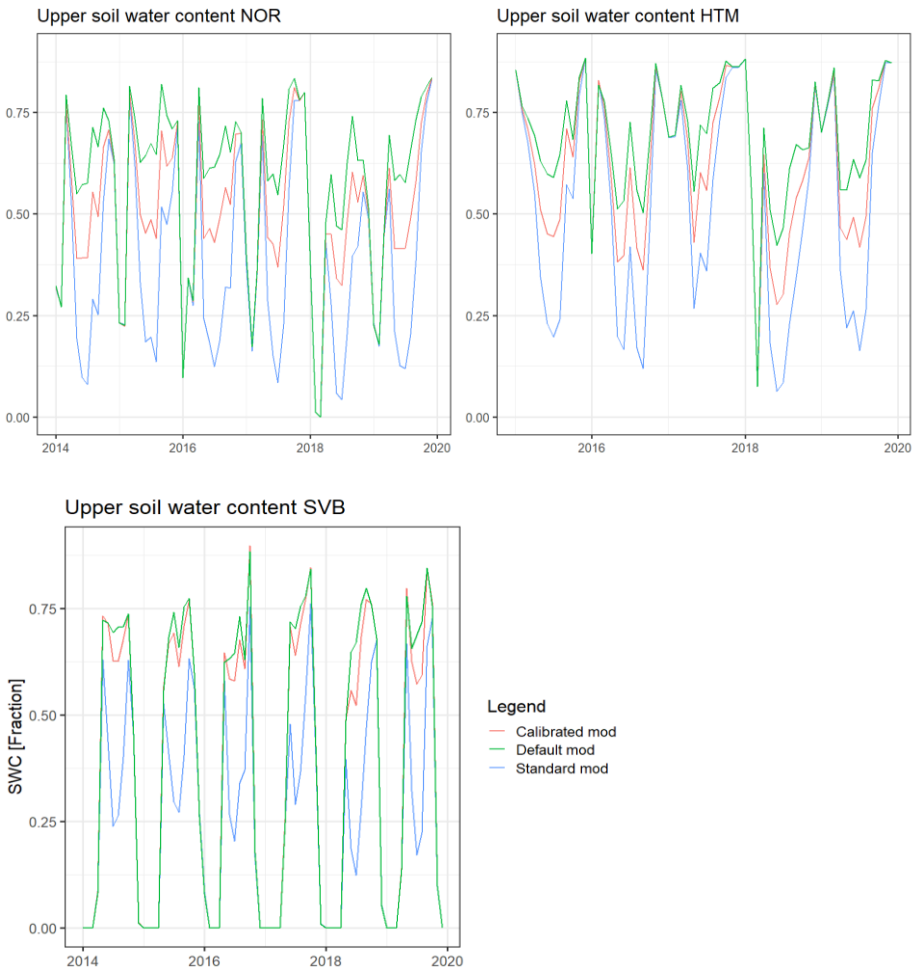

FIGURE A3*. Soil water content in the upper layers for all sites as fraction of available water holding capacity for hydraulic version (calibrated and default) and standard version.*

A.3 Second calibration – site RRMSE

A.3.1 All species included λ RRMSE

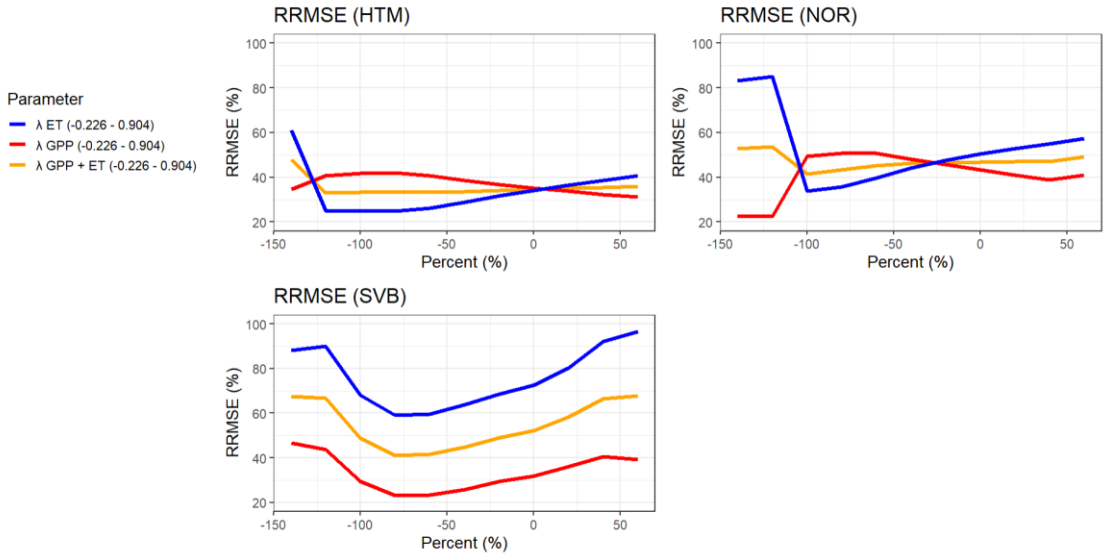

FIGURE A4: *The mean RRMSE for the specific site variation against changed parameters λ and the output ET, GPP. Blue shows the mean RRMSE of both GPP and ET.*

A.3.1 All species included $\Delta\Psi max$ RRMSE

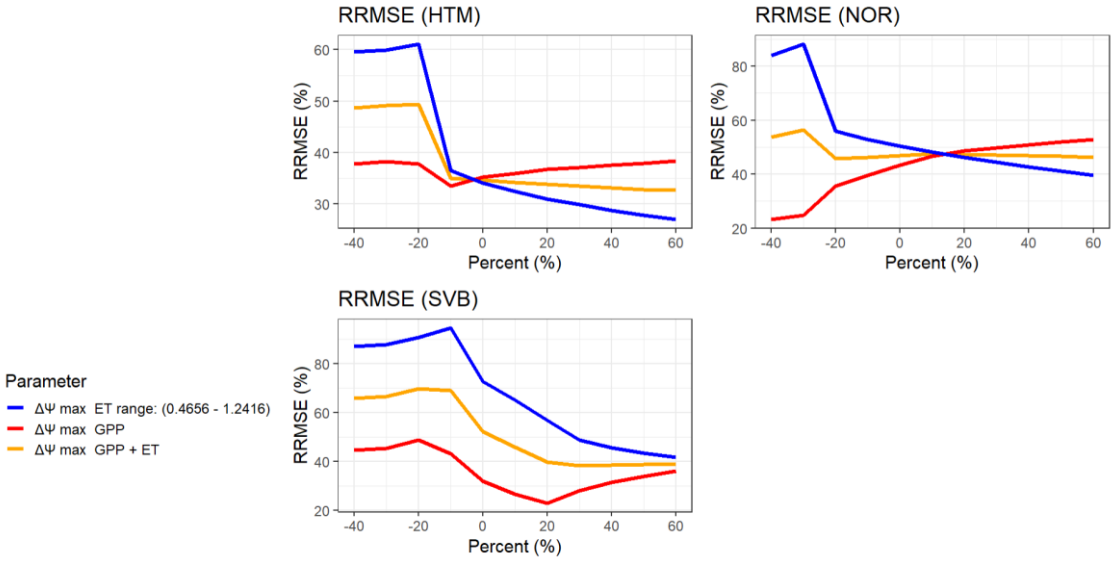

FIGURE A5: *The mean RRMSE for the specific site variation against changed parameters $\Delta\Psi$ max and the output ET, GPP. Blue shows the mean RRMSE of both GPP and ET.*

A.4 Water potential

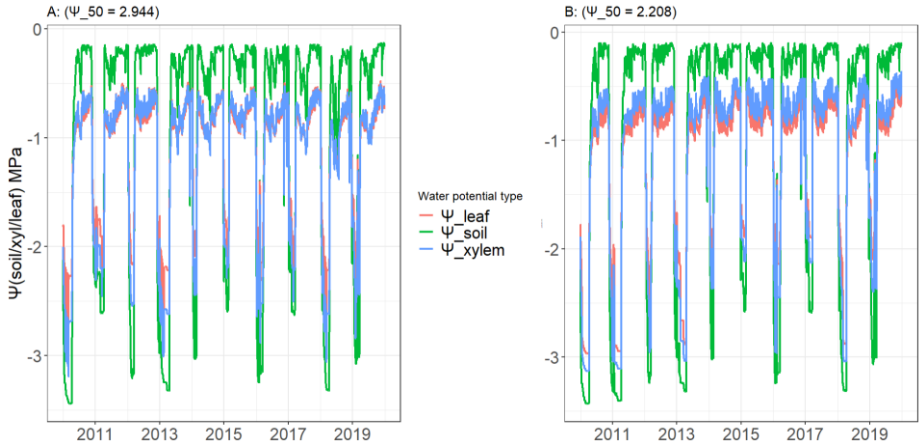

FIGURE A6: *Water potential (soil, xylem, leaf). A: Ψ50 is 2.944 MPa and B: Ψ50 is 2.208.*

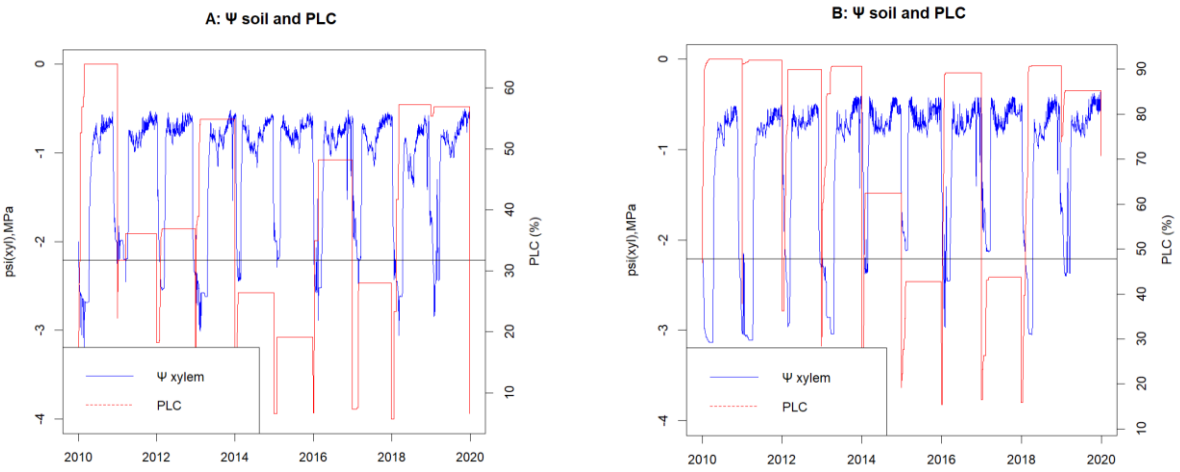

FIGURE A7: *Xylem water potential (MPa) and percent loss of cavitation for Ψ50 =2.944 MPa. B: Xylem water potential (MPa) and percent loss of cavitation for Ψ50 =2.208 MPa. Black line represents Ψ50 for xylem water potential (do not represent PLC of 50%).*

A.5 Carbon mass

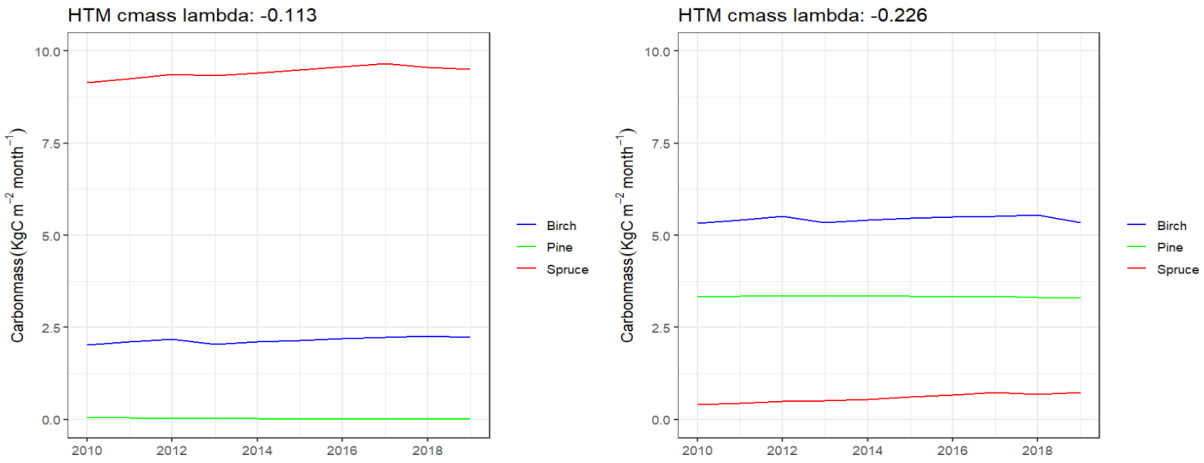

FIGURE A8: *HTM Carbon mass timeseries for each species and for λ from -0.113 to -0.226.*

λmax:

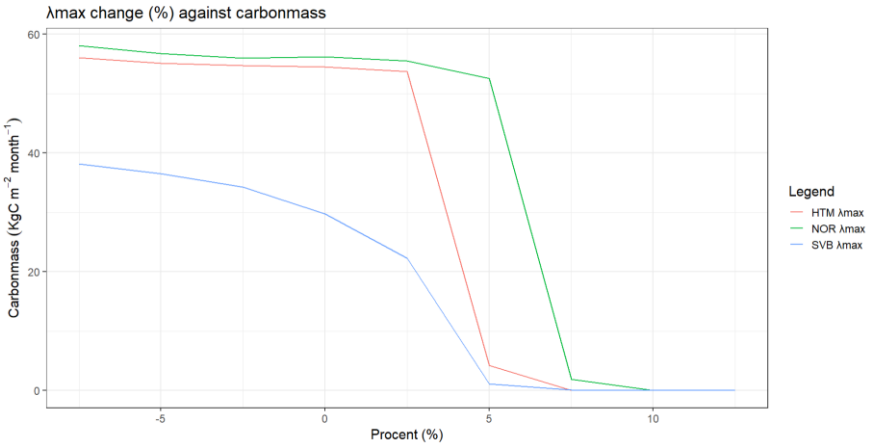

FIGURE A9: *Carbon mass changes (%) for the sites for the calibrated hydraulic model.*

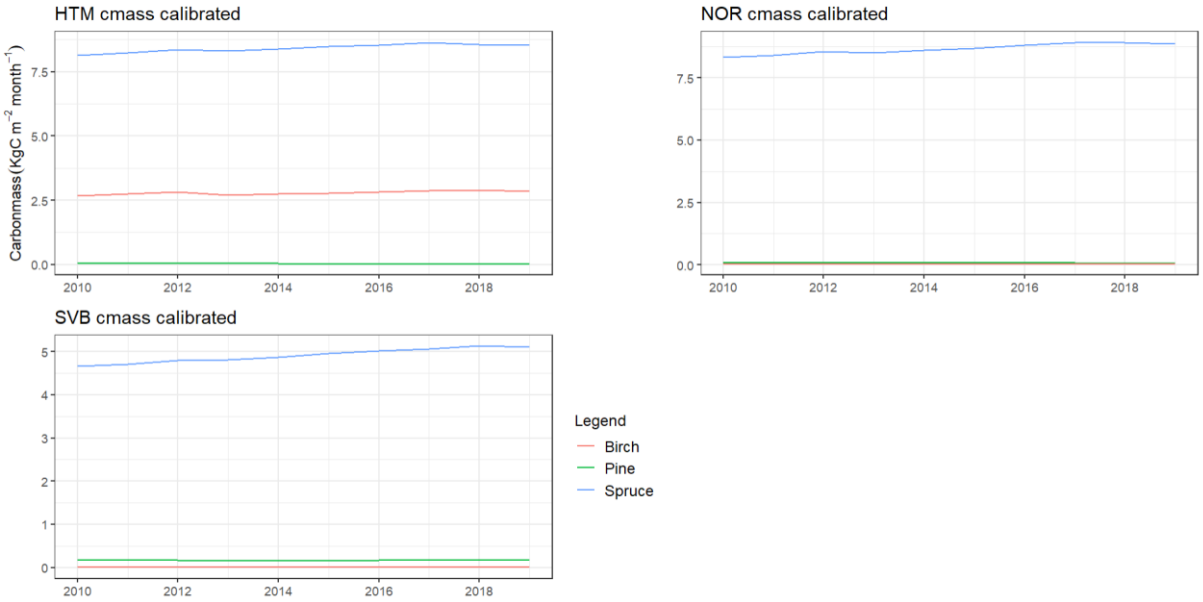

FIGURE A10: *Carbon mass timeseries for the PFT for the first calibration of the hydraulic model.*

A.6 Species/PFT settings:

A.6.1 Instruction settings

TABLE A1: The fixed settings for the tree species. **Woodens** is sapwood and heartwood density (kgC/m3), **turnover_leaf** is Leaf turnover (fraction/year), **k_latosa** is tree leaf to sapwood area ratio, sla is specific leaf area (m^2/kgC), **leaflong** is Leaf longevity (years), **kr_max** is specific root conductivity (s^{-1} MPa^{-1}), **kL_max** is specific leaf conductivity (mmol m^{-2} s^{-1} MPa^{-1}), **gmin** is canopy conductance not assoc with photosynthesis (mm/s), **gdd5min_est is** minimum GDD on 5 deg C base for establishment, **twmin_est is** minimum warmest month mean temp for establishment (deg C), **tcmin_surv is** Min 20-year coldest month mean temp for survival (deg C), **tcmin_est** is min 20-year coldest month mean temp for

establishment (deg C), **tcmax_est** is max 20-year coldest month mean temp for establishment (deg C), **rootdist** (1-5) is rootdistrubution in 1 to 5 layers and rootdist (6-12) is rootdistrubution in 6 to 15 layers.

Spruce			
wooddens	225	**gdd5min_est**	600
k_latosa	3850	**twmin_est**	5
sla	12.7588	**tcmin_surv**	-30
turnover_leaf	0.3219575	**tcmin_est**	-30
leaflong	3.106	**tcmax_est**	-1.5
kr_max	0.00112	**rootdist (1-5)**	0.12
kL_max	6.4053	**rootdist (6-15)**	0.04
gmin	0.3	**Shade tolerant**	Tolerant[1]
longevity	500		
Pine			
wooddens	282.5	**gdd5min_est**	500
k_latosa	1712.05	**twmin_est**	5
sla	9.3493	**tcmin_surv -**	-30
turnover_leaf	0.19140588	**tcmin_est**	-30
leaflong	5.2245	**tcmax_est**	-1.0
kr_max	0.00112	**rootdist (1-5)**	0.12
kL_max	5.9092	**rootdist (6-12)**	0.04
gmin	0.3	**Shade tolerant**	Intermediate[1]
longevity	350		
Birch			
wooddens	225	**gdd5min_est**	700
k_latosa	4771.4	**twmin_est**	5
sla	24.3	**tcmin_surv -**	-30
turnover_leaf	1.0	**tcmin_est**	-30
leaflong	0.7335	**tcmax_est**	7
kr_max	0.00112	**rootdist (1-5)**	0.12
kL_max	5.5704	**rootdist (6-12)**	0.04
gmin	0.5	**Shade tolerant**	Intolerant[1]
longevity	200		

1: is based on table A2 tolerant classes.

A.6.2 Shade tolerant classes

TABLE A2: The shade tolerance classes modified from Hickler et al. (2012).

Shade tolerance	**Tolerant (Spruce)**	**Intermediate (Pine)**	**Intolerant (Birch)**
Sapwood to heartwood conversion rate (year^{-1})	0.05	0.075	0.1
Growth efficiency parameter (kg C m^{-2} year^{-1})	0.03	0.06	0.135

Max. establishment rate (saplings year^{-1} patch^{-1})	0.05	0.15	0.2
Min. PAR at forest floor for establishment (MJ m^{-2} day^{-1})	0.35	2.0	2.5
Recruitment shape parameter	2.0	7.0	11.0

A.7 Latent heat to ET conversion

To calculate the energy balance corrected fluxes is based on the Bowen ratio and based on the following formula (Pastorello et al. 2020):

$$LE_{corr} = \frac{(\mathrm{NETRAD}-\mathrm{G})}{(\mathrm{H}+\mathrm{LE})} \quad (1)$$

Where *G* is soil heat flux and *H* is sensible heat flux. LE_{corr} was provided by FLUXNET (ICOS 2022).

Latent heat (LE_{corr}) is energy flux and was converted to water flux, evapotranspiration (ET_{corr}) in mm/month to validate the output monthly data from LPJ-GUESS (hydraulic and standard versions). LE_{vap} varies with temperature and therefore latent heat of vaporisation, λ provides an equation for calculating LE_{corr} with air temperature variation. Latent heat of vaporization is the amount of energy needed to change a unit mass of water from liquid to water vapor. LE_{corr} was converted to ET_{corr} using the following formula (Allen et al. 1998):

$$ET_{corr} = \frac{LE_{corr}}{\lambda} \times (60 \times 60 \times 24) \times (days\ per\ month) \quad (2)$$

$$\lambda = 2.501 \times 10^{6} - (2.361 \times 10^{-3}) \times Ta \quad (3)$$

where Ta is the mean daily air temperature.

A.8 Soil water and λ change (spruce)

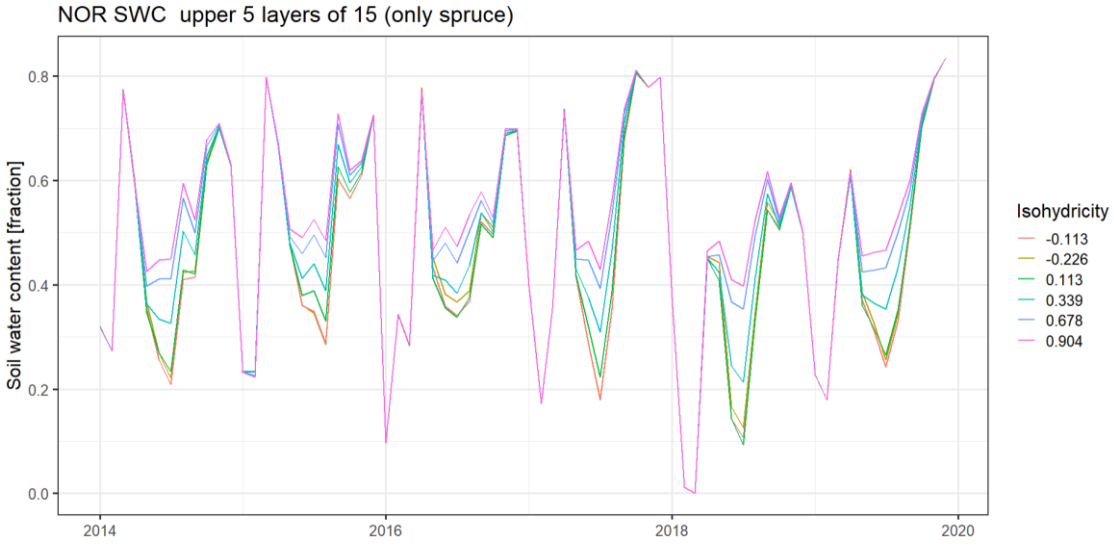

FIGURE A11: *Soil water content timeseries for spruce with changed isohydricity.*

A.9 Observation (FLUXNET) uncertainty

GPP_DT_VUT_REF values are daily data of GPP. Uncertainty estimations for GPP and ET is calculated through the following formulas:

$$\textbf{\textit{Standard error}}\ (\textbf{\textit{GPP}}) = \frac{\textit{SD}(\textit{GPP\_DT\_VUT\_REF})}{\sqrt{N}} \quad (4)$$

$$ET_{CORR_{JOINTUNC}} = \sqrt{ET_{RANDUNC}{}^2 + \left(\frac{ET_{CORR75} - ET_{CORR25}}{1.349}\right)^2} \quad (5)$$

where N is the number of measured values for one month, *GPP_DT_VUT_REF* is the Gross Primary Production, from daytime partitioning method, reference selected from GPP versions using model efficiency (MEF) , $LE_{RANDUNC}$ is the random uncertainty of ET, ET_{CORR75} and ET_{CORR25} are the 75th percentile and 25th percentile evapotranspiration flux, corrected by LE_F_MDS by energy balance closure correction factor.

ET uncertainty:

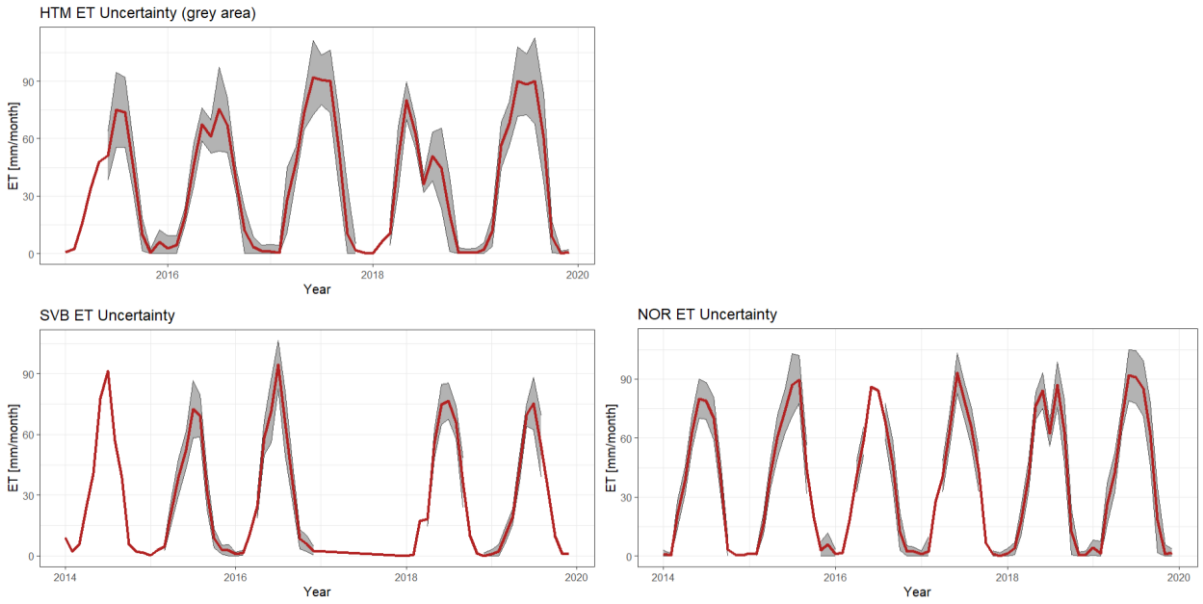

FIGURE A12: *Monthly observations of ET_{corr} for HTM, NOR and SVB (red line). Estimated uncertainty range (grey area) using joint-uncertainty from Pastorello et al. (2020). No estimated uncertainty for some of the months.*

GPP uncertainty:

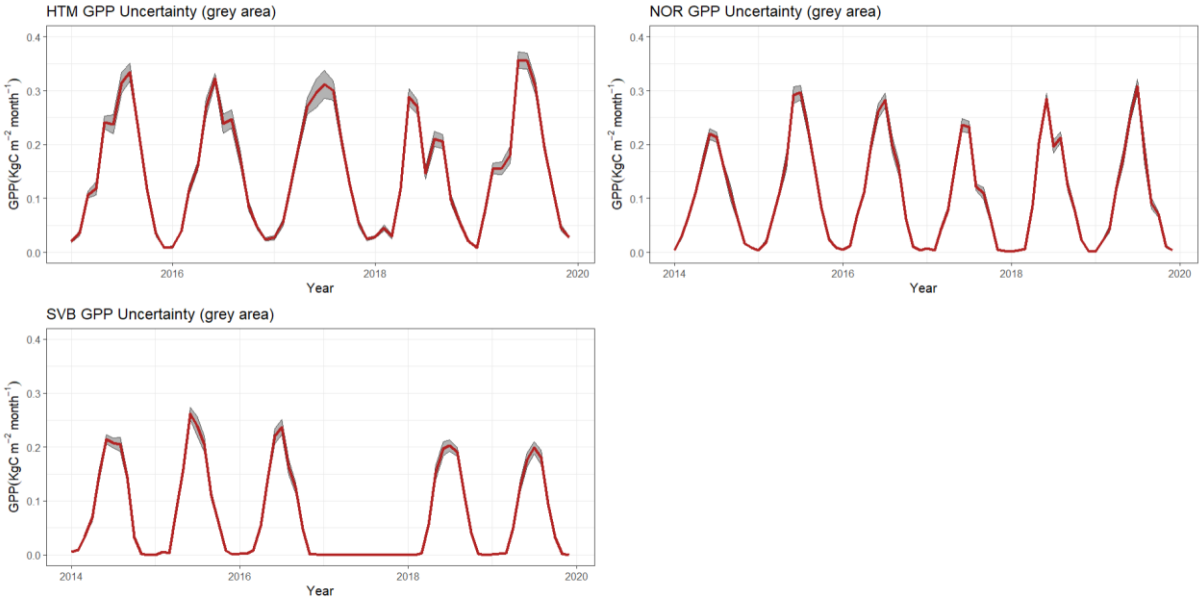

FIGURE A13: *Monthly observation of GPP for HTM, NOR and SVB (red line). Estimated uncertainty range (grey area) using standard error.*